BIOCHEMICAL, BIOPHYSICAL AND COMPUTATIONAL STUDIES OF HUMAN AND *TRYPANOSOMA CRUZI* S-ADENOSYL-L-HOMOCYSTEINE HYDROLASE

By

Sumin Cai

Bachelor of Engineering in Biopharmaceutics
China Pharmaceutical University 2000

Submitted to the Department of Molecular Biosciences and the Faculty of the Graduate School of the University of Kansas
In partial fulfillment of the requirements for the degree of Doctor of Philosophy

Dissertation Committee:

Chairperson: Krzysztof Kuczera, Ph.D.

Ronald T. Borchardt, Ph.D.

Carey K. Johnson, Ph.D.

C. Russell Middaugh, Ph.D.

Richard L. Schowen, Ph.D.

The Dissertation Committee for Sumin Cai certifies that this is the approved version of the following dissertation

BIOCHEMICAL, BIOPHYSICAL AND COMPUTATIONAL STUDIES OF HUMAN AND *TRYPANOSOMA CRUZI* S-ADENOSYL-L-HOMOCYSTEINE HYDROLASE

Committee:

Chairperson: Krzysztof Kuczera, Ph.D.

Ronald T. Borchardt, Ph.D.

Carey K. Johnson, Ph.D.

C. Russell Middaugh, Ph.D.

Richard L. Schowen, Ph.D.

October 27th 2008

Date Approved

Dedicated to:

My Paternal Great Grandmother

Erbao Cai

&

My Dad and Mom

Peifa Cai and Qihua Wang

&

My Husband

Yunsong Li

ABSTRACT

In both mammals and parasites, S-adenosyl-L-homocysteine hydrolase (SAHH) plays a crucial role in regulating S-adenosylmethionine dependent transmethylations by catalyzing the reversible conversion of adenosyl-L-homocysteine (AdoHcy) to adenosine and homocysteine. Inhibitors of parasite SAHHs (e.g., those of *Leishmania*, *Plasmodium*, *Trypanosoma*) are potential anti-parasitic agents which may present selective inhibition if their inhibitory activity is weaker for *Homo sapiens* SAHH (Hs-SAHH). This study was aimed at addressing the differences in structure and kinetic properties between Hs-SAHH and Tc-SAHH, the SAHH of *Trypanosoma cruzi*, the organism which causes Chagas disease in humans.

The available X-ray structures of Hs-SAHH and Tc-SAHH show no significant difference between the active sites of the two enzymes, providing no definite suggestions for designing selective anti-parasitic inhibitors. Therefore, we have designed a series of biochemical, biophysical and computational studies focusing on enzyme interactions with the nicotinamide cofactors. These studies showed that the equilibrium and kinetic properties of the association and dissociation of the cofactor NAD^+ from the enzymes of Hs-SAHH and Tc-SAHH are qualitatively similar but quantitatively distinct. Briefly, association of NAD^+ to both enzymes is a complex process, composed of two parts: a fast-binding phase (dead time) and a slow-binding phase. The fast-binding phase comes from one class of the homotetrameric apo-enzyme active sites, which binds cofactor weakly and generates full activity very rapidly (in less than a minute). The slow-binding phase comes from

the other class of active sites which binds cofactor more strongly but generates activity only slowly (over 30 min). These two classes of active sites appear to be numerically equal. The kinetics of slow binding of NAD^+ to two enzymes show concentration dependence, and the cofactor binds to Hs-SAHH almost 10 times faster than to Tc-SAHH. The final binding affinity of cofactor NAD^+ to Tc-SAHH persists at micromolar levels while Hs-SAHH decreases the binding affinity from micromolar to nanomolar over a period of time and its equilibrium affinity stays at nanomolar levels. In contrast to the complex kinetics of association, both enzymes undergo dissociation of NAD^+ from all four sites in a single first-order reaction. The dissociation of NAD^+ from two enzymes shows complex temperature dependence and NAD^+ leaves from Tc-SAHH much faster than from Hs-SAHH. Compared to the traditional selective inhibitor target site (the substrate-binding domain of SAHH), the identified differential features between Hs-SAHH and Tc-SAHH suggest the use of a novel target site, the cofactor (NAD^+/NADH)-binding domain.

In a detailed analysis, two structural elements, the helix 18 at the C-terminal and the β-sheet A of the Rossmann motif in the cofactor-binding domain, were identified as possible sources of the distinct properties of the two enzymes. The site-directed mutagenesis approach was employed to create two kinds of mutants: the "humanized" Tc-SAHH (helix 18 or β-sheet A of Tc-SAHH replaced by that of human enzyme) and the "parasitized" Hs-SAHH (helix 18 or β-sheet A of Hs-SAHH replaced by that of parasite enzyme). As expected, the results for the two mutants were intermediate between the two wild types: the "humanized" Tc-SAHH exhibits

similar kinetics and thermodynamics to wild type Hs-SAHH while the “parasitized” Hs-SAHH has properties close to wild type parasite enzymes.

Moreover, in an alanine scanning computational study, two conserved residues at the C-terminus, a Lys and a Tyr, are found to be involved in the differential kinetic properties of the two enzymes. All these data support the view that the cofactor-binding domain is a good target for designing selective inhibitors against parasite enzymes.

In addition, this work found a selective inhibitor which bound to the traditional target site – the substrate binding site, and studied its inactivation mechanism and kinetic features. Ribavirin, an analogue of adenosine, exhibits preferential time-dependent inactivation on Tc-SAHH over Hs-SAHH and provides a structural lead to design more selective inhibitors.

Overall, studies on differential cofactor association and dissociation properties between Hs-SAHH and Tc-SAHH will help us understand better on these two enzymes and lead to design potential selective inhibitors targeting at cofactor-binding sites for treatment of Chagas disease.

Acknowledgements

Without the help from my advisor Dr. Krzysztof Kuczera and my close committee members Dr. Ronald T. Borchardt and Dr. Richard L. Schowen, I would never gain my current achievements. I am very grateful to Dr. Kuczera and Dr. Borchardt who gave me the chance to join the SAHH project four years ago when my previous advisor moved to another university. I transferred the research field from cell biology to biochemistry at that time and I was so lucky to be guided patiently by above three excellent scientists in the new field and to be trained carefully in different aspects: experimental design, data analysis, scientific presentation and writing. Although scientific research is hard and produces repeated failures, my Ph.D. training was filled with fun. I enjoyed in working with Dr. Schowen and deeply impressed by his distinguished scientific qualities: limitless knowledge, strict scientific aptitude and incredible ideas.

I am also indebted to the co-workers and the people who gave me great assistance in my research. Dr. Qing-Shan Li, a previous postdoc, taught me how to do biochemistry experiments when I first joined the SAHH project. Dr. Jianwen Fang, an expert in the computer area, kindly guided me in the use of computational software. Later there was happy and effective cooperation among Dr. Li, Dr. Fang and me on a series of publications. Moreover, my thanks go to previous and current lab members: Mengmeng Wang, Chen Hu, Becky Bross, Kevin Head and Dan Mudra as well as my committee members: Dr. Russ C. Middaugh, Dr. Carey K. Johnson who gave me lots of valuable comments and suggestions. In addition, I appreciate all the help from the

faculty, who taught me classes and/or guided me on research in the Department of Molecular Biosciences, and the help from the groups of Dr. Topp, Dr. Middaugh, Dr. Siahaan and Dr. Laurence in the Department of Pharmaceutical Chemistry.

My appreciation also goes to the loyal friendship of Jiang Xu, who became my best friend at KU and always gave me encouragement, support and help in my Ph.D. study. I also thank for the cordial friendship of Chuck and Marsh McPheeters.

Most importantly, I would like to express my deepest gratitude to my dearest dad and mom, Peifa Cai and Qihua Wang. They give me a happy family and always support me with endless love in my study and life. I am the only kid of my parents and I know they made a great sacrifice to let me study abroad for such a long time and in such a far country. Although I cannot stay with them everyday, what I wish is to be a daughter they are proud of.

I give the SPECIAL thanks to my husband, Dr. Yunsong “Frank” Li. It was our fate to join KU together in August 2002 and since he knew me in the new student orientation, he never let me feel lonely and helpless in the United States. I am grateful from my heart to his support and respect for my research and his sincere care of my life. As a wife, I will stay with my husband together to build a family full of love, pleasure and fun.

Last but not the least, I would like to share my great happiness with all who helped me, supported me and loved me during the past six years of my Ph.D. study no matter they are in the United States or in my home country China.

Table of Contents

Chapter 1

Introduction to Hs-SAHH and Tc-SAHH

1.1. The role of SAHH in methyl transfer

S-adenosyl-L-homocysteine (AdoHcy) hydrolase (SAHH; EC 3.3.1.1.) is the only known enzyme responsible for the reversible conversion of AdoHcy to adenosine (Ado) and homocysteine (Hcy) (Scheme 1.1.), which occurs downstream of the S-adenosylmethionine (AdoMet)-dependent transmethylation metabolic pathway [1, 2]. AdoMet-dependent methyl transfers are involved in a wide variety of important biological functions and the corresponding methyl acceptors in this pathway include macromolecules such as proteins, nucleic acids, polysaccharides and also include small molecules such as histamines and phospholipids [3]. Since AdoHcy is a powerful product inhibitor which functions as a switch to regulate the AdoMet-dependent methyl transfers, SAHH plays a crucial role in the AdoMet-dependent transmethylation pathway through controlling the intracellular levels of AdoHcy [1]. The catabolic reaction of AdoHcy favors the hydrolytic direction under physiological conditions [1]. Thus, inhibition of SAHH in mammalian cells will result in increased cellular level of AdoHcy and further blocking of the methyl cycle.

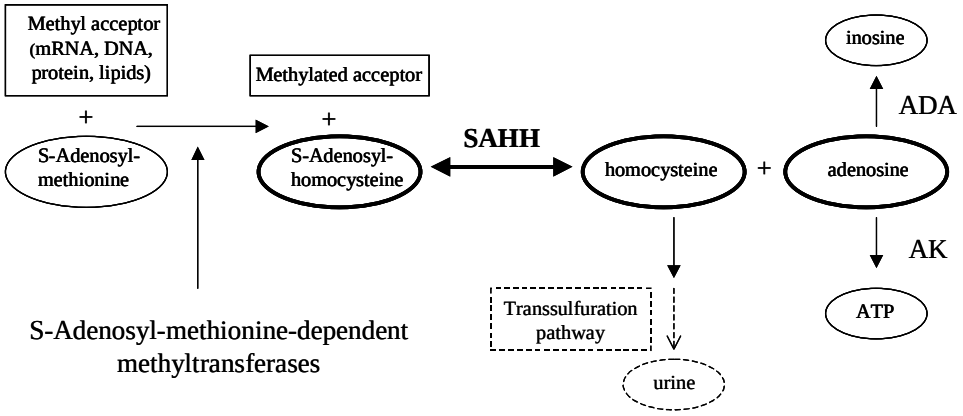

Scheme 1.1. The role of SAHH in methyl transfer and its metabolic pathways. Abbreviations: ADA, adenosine deaminase; AK, adenosine kinase.

Since it has a unique role in methyl transfer, SAHH has been considered as an antiviral target in chemotherapy for decades, since the 5'-terminal residue of viral mRNA is an AdoMet-dependent transmethylase substrate [4, 5]. Moreover, overactive malfunction of SAHH will result in abnormally high blood levels of Hcy, which increases the risk of cardiovascular disease [6-8] and possible amyloid diseases [9], and so SAHH has been considered as a target for treatment of above diseases as well. Recently, a new pharmacological interest has developed in SAHH as an anti-parasitic agent [10].

1.2. The importance of selective inhibitors against Tc-SAHH and therapeutics in Chagas disease

Besides mammalian organisms, parasites such as *Trypanosoma cruzi* [11], *Plasmodium falciparum* [12] and *Leishmania donovani* [10, 13] also encode their own SAHHs (Tc-SAHH, Pf-SAHH and Ld-SAHH, respectively) as well as AdoMet-dependent methyltransferases [14]. Similar to mammalian organisms, parasites use their AdoMet-dependent methyltransferase to methylate the 5'-cap of their mRNAs, which are important for their growth [14]. Thus, inactivation of parasitic SAHH will result in the blocking of methyl transfer and further suppress the growth of parasites. Earlier studies [10, 11] have shown that there are differences of the kinetic and thermodynamic parameters between human and parasite enzymes. Parasite enzymes have weaker binding affinities for NAD^+ and/or lower catalytic activities than those

of the human enzyme [10, 11]. These differences provide the possibility of designing selective inhibitors against parasite SAHHs without inactivation of human SAHH (Hs-SAHH).

In this study we are specifically interested in *Trypanosoma cruzi*. There currently are 8-11 million people infected with Chagas disease (also known as American trypanosomiasis) by the protozoan parasite *Trypanosoma cruzi* (Center for Disease and Control, Chagas Disease Fact Sheet, June 2007). This disease is transmitted by triatomine insects when they feed on the blood of human hosts [15]. Chagas disease mainly resides in rural areas of Mexico, Central America and South America and seriously threatens the public health there [15]. Because of increased population movement, it has been reported that there are rare cases in southern parts of the USA (Center for Disease and Control, Chagas Disease Fact Sheet, June 2007). It is therefore useful to continue biochemical, biophysical and computational studies on the distinguishing features between Hs-SAHH and Tc-SAHH because these studies could lead to development of compounds with clinical potential as anti-parasitic agents and eventually to improved treatments of Chagas disease.

1.3. Structural similarities between Hs-SAHH and Tc-SAHH

So far there are eleven available X-ray structures of SAHH from different sources (Protein Data Bank files: 1a7a, 1ky4, 1ky5, 1li4, 1d4f, 1ky4, 1xwf, 1k0u,

2h5i, 1xbe, 1v8b) including wild types of human placenta, rat liver, *Plasmodium falciparum* and *Trypanosoma cruzi* (unpublished data from our group) as well as various mutated forms, providing highly useful information for SAHH investigations. The alignment of SAHH amino acid sequences from different sources shows the primary structure is highly conserved [1].

1.3.1. The structure of Hs-SAHH

Hs-SAHH is a homotetramer (Figure 1.1.) composed of four ~ 47.5 kDa monomers [1, 16]. Each monomer has 432 residues and can be divided into three parts: one substrate-binding domain, one cofactor-binding domain (complexed to a molecule of NAD^+/NADH) and a small extended C-terminal "tail" [1, 16]. Both structure and normal mode analysis identify a hinge region [residues 182-196 (hinge region 1) and 352-356 (hinge region 2)] which connects the substrate-binding domain (SBD, residues 5-180 and 357-374) with the cofactor-binding domain (CBD, residues 191-356) [1, 17, 18]. This hinge regulates a ~ 19 ° reorientation of the SBD relative to the CBD in the direction of the open-to-closed transition and enables a conformational change in SAHH, which plays an important role in substrate capture and in the subsequent series of catalytic reactions [16, 17].

Between the SBD and the CBD there is a deep cleft which works as a channel for substrates entering the active site and also for products being released into

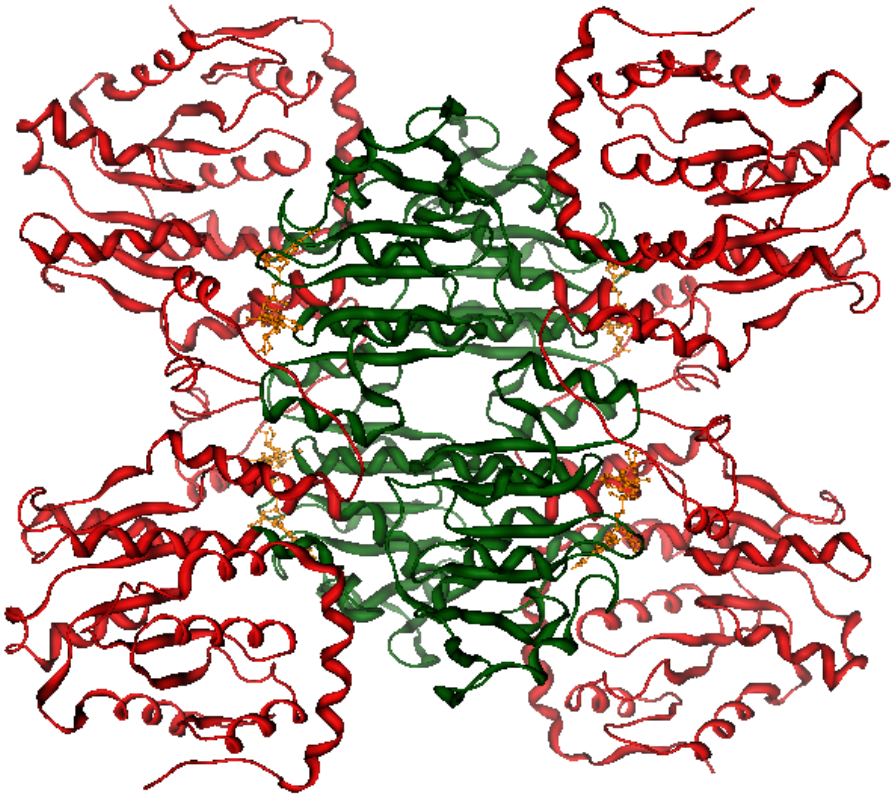

Figure 1.1. The tetramer structure of SAHH containing cofactor NAD^+ (Brown) (pdb code: 1KY4). Four cofactor-binding domains (green) form the central core and four substrate-binding domains (red) are located outside.

solution [1]. In terms of quaternary structure, the tetramer is composed of two dimers, formed by monomers A and B, and monomers C and D, *respectively*. The two dimers bind each other tightly and build a "dimer of dimers" [1]. The short tail (residue 380-432) of monomer A extends to monomer B and helps to cover monomer B's cofactor-binding site, and *vice versa* [1]. This tail exchange also occurs between the C and D monomers [1]. Moreover, the four cofactor-binding domains from four monomers bind each other tightly to form a central core with the four substrate-binding domains facing outside [1].

Comparing the available X-ray structures, there are two different conformations of SAHH: the open form and the closed form. Since rat SAHH shares 97 % sequence identity with the human enzyme, the entire protein structure of rat SAHH is assumed to be very similar to that of the human enzyme [19]. The open conformation comes from the structure of that rat enzyme (PDB code: 1KY4) [20] while the closed conformation is from the human source structure [PDB code: 1A7A [1] or 1LI4 [16]]. It is worth emphasizing that the X-ray structure (PDB:1A7A) of SAHH which contains the inhibitor DHCeA shows a twisted-closed conformation: a 14 º reorientation of two halves of the homotetramer to tightly seal the active core [1]. Comparison of the open and closed conformations, Figure 1.2. shows a 19° rotation of the substrate binding domain toward the cofactor binding domain, which transits the open to the closed conformation. The open-to-closed conformational transition is related to the catalytic reactions involving the substrate and cofactor

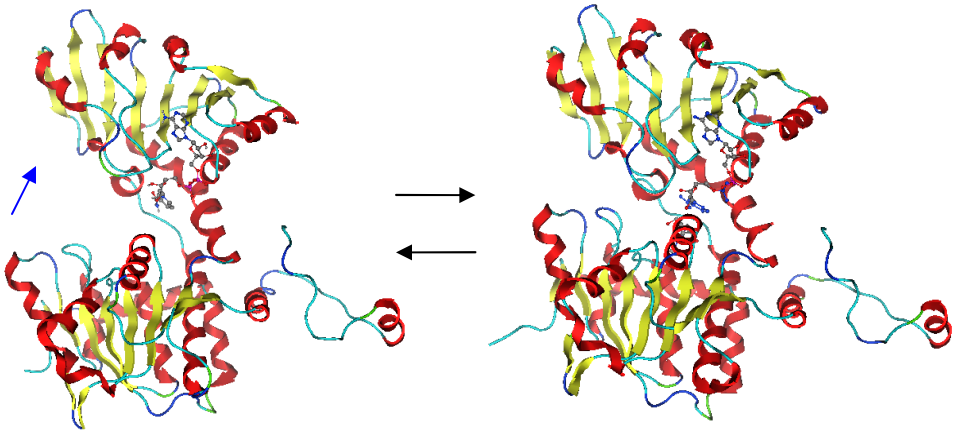

Open **Closed**

Figure 1.2. Open conformation (pdb: 1KY4, rat source) and closed conformation (pdb: 1LI4, human source) of SAHH monomer from crystallization (created by Molecular Operation Environment). The top domain is the cofactor-binding domain; the bottom domain is the substrate-binding domain; the right loop is the C-terminal tail. SAHH in open conformation only contains cofactor NAD^+ (ball-and-stick) and SAHH in closed conformation contains cofactor NADH (ball-and-stick) and oxidized inhibitor-NepA (ball-and-stick). Comparison of open conformation and closed conformation, the substrate-binding domain rotates ~ 19 ° toward to the cofactor binding domain to form an active site for catalysis.

NAD(H) in the active site. The open conformation of SAHH enables substrate binding and the closed conformation provides a closer contact between substrate and cofactor in active site needed for catalysis. The enzyme converts back to the open conformation upon product release [21].

Besides the X-ray structures, there is other evidence for SAHH domain motions. Computationally, normal mode analysis of low-frequency collective motions of SAHH reveals the different mechanical properties of the open and closed forms of SAHH. The hinge-bending motion in the direction of the open-to-closed conformational transition is unique to the open form of SAHH and occurs independently of other protein vibrations [17]. In the closed form, normal mode calculations show the amplitude of the hinge-bending motion in each subunit of SAHH is smaller than that in the open form, and the hinge bending motions of individual subunits are strongly coupled to each other and other low frequency vibrations, including subunit reorientations [17]. This mechanical coupling, a characteristic of the closed form, may transmit the information of any structural changes related to the catalytic reactions in one of the four active sites to other active sites. Normal mode analysis also identified that the 20-ps hinge-bending vibrations of subunits only reach an amplitude motion of ~ 1° which is much smaller than the amplitude of 19° in the global structural transition, so the 19° SBD vs. CBD reorientation cannot be described as a simple elastic deformation [17].

Experimentally, time-resolved fluorescence anisotropy measurements were carried out on native SAHH and three catalytically active mutants, M351P, H353A and P354A, all labeled with the fluorescent probe PMal at residues C^{113} and C^{421} [18]. Data analysis was focused on the time constants for reorientation motions and the data for wild type SAHH with/without ligand provides important information on the effect of ligand binding and oxidation on hinge-bending motions. Wild type SAHH without substrate exhibits three rotational correlation times: 0.5 ns reflecting local chromophore reorientations and protein vibrations; 14 ns involving domain reorientation; and 82 ns manifesting the overall protein tumbling in solution [18]. Wild type SAHH bound with 3'-deoxyAdo/NAD^+ or 3'-keto-Ado/NADH (Ado/NAD^+) shows similar three-component anisotropy decay, but for wild type SAHH bound with 3'-keto-NepA/NADH, the 10-20 ns domain reorientation is not detected [18]. These results indicate that there is an equilibrium between open and closed structures of SAHH. This equilibrium is shifted toward to a more mobile open form in the presence of the substrate-free enzyme (E-NAD^+), as well as in the presence of the intermediates which are formed early in the catalytic cycle after substrate binding or formed late prior to product release (E-NAD^+/ligand). This equilibrium is shifted toward the more rigid closed form in the presence of SAHH with substrates/analogues of the central catalytic intermediate (E-NADH/ligand) [18]. In addition, the fluorescence anisotropy studying of three mutations with/without ligand was used to investigate the roles of these residues in the hinge region 2 (residues 352-356) in hinge bending motions. Mutants M351P and P354A show a

similar pattern of behavior to wild type SAHH, which indicates that residues M351 and P354 have no significant effects on domain motion [18]. For the H353A mutant, the 10-20 ns domain motion wasn't detected with/without ligand, and the longest component was shortened to 55-71 ns for all four ligation states of mutant H353A. This indicates mutant H353A changes its domain motion dynamics independent of presence of ligand or oxidation state of cofactor [18]. Since the H353A mutant remains catalytically active, this mutant may slow down its hinge bending motions to a long time scale similar as that of overall protein tumbling or longer, or exhibit modified shape and size of the protein [18]. If the hinge bending motions slow down to the time scale of the enzyme's turnover (the order of a second), this would be out of the detectable range for the fluorescence anisotropy study (0.1 - 200 ns) [18]. Overall, hinge region 2 doesn't make a direct contribution to catalytic activity. In contrast, hinge region 1 contains residues N181, K186, N190, N191 which are in the active site, which are involved in binding the substrate and thus are directly able to affect the activity [18].

To get a direct and clear picture of the domain motions of SAHH, a 15 ns dynamics simulation of the open form of SAHH with explicit solvent was performed using Amber7 software. Very similar to the X-ray structure, the trajectories show that at the tetramer level the four cofactor binding domains form a central core which remains relatively rigid, and that the four substrate binding domains, located at the protein exterior, exhibit flexible reorientations of large amplitude. Interestingly, the

fluctuations of domains between open and closed conformations within each subunit constitute only ~ 20 % of the trajectory domain motions. At the tetramer level, the remaining ~ 80 % of the domain motions are perpendicular to the direction of the open-to-closed structural transition, and may be described as a “breathing-type” motion with substrate-binding domains moving to and from the tetrameric core of SAHH. Furthermore, the domain reorientations in solution can be represented as a combination of a faster process with 20-50 ps rotational correlation times and 3-4° amplitude, and a slower process with 8-23 ns correlation times and 14-22° amplitude. The time scale of the faster process is very close to that of the hinge-bending vibrations which were found in the normal mode analysis while the slow process well matches the fluorescence anisotropy decay measurements, which detected the 10-20 ns domain motion with ca. amplitude of 26° in SAHH without substrate. Therefore, the slow process is assigned to the rotational diffusion of the domains within a core with 10-20° half-angle. Overall, the results of the simulation agree with the previous data and help us to better understand SAHH domain motions in solution [22].

The X-ray structures are especially important tools in structural and functional studies of SAHHs. Below is a summary of the X-ray structures of six wild types of SAHH (data available from the Protein Data Bank).

(1.) 1KY4 [20] [refined from 1B3R [19]]: structure of the rat enzyme with cofactor NAD^+ with no substrate.

(2.) 1A7A [1]: structure of the human enzyme with cofactor NADH reduced by the substrate analogue DHceA, which is oxidized to the 3'-keto form and bound to the active site. This structure is a twisted-closed form with a ~14° rotation of the AB dimer relative to the CD dimer.

(3.) 1K0U [23]: structure of the rat enzyme with bound D-eritadenine, an acyclic-sugar analog of Ado, with the cofactor in the NAD^+ state.

(4.) 1LI4 [16]: structure of the human enzyme with bound oxidized 3'-keto-NepA, an analogue of the intermediate 4',5'–didehydro-5'-deoxy-3'-ketoAdo, and with the cofactor in the NADH state.

(5.) 1XBE (unpublished data, Dr.s Q.-S. Li and Huang W.): structure of the *Trypanosoma cruzi* enzyme bound to oxidized 3'-keto-NepA, an analogue of the intermediate 4', 5'–didehydro-5'-deoxy-3'-ketoAdo, and with the cofactor in the NADH state.

(6.) 1V8B [24]: structure of the *Plasmodium falciparum* enzyme complexed to the substrate Ado and the cofactor NAD^+.

The nature of the residues involved in substrate and cofactor binding are crucial for understanding the catalytic mechanism of SAHH and to help design inhibitors. These residues could be identified from the above available high-resolution crystal structures; the importance of some of them has already been verified by mutagenesis. Figure 1.3. (a and b) shows the position of the residues (E156, N181, K186, D190, N191, N80, D134 and F302) involved in binding the

A

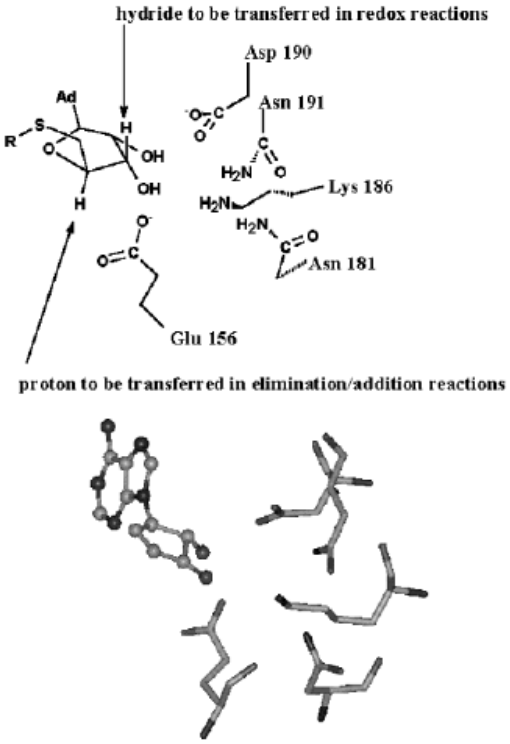

B

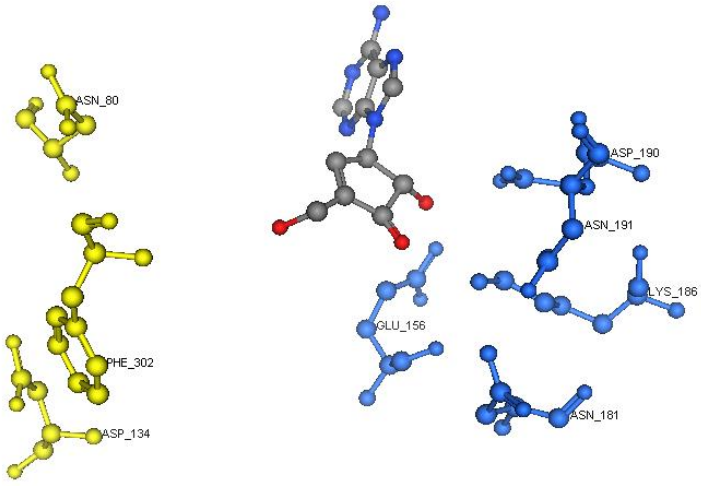

Figure 1.3. (a) The residues involved in substrate binding. (Adopted from Elrod, et al. 2002 [25]); (b) The residues involved in Hcy binding (N80, D134, F302) are shown in yellow. (Created by Molecular Operation Environment)

substrate AdoHcy and the position of other residues located in active site. Table 1.1 in the Appendix lists all known mutations of SAHH from human and rat sources including residues involved in catalysis (Redox), hinge bending, cofactor binding and substrate binding (adenine/ribose/ Hcy).

1.3.1.1. The Rossmann motif and α- helix 18 of SAHH

There are two important sub-structures of SAHH, the Rossmann motif fold and a helix at the C-terminal tail, which are involved in cofactor binding. An introduction to these two sub-structures is given briefly below. Detailed studies of the roles of these two structures in cofactor association with and dissociation from SAHH are described in Chapters 3 and 4.

The Rossmann motif (Fig. 1.4.) can be found in most classical nicotinamide adenine dinucleotide (NAD^+) binding proteins [26]. Its βαβαβ unit associated with an additional β strand forms a "core", the minimum secondary necessary structure to bind the cofactor in this motif [27]. In addition, the first 30-35 amino acids of the "core" are a fingerprint region for the identification of dinucleotide binding. There are several conserved characteristics within this fingerprint sequence: 1) a six residue glycine-rich sequence (GXGXXG) involved in phosphate binding; 2) six conserved positions only containing hydrophobic amino acids; 3) a conserved negatively charged residue and 4) a conserved positively charged residue [26]. Specifically, the

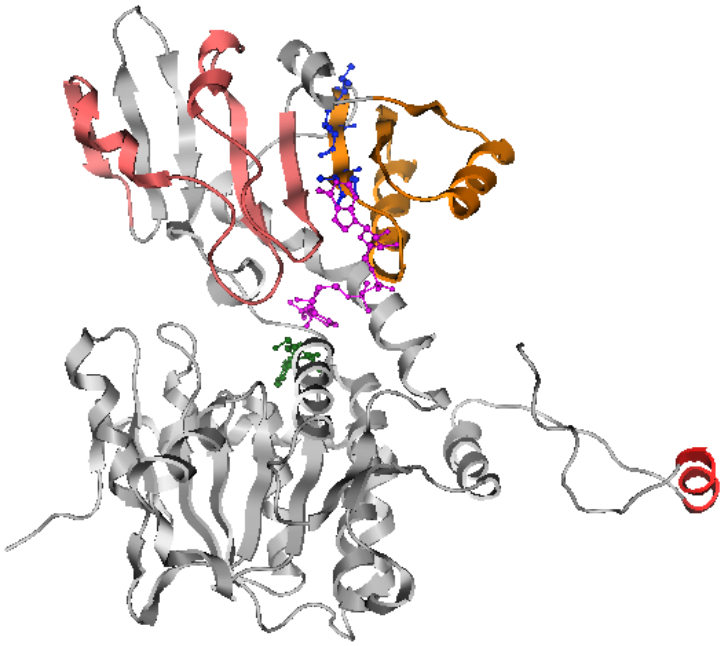

Figure 1.4. Rossmann motif in the cofactor-binding domain of Hs-SAHH (pdb: 1LI4) contains two βαβαβ units (one is brown, one is pink). (Created by Molecular Operation Environment)

six conserved hydrophobic residues are located on the first β-sheet, the first α-helix and the second β-sheet, which form a hydrophobic core and are crucial to pack the β-sheets against the α-helix in crucial secondary structure interactions [27]. Moreover, a second repeated βαβαβ unit, related to the first one by a two-fold rotation, can usually be found in $NAD(P)^+$ binding proteins [27].

There are two classical Rossmann motifs seen in each subunit of SAHH (Fig. 1.4.): one in the substrate-binding domain and the other in the cofactor-binding domain. The Rossmann motif in the NAD^+ binding domain has a second repeated βαβαβ unit. Alignment of the fingerprint sequences (first 30-35 amino acids) of the Rossmann motif in the NAD^+-binding domain of human and parasitic SAHHs reveals that the two small conserved hydrophobic residues on the first β-sheet of the Rossmann motif are conserved in Hs-SAHH and Pf-SAHH, but replaced by two hydrophilic residues in Tc-SAHH and Ld-SAHH. The replacement of the hydrophobic residues by two hydrophilic residues may weaken the hydrophobic interactions and increase the flexibility of the hydrophobic core formed by the six hydrophobic residues and other residues, which further influences NAD^+ binding and dissociation.

The C-terminal tail of SAHH is a flexible structure. The tail includes a short helix - 18 (Fig. 1.5.), located 8 amino acid residues ahead of the last Lys among Hs-

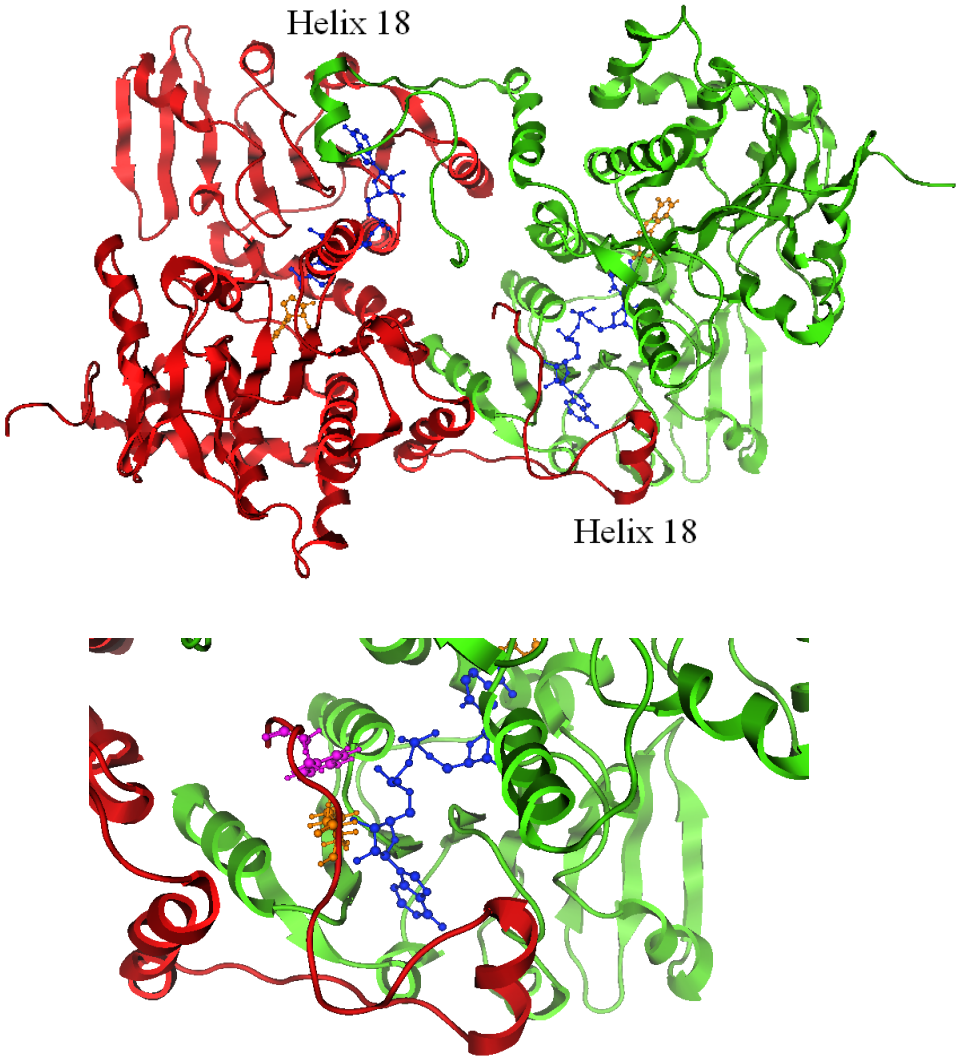

Figure 1.5. Top: The structure and position of helix 18 from the X-ray structure of Hs-SAHH (pdb: 1A7A). The helix 18 located on the C-terminal tail is close to the cofactor NAD(H) (blue) of the neighboring subunit. Bottom: Lys426 (yellow) and Tyr430 (purple) are on the end of the tail, which is involved in direct interaction with the cofactor NAD(H) (blue). (Created by Molecular Operation Environment)

SAHH and parasitic SAHHs (Tc-SAHH, Ld-SAHH and Pf-SAHH). The residues Lys^{426} and Tyr^{430} in the C-terminal loop of Hs-SAHH are observed close to NAD^+ in X-ray structures, and may form hydrogen bonds with NAD^+. A stable helix 18 may help to locate residues Lys^{426} and Tyr^{430} at suitable positions in the NAD^+ binding pocket. Therefore, the relative stability of helix 18 is important for determining the differences in cofactor-binding affinity between human and parasitic enzymes.

1.3.1.2. Subunit interactions

Inter-subunit binding may be involved in understanding such mechanistic features as active-site "sealing" (see above on the dimer-dimer rotation) and also cooperative phenomena that may be important in enzyme function (see Chapter 2 for cooperativity in the kinetics of cofactor association). It has been reported that K426 of Hs-SAHH, which is located on the C-terminal tail, is a residue involved in subunit binding. The mutant K426A of Hs-SAHH lost almost 100 % catalytic activity in both the synthetic and hydrolytic direction. This mutant retains only 48 % of its tetrameric structure. Its cofactor binding affinity also decreased dramatically (NAD^+ content of purified coenzyme is only 9 % while NADH content of purified coenzyme is 28 %) [28].

Moreover, there are several residues in the hinge region 2 whose mutations also perturb the quaternary structure, such as H353F, F356A, T363A, T363P (Dr. M.

Wang-dissertation). In addition, previous data of Dr. X. Yang (unpublished) shows that the binding of NAD^+ to Hs-SAHH exhibits some positive cooperativity and may be fit to a two-site model. However, there is no suggestion from the crystallographic structures to explain the dimer-dimer cooperativity, since SAHH is homotetramer and the dimers AB and CD do not exhibit any structural differences [1].

1.3.1.3. Isoforms of SAHH

A random investigation of red blood cell samples from a hospital laboratory was performed and several polymorphic isoforms named SAHH-1 to 4 were identified by horizontal starch gel electrophoresis [29]. SAHH-1 (SAHH; EC 3.3.1.1.) in this study is the wild type form encoded by *Homo sapiens* [1]. Functional analysis shows that isoforms SAHH-2 and SAHH-3 exhibit more than 94 % catalytic activity of the wild type SAHH-1 and their kinetic parameters are very similar to that of the wild type enzyme [30]. Tracing the genetic background, a single nucleotide polymorphism (SNP) results in one amino acid change in isoform SAHH-2 (nucleotide C112_T; amino acid R38W) and isoform SAHH-3 (nucleotide G377_A; amino acid G123R) [30]. However, isoform SAHH-4 exhibits no change at the gene level. Possible explanations for the difference between properties of SAHH-1 and SAHH-4 might be some unknown posttranslational modifications [30]. Moreover, individuals with isoform SAHH do not report having any clinical symptoms such as SAHH deficiency or high levels of plasma AdoHcy [29].

1.3.2. The structure of Tc-SAHH

The SAHH of *Trypanosoma cruzi* (437 aa and ~ 48 kDa per subunit) was cloned and purified by former scientists in our laboratory [11]. The sequence of Tc-SHAH shares 74 % identity with Hs-SAHH [11]. The X-ray structure of Tc-SAHH treated with the inhibitor Neplanocin A has been recently determined (unpublished data, Drs. Q.-S. Li and W. Huang). Comparison of the X-ray structures of Hs-SAHH and Tc-SAHH shows that there is no significant difference between them at the structural levels of the tetramer, subunit, CBD, SBD and C-terminal tail. The residues directly interacting with the substrate and the residues directly interacting with NAD^+ are all conserved. However it was reported that parasitic enzymes such as Tc-SAHH [11], Ld-SAHH [10] and Pf-SAHH bound cofactor NAD^+ less tightly than Hs-SAHH (unpublished data, S. Cai), which suggests that there are some structural factors causing the differences in properties between Hs-SAHH and parasite enzymes.

1.4. The catalytic mechanism of SAHH

SAHH is a hydrolase for which the catalytic mechanism was the topic of intense earlier studies. Briefly, the catalytic reaction of SAHH for human and parasite is the reversible hydrolysis and synthesis of AdoHcy to/from Ado and Hcy.

$$\text{AdoHcy} + H_2O \rightleftharpoons \text{Ado} + \text{Hcy}$$

This equilibrium favors the hydrolytic direction *in vivo* because of rapid removal of products - Ado catalyzed by Ado deaminase and Hcy by the transsulfuration pathway. In contrast, this equilibrium favors the synthetic direction in the biochemical assays *in vitro* [1].

The total catalytic process can be divided into two independent parts: a reduction/oxidization portion and an elimination/addition part, which is shown as a cycle in Scheme 1.2. [16, 31, 32]. The redox part utilizes a tightly bound NAD^+/NADH as a cofactor for hydrogen transfer. In the hydrolysis direction, the 3'-OH group of substrate AdoHcy transfers hydrogen to NAD^+, which forms 3'-keto-AdoHcy and NADH. The 3'-keto-AdoHcy makes its 4'-CH bond susceptible to attack and activates elimination of Hcy from the 4'-CH bond, followed by Michael addition of water to form 3'-keto-Ado. Tightly bound NADH returns hydrogen to 3'-keto-Ado and this catalytic process is completed with Ado released from the SAHH containing the cofactor NAD^+.

This catalytic cycle involves in two enzyme conformational changes (Protein Data Bank code 1A7A) [1, 21]: an open-closed interconversion of each monomer, which regulates substrate binding and product release, and a ~14° rotation of one dimer relative to the second dimer, which leads to a reduction in the volume of

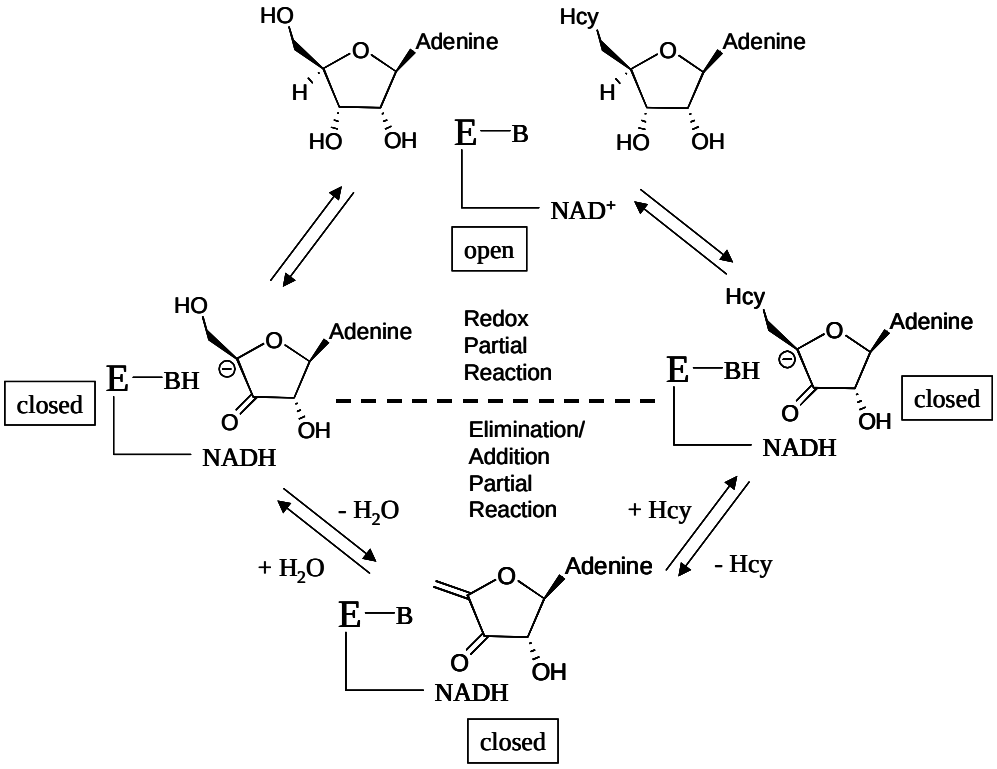

Scheme 1.2. Catalytic cycle of SAHH in both hydrolytic and synthetic directions with redox partial reactions and elimination/addition partial reaction. Shown B represents the enzyme accepting and returning the proton at the 4' position. SAHH with NAD^+ stay in an open conformation while SAHH with NADH stay in a closed conformation for a series of catalytic reactions.

the tetramer and may serve to “seal” the closed form. The “sealed” active sites help to prevent contact of intermediates with the environment during a series of transition states [21, 33].

The kinetics of individual steps in the SAHH catalytic cycle have been measured and a model suggested that integrates the kinetics, the structural and dynamic results, and the findings from site-directed mutagenesis [16]. The model emphasizes the roles of avoidance of abortive reactions and stabilization of transition states in achieving efficient level of catalysis [16, 34-36]. There are three 3’-keto intermediates in the catalytic cycle and none of them can survive exposure to the aqueous buffer environment [16].

Any release and/or exposure of intermediates will result in abortive products and an uncompleted catalytic cycle. Instead, a tight closure of the active site builds a barrier of 110 kJ/mol for abortive release of intermediates, which is ~ 50 kJ/mol higher than diffusional limits and decreases the rate of abortive release by 10^8-10^9 fold when the concentrations of AdoHcy, Ado and Hcy are at 1 μM [16]. In addition, the central intermediate 4’, 5’-didehydro-5’-deoxy-3’-keto-adenosine also needs to be protected from the nearby cofactor NADH to avoid premature reduction of the 3’-keto group of the intermediate [16]. This 3’-keto structure of the central intermediate is crucial for activation of the next step of Michael addition of water/Hcy to the 4’,5’-double bond. To achieve the necessary protection, residue His 301 shifts its position

so that its side chain buttresses the cofactor NADH at a greater separation from the intermediate. The result is an apparent increase in distance between C-4' (cofactor NADH) and C-3' (substrate) of about 0.4 Å [16]. The barrier for the abortive reduction of the central intermediate is 86-89 kJ/mol, which is 22-24 kJ/mol higher than the barrier for productive reduction (65-67 kJ/mol). This difference in barrier heights results in a rate of productive reduction that is faster by 10^3-10^4 fold than the rate of abortive reduction [16]. The catalysis of most steps in the reaction depends on acid-base catalysis for transition-state stabilization, so that the potentially needed exchange of protons with the medium would seem to be difficult in the closed conformation. However, SAHH depends on a chain of water molecules to deliver protons between the active site and the buffer environment to maintain the suitable protonation states of functional residues during the catalytic cycle [16].

Many attempts have been made to design mechanism-based inhibitors targeting the substrate binding site and utilizing its catalytic potentialities, and some progress has been achieved [1, 2, 37]. The partial "oxidative" reaction (reduction/oxidation) and partial "hydrolytic" (elimination/addition) reaction provide two design targets [37]. Type I inactivators, which are oxidized to the 3'-keto form with SAHH catalysis and conversion of NAD^+ to NADH, target the oxidative partial reaction [38]. Neplanocin A (NepA) with K_i of 8.4 nM is an example of type I inactivators and its catalytic reaction stops after oxidation at the 3' position produces a material that is structurally an analogue of the central intermediate 4', 5'-didehydro-

5’-deoxy-3’-keto-adenosine [1, 39]. On the other hand, type II inactivators are not only oxidized in the 3’-position by SAHH but also form covalent bonds with enzyme in reactions analogous to the elimination/addition partial reaction [38]. For example, (E)-5’, 6’-didehydro-6’-deoxy-6’fluorohomoadenosine (EDDFHA) is a type II inactivator by generating electrophiles at the active site and forming a covalent bond to irreversibly inactivate the enzyme [40]. Figure 1.6. shows the structures of the above two types of inhibitors and their inactivation mechanisms.

The question of approaches to drug design will be treated further in Chapter 6 of this study.

1.5. Scope of this dissertation

Major studies of the structure, function and catalytic mechanism of SAHH have been performed over the past decades. This has built the foundation for the new research and forms the basis of this work which involves the comparison of the properties between human and parasitic SAHHs. This is aimed at developing effective antiparasitic medicines against serious human diseases. Tc-SAHH, which was cloned, purified and crystallographically analyzed in our laboratory, is the object of my study which is to identify distinguishing features between Hs-SAHH and parasitic enzymes by use of biochemical, biophysical and computational approaches. The results are intended to lead to the design of selective inhibitors against Tc-SAHH

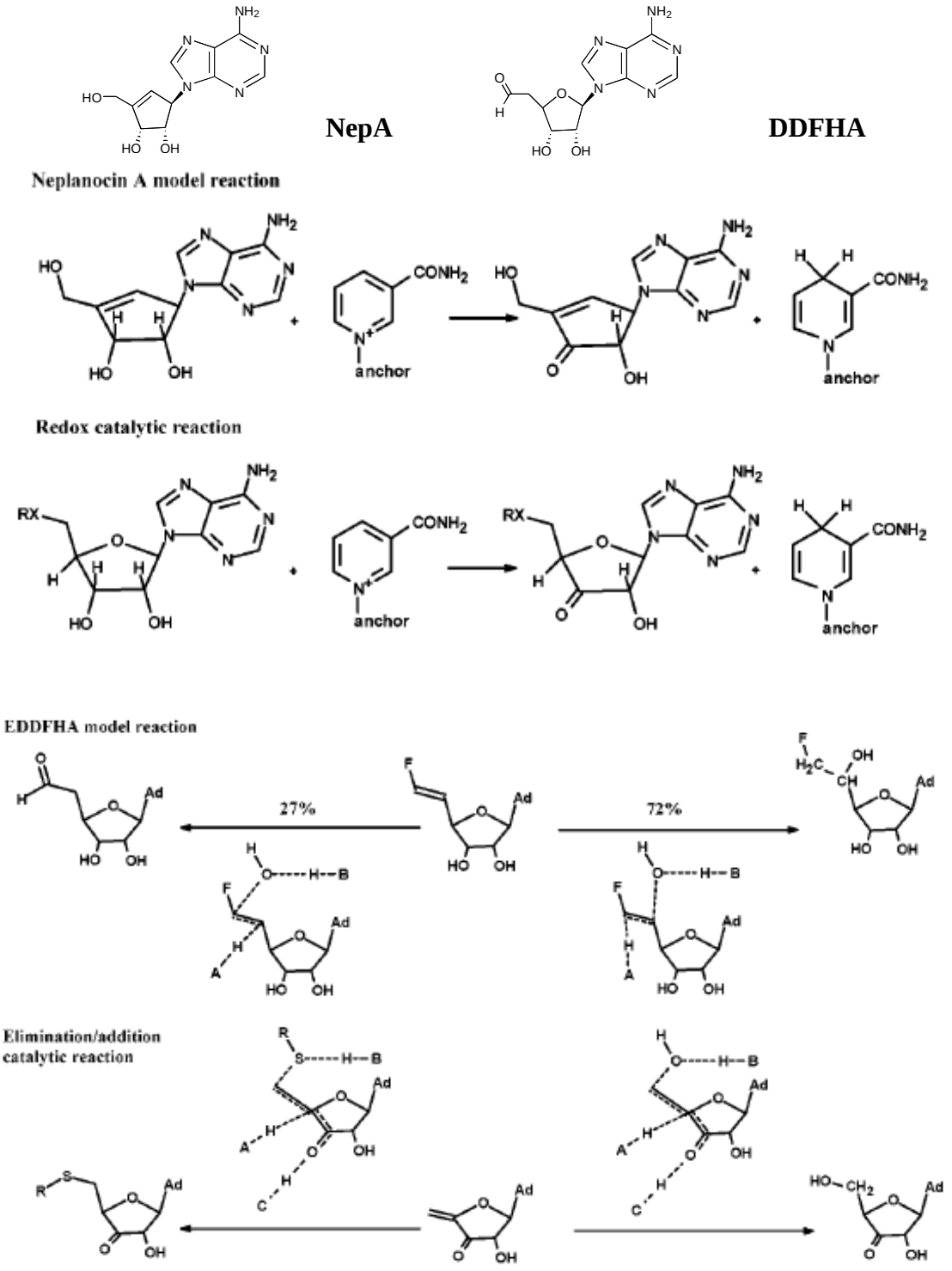

Figure 1.6. Type I inhibitor (NepA) and Type II inhibitor (EDDFHA) structure and its inactivation mechanism (adopted from Elrod, et al. 2002 [25]).

as anti-parasitic agents at the traditional substrate binding site or new targeting sites (e.g. cofactor binding site). Furthermore, this work includes kinetics, and mechanistic studies of a selective compound, which deepens our understanding of selective inhibition against Tc-SAHH.

Summary of the Contents in this Dissertation:

In this chapter, the structures and functions (biological role and catalytic mechanism) of Hs-SAHH and Tc-SAHH are reviewed. In Chapter 2, the basic features of association and dissociation of cofactor NAD(H) to Hs-SAHH and Tc-SAHH are described. Chapters 3 and 4 include studies on the role of the stability of helix 18 and the role of two conserved hydrophobic residues on the first β-sheet of the Rossmann motif of the cofactor-binding domain in the differential cofactor-binding features of Hs-SAHH and Tc-SAHH, respectively. In Chapter 5, computational alanine scanning is performed to predict the residues important for the differential cofactor-binding features of Hs-SAHH and Tc-SAHH and experimental mutagenesis is carried out to test two predicted residues (a Lys and a Tyr on the C-terminal tail). In Chapter 6, the kinetics and inactivation mechanism of ribavirin, a selective inhibitor which is structurally similar to adenosine, were studied for a traditional targeting site in the substrate binding domain. Conclusions and limitations are described in Chapter 7.

1.6. References:

1. Turner, M.A., et al., *Structure and function of S-adenosylhomocysteine hydrolase.* Cell Biochem Biophys, 2000. **33**(2): p. 101-25.
2. Yin, D., et al., *Mechanism-based S-adenosyl-L-homocysteine hydrolase inhibitors in the search for broad-spectrum antiviral agents.* Biomedical Chemistry: Applying Chemical Principles to the Understanding and Treatment of Disease (P.F. Torrence, Ed.), John Wiley & Sons, Inc., New York, 2000: p. 41-71.
3. Chiang, P.K., *Biological effects of inhibitors of S-adenosylhomocysteine hydrolase.* Pharmacol Ther, 1998. **77**(2): p. 115-34.
4. De Clercq, E., *Carbocyclic adenosine analogues as S-adenosylhomocysteine hydrolase inhibitors and antiviral agents: recent advances.* Nucleosides Nucleotides, 1998. **17**(1-3): p. 625-34.
5. Robins, M.J., et al., *Inactivation of S-adenosyl-L-homocysteine hydrolase and antiviral activity with 5',5',6',6'-tetradehydro-6'-deoxy-6'-halohomoadenosine analogues (4'-haloacetylene analogues derived from adenosine).* J Med Chem, 1998. **41**(20): p. 3857-64.
6. Schnyder, G., et al., *Decreased rate of coronary restenosis after lowering of plasma homocysteine levels.* N Engl J Med., 2001. **345**(22): p. 1593-600.
7. Ashfield-Watt, P.A., et al., *Folate, homocysteine, endothelial function and cardiovascular disease. What is the link?* Biomed Pharmacother., 2001. **55**(8): p. 425-33.

8. Ueland, P.M., H. Refsum, and L. Brattstrom, *Plasma homocysteine and cardicascular disease.* Arteriosclerotic Cardiovascular Disease, Hemostasis and Endothelial Function (Francis, R.B., Jr., Ed.), Marcel Dekker, New York, 1992: p. 183-196.

9. Kruman, I.I., et al., *Folic acid deficiency and homocysteine impair DNA repair in hippocampal neurons and sensitize them to amyloid toxicity in experimental models of Alzheimer's disease.* J Neurosci. , 2002. **22**(5): p. 1752-62.

10. Yang, X. and R.T. Borchardt, *Overexpression, purification, and characterization of S-adenosylhomocysteine hydrolase from Leishmania donovani.* Arch Biochem Biophys, 2000. **383**(2): p. 272-80.

11. Parker, N.B., et al., *Trypanosoma cruzi: molecular cloning and characterization of the S-adenosylhomocysteine hydrolase.* Exp Parasitol, 2003. **105**(2): p. 149-58.

12. Nakanishi, M., et al., *Mutational analyses of Plasmodium falciparum and human S-adenosylhomocysteine hydrolases.* Mol Biochem Parasitol, 2005.

13. Henderson, D.M., et al., *Cloning of the gene encoding Leishmania donovani S-adenosylhomocysteine hydrolase, a potential target for antiparasitic chemotherapy.* Mol Biochem Parasitol. , 1992. **53**(1-2): p. 169-183.

14. Shuman, S., *The mRNA capping apparatus as drug target and guide to eukaryotic phylogeny.* Cold Spring Harb Symp Quant Biol. , 2001. **66**: p. 301-12.

15. Teixeira, R.A., et al., *Chagas disease.* Postgrad Med J., 2006. **82**(974): p. 788-798.

16. Yang, X., et al., *Catalytic strategy of S-adenosyl-L-homocysteine hydrolase: transition-state stabilization and the avoidance of abortive reactions.* Biochemistry, 2003. **42**(7): p. 1900-9.

17. Wang, M., et al., *Domain motions and the open-to-closed conformational transition of an enzyme: a normal mode analysis of S-adenosyl-L-homocysteine hydrolase.* Biochemistry, 2005. **44**(19): p. 7228-39.

18. Wang, M., et al., *Effects of ligand binding and oxidation on hinge-bending motions in S-adenosyl-L-homocysteine hydrolase.* Biochemistry, 2006. **45**(25): p. 7778-86.

19. Hu, Y., et al., *Crystal structure of S-adenosylhomocysteine hydrolase from rat liver.* Biochemistry, 1999. **38**(26): p. 8323-33.

20. Takata, Y., et al., *Catalytic mechanism of S-adenosylhomocysteine hydrolase. Site-directed mutagenesis of Asp-130, Lys-185, Asp-189, and Asn-190.* J Biol Chem, 2002. **277**(25): p. 22670-6.

21. Yin, D., et al., *Substrate binding stabilizes S-adenosylhomocysteine hydrolase in a closed conformation.* Biochemistry, 2000. **39**(32): p. 9811-8.

22. Hu, C., et al., *Molecular dynamics simulations of domain motions of substrate-free S-adenosyl- L-homocysteine hydrolase in solution.* Proteins, 2008. **71**(1): p. 131-43.

23. Huang, Y., et al., *Inhibition of S-adenosylhomocysteine hydrolase by acyclic sugar adenosine analogue D-eritadenine. Crystal structure of S-adenosylhomocysteine hydrolase complexed with D-eritadenine.* J Biol Chem, 2002. **277**(9): p. 7477-82.

24. Tanaka, N., et al., *Crystal structure of S-adenosyl-L-homocysteine hydrolase from the human malaria parasite Plasmodium falciparum.* J Mol Biol, 2004. **343**(4): p. 1007-17.

25. Elrod, P., et al., *Contributions of active site residues to the partial and overall catalytic activities of human S-adenosylhomocysteine hydrolase.* Biochemistry, 2002. **41**(25): p. 8134-42.

26. Rossmann, M.G., et al., *Evolutionary and structural relationships among dehydrogenases.* . The Enzymes, 3rd edn (Boyer, P. D., ed.) Academic Press, New York., 1975. **XI**: p. 61-102.

27. Wierenga, R.K., De Maeyer, M. C. H., and Hol, W. G. J., *Interaction of pyrophosphate moieties with helixes in dinucleotide binding proteins.* Biochemistry, 1985. **24**(6).

28. Ault-Riche, D.B., C.S. Yuan, and R.T. Borchardt, *A single mutation at lysine 426 of human placental S-adenosylhomocysteine hydrolase inactivates the enzyme.* J Biol Chem, 1994. **269**(50): p. 31472-8.

29. Kloor, D., et al., *Studies of S-adenosylhomocysteine-hydrolase polymorphism in a Croatian population.* J Hum Genet., 2006. **51**(1): p. 21-4.

30. Fumić, K., et al., *Functional analysis of human S-adenosylhomocysteine hydrolase isoforms SAHH-2 and SAHH-3.* Eur J Hum Genet., 2007. **15**(3): p. 347-51.

31. J.L., P. and A. R.H., *Mechanism for enzymatic thioether formation. Mechanism of action of S-adenosylhomocysteinase.* J Biol Chem. , 1976. **251**(18): p. 5817-9.

32. J.L., P. and A. R.H., *The mechanism of action of S-adenosylhomocysteinase.* J Biol Chem. , 1979. **254**(4): p. 1217-26.

33. Hu, Y., et al., *Computational characterization of substrate binding and catalysis in S-adenosylhomocysteine hydrolase.* Biochemistry, 2001. **40**(50): p. 15143-52.

34. Porter, D.J. and F.L. Boyd, *Mechanism of bovine liver S-adenosylhomocysteine hydrolase. Steady-state and pre-steady-state kinetic analysis.* J Biol Chem, 1991. **266**(32): p. 21616-25.

35. Porter, D.J. and F.L. Boyd, *Reduced S-adenosylhomocysteine hydrolase. Kinetics and thermodynamics for binding of 3'-ketoadenosine, adenosine, and adenine.* J Biol Chem, 1992. **267**(5): p. 3205-13.

36. Porter, D.J., *S-adenosylhomocysteine hydrolase. Stereochemistry and kinetics of hydrogen transfer.* J Biol Chem, 1993. **268**(1): p. 66-73.

37. Yuan, C.-S., et al., *Design and synthesis of S-adenosylhomocysteine hydrolase as broad-spectrum antiviral agents.* Advances in Antiviral Drug Design (E. De Clercq, Ed.), JAI press, Inc., Greenwicl, CT, 1996. **2**: p. 41-88.

38. Wolfe, M.S. and R.T. Borchardt, *S-adenosyl-L-homocysteine hydrolase as a target for antiviral chemotherapy.* J Med Chem. , 1991. **34**: p. 1521-30.

39. Borchardt, R.T., B.T. Keller, and U. Patel-Thombre, *Neplanocin A. A potent inhibitor of S-adenosylhomocysteine hydrolase and of vaccinia virus multiplication in mouse L929 cells.* J Biol Chem., 1984. **259**(7): p. 4353-8.

40. Yuan, C.S., et al., *(E)-5',6'-didehydro-6'-deoxy-6'-fluorohomoadenosine: a substrate that measures the hydrolytic activity of S-adenosylhomocysteine hydrolase.* Biochemistry, 1994. **33**(40): p. 12305-11.

Appendix: Table 1.1. Mutations of SAHH from human, rat and trypanosomal resources.

SAHH of Human or Rat Sources	Function/ Location of Mutation	Tc-SAHH	Function/ Location of Mutation
H54N-rat	catalysis		
H55A	redox		
C79A	redox		
N80S	Hcy		
D130N-rat	catalysis		
D134N	Hcy		
E155Q-rat	catalysis		
E155D-rat	catalysis		
E156A	active		
N181A	active		
K185N-rat	catalysis		
K186A	active		
D189N-rat	catalysis		
N190S-rat	catalysis		
D190A	catalysis		
N191A	active		
D244E-rat	cofactor binding		
H300N-rat			
H301A	redox		
F302G	Hcy		

SAHH of Human or Rat Sources	Function/ Location of Mutation	Tc-SAHH	Function/ Location of Mutation
D303S	Hcy		
M351P	Hinge		
H352N-rat			
H353A	Hinge		
H353F	Hinge		
P354A	Hinge		
F356A	Hinge		
T363A	Hinge		
M367A	Hinge		
K426A	Tail (Monomer)	K431A	Tail
K426E	Monomer		
K426R	Quaternary		
Y430F	Tail		
Y430A	Tail	Y435A	Tail
R431A	Tail		
Hs-18Pf-SAHH: E411D_K412N_ A414C_Y416F	Helix 18	Tc-18Hs-SAHH: A416E_R417K_ D420Q _I422L	Helix 18
Hs-18Tc-SAHH: E411A_K412R_Q415D	Helix 18		
Hs-βATc-SAHH: V215T_V217C	β sheet-A	Tc-βAHs-SAHH: T214V_C216V	β sheet-A

Chapter 2

Basic Features of the Association and Dissociation Processes in Comparative Kinetics of Cofactor Association and Dissociation for Hs-SAHH and Tc-SAHH.

2.1. Introduction

The enzymes from *T. cruzi* and *L. donovani* were reported to bound NAD^+ less tightly than the human enzyme, and the enzyme from *P. falciparum* was observed to bound NAD^+ less tightly than the human enzyme (unpublished data). Therefore, the cofactor-binding site and its properties have become a focus of interest for finding those distinguishing features among these enzymes that might permit differential inhibition. In the present work, we have systematically analyzed the comparative kinetics of cofactor association and dissociation and their temperature dependences for Hs-SAHH and Tc-SAHH.

2.2. Methods

2.2.1. Expression and purification of Hs-SAHH and Tc-SAHH.

The expression of the two enzymes was basically the same as previously described [1, 2]. Briefly, in separate experiments the gene encoding each enzyme was inserted into the vector pPROK-1 (Clonetech, CA) and the recombinant plasmids were transferred into *E. coli* strain JM109. The transformed *E. coli* cells grew in 1 L of 2×YT medium containing ampicillin (100 mg/L) at 37 ^{o}C. When the absorbance at 600 nm reached 0.4 ~ 0.8, 1 mM isopropyl-1-thio-β-D-galactopyranoside was added to induce protein expression during incubation at 37 ^{o}C for 8 h for Hs-SAHH and at 25 ^{o}C for 12 h for Tc-SAHH.

The procedures for purification of the two enzymes were the same except that 50 μM NAD^{+} was added to the buffer before purification of Tc-SAHH. The harvested *E. coli* cells containing the enzyme were stored at -80 ^{o}C. Preparation of a cell-free extract was carried out as previously described [1, 2]. The enzyme was purified from cell-free extract by means of four columns in an FPLC system (Amersham Biosciences). The buffer during all purification processes was 50 mM TrisHCl, pH 7.4, containing 1 mM EDTA. A typical procedure is as follows. The cell-free extract was loaded onto a Q-sepharose Fast Flow column (26/10) and the enzyme was eluted with 50 to 150 mM NaCl in buffer. The enzyme sample was then passed through a Hiload Phenyl-sepharose column (26/10), a Hiload superdex 200 (16/60) column, and placed on a MonoQ (10/10) column from which the purified enzyme was eluted with 50 to 300 mM NaCl in buffer.

2.2.2. Enzyme activity assay and determination of kinetic properties.

SAHH activity was assayed in the synthetic direction by measuring the rate of formation of AdoHcy from Ado and Hcy by use of HPLC as previously described [3, 4]. The enzyme activity in the hydrolytic direction was determined by coupling the conversion of AdoHcy to Ado and Hcy to the deamidation of Ado with catalysis by Ado deaminase [4].

2.2.3. Determination of apo-enzyme concentrations by titration with NAD^+.

Apo-enzyme was prepared as previously described [5]. All enzyme and apo-enzyme concentrations used in this paper are given as formal concentrations of monomeric subunit. Because NAD^+ binds to both Hs-SAHH and Tc-SAHH very tightly at 22 ^oC (K_d below 50 nM at 22 ^oC for both enzymes), the concentration of apo-enzyme can be determined by NAD^+ titration. To a volume of 10 μl containing initially 40 μM of apo-enzyme were added successive 10-μl portions of NAD^+ stock solution to produce concentrations from 1.5 to 180 μM. The solutions were then incubated at 22 ^oC till no further increase was observed in enzyme activity (usually from 20 to 90 min). Enzyme activity was measured in the hydrolytic direction. Concentrations of NAD^+ were increased to approximately 9 times the saturation value and the enzyme concentration (monomers) was taken as equal to the concentration of

enzyme-bound NAD^+ under saturation conditions. At values of $[NAD^+]$ below the equivalence point, the activity is equal to $\gamma[NAD^+]$, where γ is the activity per occupied active site and is equal to the slope of the plot of activity vs. $[NAD^+]$. Above the equivalence point, the slope becomes zero and the intercept becomes $\gamma[E]_{tot} = \gamma [NAD^+]_{bound}$ where $[E]_{tot}$ is the total enzyme concentration expressed as monomers. The ratio intercept/slope thus yields $[E]_{tot} = [NAD^+]_{bound}$. The values of $[E]_{tot}$ corresponded closely to the values calculated from the protein concentration.

2.2.4. Determination of rate constants for association of NAD^+ and NADH with apo-enzyme (apparent first-order rate constant k_{app} and apparent second-order rate constant k_{on}).

Typically, to a 50 μl solution (50 mM phosphate buffer, pH 7.4, 1 mM EDTA) containing 2 μM apo-enzyme were added successive portions of 50 μl of stock solution to produce concentrations of NAD^+ from 1 to 300 μM. Samples were taken for activity assay at measured times during incubation at the desired temperature. The measured activities A were either converted to the amount of enzyme: NAD^+ complex or used directly in eq. 1.

$$A = A_f - (A_f - A_o)[\exp(-k_{app}t)] \qquad (1)$$

Here, A is the activity measured at time t, A_o is the activity at the apparent time zero (reflecting reaction during the dead-time of the experiment), A_f is the activity at the end of the experiment, and k_{app} is a first-order rate constant for association that

generally will be a function of [NAD^+]. At [NAD^+] = 5 μM, A_o is quite small and k_{app} is approximately proportional to [NAD^+]; an apparent second-order rate constant for the association reaction k_{on} was therefore calculated from data at this concentration as $k_{on} = k_{app}/[NAD^+]$ and was used in the calculation of the equilibrium dissociation constant (see below).

In the measurement of k_{app} for NADH, the bound NADH was monitored by a fluorescence method as previously described [3].

2.2.5. Determination of the rate constants for dissociation of NAD^+ from Hs-SAHH and Tc-SAHH (k_{off}).

A 200 μL solution containing 4 μM SAHH, 80 U/ml alcohol dehydrogenase, 30 mM 2-propanol, 2 mM NADH and 1 mM EDTA in a 50 mM phosphate buffer at pH 7.4 was incubated at a desired temperature. Samples were taken at measured times for determination of enzyme activity. The concentration of NADH, binding of which to the enzyme rendered the dissociation of NAD^+ irreversible, was in large excess over the enzyme concentration and did not significantly change during the experiments. As a control for thermal inactivation of the enzyme, the activity of SAHH was also determined under the same conditions as above except that no NADH or alcohol dehydrogenase was present. The time dependence of relative

enzyme activity (A/A_o) in both the dissociation experiment and the thermal inactivation control fitted to eq (2), which is equivalent to eq (1) with $A_f = 0$.

$$A/A_o = \exp(-k_{obs}\, t) \qquad (2)$$

In the control experiment for loss of activity by thermal inactivation, $k_{obs} = k_{ina}$, the first-order rate constant for thermal inactivation of the enzyme. When thermal inactivation and NAD^+ dissociation were occurring simultaneously, $k_{obs} = k_{tot} = k_{ina} + k_{off}$, where k_{off} is the apparent first-order rate constant for dissociation of NAD^+. The rate constant k_{off} for NAD^+ dissociation was then obtained from $k_{off} = k_{tot} - k_{ina}$.

2.2.6. Thermal stability determinations by circular dichroism (CD) spectroscopy.

CD spectra were measured with a Jasco J-720 spectropolarimeter equipped with a Peltier temperature controller. Enzyme samples (0.1 mg/mL in 50 mM phosphate buffer, pH 7.4 and 1 mM EDTA) were contained in 0.1 cm path length cells. A resolution of 0.2 nm and a scanning speed of 20 nm/min with a 2 s response time were employed. Spectra presented are an average of three consecutive spectra. For the thermal stability experiment, the signal at 222 nm was measured at 0.1 °C intervals with use of a 60 °C/hour temperature ramp rate.

2.2.7. Thermal stability measurements by differential scanning calorimetry (DSC).

Apo-enzyme samples (2 mg/mL) were degassed under mild vacuum for 15 minutes before obtaining thermograms with a Microcal DSC instrument (Northampton, MA). A 0.9 ml solution of buffer containing 50 mM phosphate and 1 mM EDTA, pH 7.4, was placed in the reference cell and the apo-enzyme sample in the same buffer was placed in the sample cell. Thermograms from 25 to 80 °C were collected at a scan rate of 60 °C/hr. Similar scans obtained with buffer in both the reference and sample cells were subtracted from the apo-enzyme thermograms.

2.2.8. Determination of the equilibrium dissociation constants (K_d) for NAD^+ and NADH.

The equilibrium dissociation constants for NAD^+ were calculated from the ratio of the dissociation and association rate constants, $K_d^{NAD+} = k_{off}/k_{on}$, which were measured as described above.

The equilibrium dissociation constants for NADH were calculated from the loss of enzyme activity as NADH replaces NAD^+ in the enzyme active sites. In the absence of added NADH, the activity of the enzyme will be proportional to the fraction of enzyme associated with NAD^+ as in eq (3)

$$A([NADH] = 0) = \alpha E_{tot}[[NAD^+]/(K_d^{NAD+} + [NAD^+])] \quad (3)$$

where α is a known function of the enzyme kinetics (for the hydrolytic direction of SAHH action, α is proportional to $k_{cat}[AdoHcy]/(K_M + [AdoHcy])$ and $[E_{tot}]$ is the total concentration of enzyme in all forms (E and $E:NAD^+$). In the presence of NADH, the activity A is proportional to a total enzyme concentration given by eq (4a),

$$[E_{tot}] = [E] + [E:NAD^+] + [E:NADH] =$$

$$[E:NAD^+](K_d^{NAD+}/[NAD^+] + 1 + K_d^{NAD+}[NADH]/K_d^{NADH}[NAD^+]) \quad (4a)$$

so that the activity is given by eq (4b).

$$A = \alpha[E_{tot}] / (K_d^{NAD+}/[NAD^+] + 1 + K_d^{NAD+}[NADH]/K_d^{NADH}[NAD^+]) \quad (4b)$$

Combining eqs 3 and 4b then gives eq (5):

$$A([NADH] = 0)/A = 1 + ([NADH]/K_d^{NADH})(K_d^{NAD+}/(K_d^{NAD+} + [NAD^+])) \quad (5)$$

Because K_d^{NAD+} is known, non-linear least-squares fitting (Origin, Microcal) of A as a function of [NADH] to eq (5) then yields K_d^{NADH}.

2.2.9. Inhibition of Hs-SAHH and Tc-SAHH by the NAD(H) analogs, S-NAD^+ and S-NADH.

Thionicotinamide adenine dinucleotide (S-NAD^+) was obtained from Sigma (T7375). The reduced form of thionicotinamide adenine dinucleotide (S-NADH) was prepared from the oxidized form by use of alcohol dehydrogenase (Sigma, A-3263).

Reduction of the oxidized form of S-NAD^+ was followed by HPLC using the procedure described under enzyme activity assay. Loss of activity of Hs-SAHH and Tc-SAHH was monitored as above, and equilibrium dissociation constants of the thione-analogs S-NAD^+ and S-NADH were calculated by the same method used for NADH. To determine k_{off} for S-NAD^+ and S-NADH, 20 μL volumes of solutions of Hs-SAHH or Tc-SAHH reconstituted with S-NAD^+ and S-NADH (and thus catalytically inactive) were incubated in the presence of 5 mM NAD^+ at 37 °C. Samples were taken at desired times and the activity was measured. The fractional gain in activity with time was taken as equal to the fractional release of S-NAD^+ or S-NADH.

2.3. Results

2.3.1. Kinetics of the dissociation of NAD^+ from Hs-SAHH and Tc-SAHH.

Fig. 2.1. shows the loss of fractional activity as a function of time as NAD^+ dissociates from Hs-SAHH and Tc-SAHH. The data are described by a simple single-exponential function (eq 2) and after correction for thermal inactivation (negligible under these circumstances) yield the dissociation constant k_{off}.

2.3.2. Temperature dependence of the kinetics of the dissociation of NAD^+ from Tc-SAHH and Hs-SAHH.

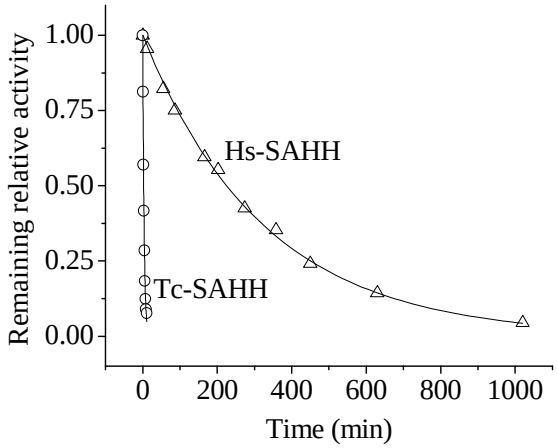

Figure 2.1. The time course of the loss in enzyme activity at 37 °C as NAD^+ dissociates from Hs-SAHH (shallow curve, $k_{obs} = k_{off} = 5.1 \pm 0.1 \times 10^{-5}\ s^{-1}$) and Tc-SAHH (steep curve, $k_{obs} = k_{off} = 4.7 \pm 0.1 \times 10^{-3}\ s^{-1}$). The solid lines are exponential functions (eq (2) above).

Fig. 2.2. presents Eyring plots of the first-order rate constants k_{off} for dissociation of the cofactor NAD^+ from Hs-SAHH (31 °C to 45.5 °C) and from Tc-SAHH (21 °C to 37 °C). The Eyring plots are non-linear for both enzymes, consisting of a linear low-temperature regime and a linear high-temperature regime. Two expressions [(eqs (6a) and (6b)] were considered for fitting of the data, corresponding to mechanistic models treated in the Discussion Section.

$$k_{off} / (kT/h) = \exp (\Delta S^{\ddagger}_{\ell} / R - \Delta H^{\ddagger}_{\ell} / RT) + \exp (\Delta S^{\ddagger}_{h} / R - \Delta H^{\ddagger}_{h} / RT) \qquad (6a)$$

$$k_{off} / (kT/h) = [\exp(\Delta S^{\ddagger}_{\ell} / R - \Delta H^{\ddagger}_{\ell} / RT)](1/\{1 + [\exp(\Delta S^{o}_{\ell h} / R) - \Delta H^{o}_{\ell h} / RT]\}) + [\exp (\Delta S^{\ddagger}_{h} / R) - \Delta H^{\ddagger}_{h} /RT)]([\exp(\Delta S^{o}_{\ell h} / R) - \Delta H^{o}_{\ell h} / RT]/\{1 + [\exp(\Delta S^{o}_{\ell h} / R - \Delta H^{o}_{\ell h} / RT)]\}) \qquad (6b)$$

The expression of eq (6a), where the subscript ℓ denotes the quasi-thermodynamic parameters of activation for the low-temperature regime and the subscript h denotes those for the high-temperature regime, corresponds to parallel dissociation reactions with different activation parameters. Attempts to fit this expression to the data produced very large errors in the adjustable parameters and plots that failed to intersect some of the points. This expression produces curvature that is too gentle to correspond to all the data.

The expression of eq (6b) allows for a more abrupt shift from the low-temperature to the high-temperature regime in a transition with equilibrium thermodynamic parameters $\Delta S^{o}_{\ell h}$ and $\Delta H^{o}_{\ell h}$. This approach requires determination of

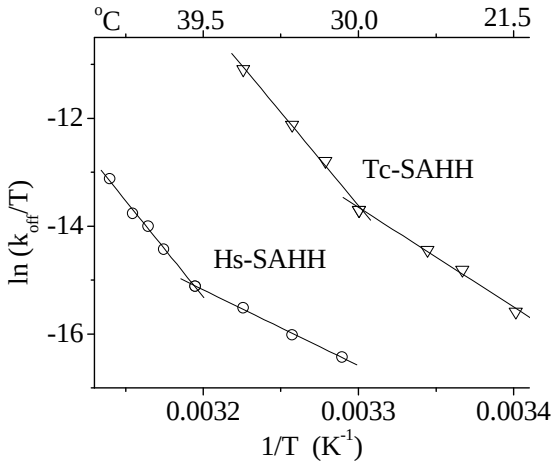

Figure 2.2. The temperature dependence of the rate constant for dissociation of NAD^{+} from Hs-SAHH (lower curve) and from Tc-SAHH (upper curve). The lines are intersecting Eyring plots with the parameters given in Table 2.1.

six adjustable parameters. Since the data sets contain only seven (Tc-SAHH) and eight (Hs-SAHH) experimental points, the full-scale fitting exercise is futile. Therefore the two temperature regimes were independently fitted to an Eyring expression [eqs (6c) and (6d)] for each set of data.

$$k_{off} / (kT/h) = \exp (\Delta S^{\ddagger}_{\ell} / R - \Delta H^{\ddagger}_{\ell} / RT) \qquad (6c)$$

$$k_{off} / (kT/h) = \exp (\Delta S^{\ddagger}_{h} / R - \Delta H^{\ddagger}_{h} / RT) \qquad (6d)$$

The values of the quasi-thermodynamic parameters of activation are given in Table 2.1.The conversion temperature T_o for passage from the low-temperature regime to the high-temperature regime is given by eq (7) and values are given in Table 2.1.

$$T_o = (\Delta H^{\ddagger}_{h} - \Delta H^{\ddagger}_{\ell}) / (\Delta S^{\ddagger}_{h} - \Delta S^{\ddagger}_{\ell}) \qquad (7)$$

2.3.3. Kinetics of the association of NAD^+ with Tc-SAHH and Hs-SAHH.

In contrast to the simple first-order reaction of cofactor dissociation, the association of NAD^+ with rat-liver SAHH has been reported [5] to exhibit biphasic kinetics, with half of the full complement of the cofactor binding during the dead-time of the experiment and the other half binding over about an hour (concentrations of apo-enzyme 15.9 μM and NAD^+ 185-555 μM). Fig. 2.3. shows the association kinetics for Tc-SAHH and Hs-SAHH for 1 μM apo-enzyme (as monomers) reacting

with 1-100 μM NAD^+ (further experiments, not shown, extended the range of [NAD^+] to 300 μM). Both enzymes exhibit first-order kinetics of cofactor association at all

Table 2.1. Quasi-thermodynamic parameters of activation and conversion temperatures [a, b] for NAD^+ dissociation from Hs-SAHH (30 °C to 37 °C) and Tc-SAHH (20 °C to 37 °C), pH 7.4.

Enzyme	$\Delta S^{\ddagger}_{\ell}$ (J/mol-K)	$\Delta H^{\ddagger}_{\ell}$ (kJ/mol)	$\Delta S^{\ddagger}_{h}$ (J/mol-K)	$\Delta H^{\ddagger}_{h}$ (kJ/mol)	T_o, K
Hs-SAHH	24 ± 1	116 ± 4	600 ± 25	297 ± 9	314 ± 21 (41 °C)
Tc-SAHH	170 ± 15	154 ± 8	610 ± 30	287 ± 8	302 ± 34 (29 °C)

[a] *Values in the table above obtained from fits to eqs (6) and (7) of the data shown in Fig. 2.2.*

[b] *Temperature of intersection of the high-temperature and low-temperature limbs of the temperature dependence and thus the temperature of conversion between the two regimes.*

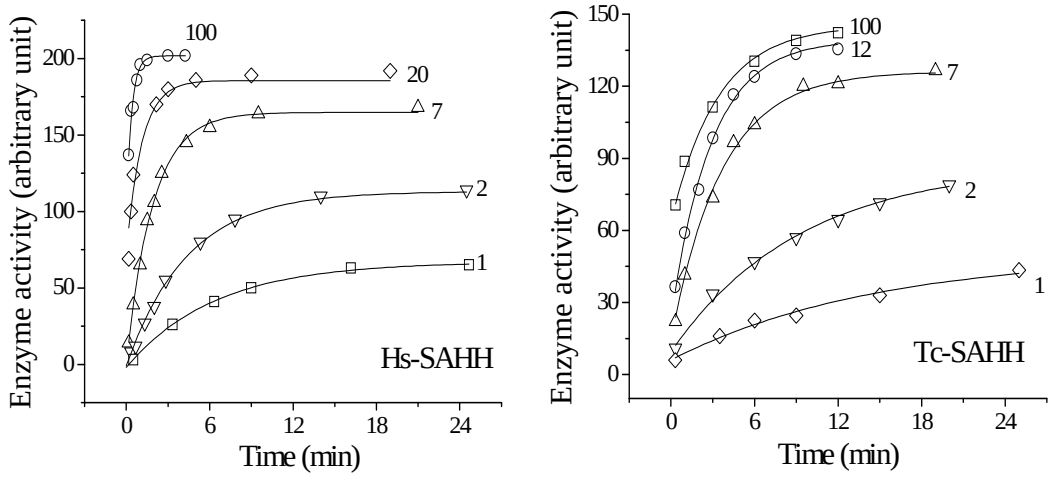

Figure 2.3. The time course of the rise in enzyme activity as NAD^+ associates with the apo-forms of Hs-SAHH and Tc-SAHH at 23 °C and pH 7.4. In each case, representative curves are shown for low, medium, and high concentrations of NAD^+ (identified on the graphs by values of [NAD^+] in μM). The lines are plots of eq (8), with parameters A_o (the initial activity, reflecting the fast-binding component), A_f (the final activity, reflecting the sum of fast-binding and slow-binding components), and k_{app} (the rate constant for the slow-binding component) the values of which will be presented in figures below. Note that all three parameters rise as [NAD^+] rises.

cofactor concentrations, with the rise in enzyme activity A upon cofactor binding following eq (8), equivalent to eq. (1) above, with A_o the activity at the apparent time zero, A_f the activity at very long times, and k_{app}, the first-order rate constant, all being functions of $[NAD^+]$.

$$A = A_f - [(A_f - A_o) \exp (- k_{app} t)] \qquad (8)$$

Particularly at cofactor concentrations greater than about 7 μM, considerable binding occurs during the mixing period or dead-time of the experiment (*fast binding*) and is measured by A_o. The remainder of the sites is occupied more slowly with a rate constant k_{app} (*slow binding*) to produce a total final activity A_f which is the sum of activities generated by the fast-binding component and the slow-binding component.

A model to be presented in the Discussion Section suggests that the magnitudes of the fast-binding component of activity A_o, the sum of fast-binding and slow-binding components of activity A_f, and the rate constant k_{app} for the slow-binding component of activity should depend on $[NAD^+]$ according to eqs (9a), (9b), and (9c), respectively.

$$A_o = (A_t/2)[[NAD^+]^n /(K_o^n + [NAD^+]^n)] \qquad (9a)$$

$$A_f = A_t[[NAD^+]/(K_f + [NAD^+])] \qquad (9b)$$

$$k_{app} = k_a[[NAD^+]/(K_a + [NAD^+])] \quad (9c)$$

Here A_t is the total enzyme activity at saturating $[NAD^+]$ after completion of slow binding, k_a is the limiting rate constant for slow binding at high $[NAD^+]$, n is a Hill coefficient needed to give an approximate account of apparent cooperativity, and K_o, K_f, and K_a are equilibrium dissociation constants of NAD^+ from three different forms of the active site (more detail is given in the Discussion Section). The data in Fig. 2.4. were fit to eq (9c) resulting in the values of k_a and K_a shown in the figure.

The dependence of the rate constant k_{app} on cofactor concentration for the slow-binding reaction thus exhibits saturation above about 30 μM for both enzymes (Fig. 2.4.), consistent with the previous report for the rat-liver enzyme [6] that the slow-binding rate constant is independent of cofactor concentration in the concentration range studied by those authors (185-555 μM). Furthermore, the affinities for NAD^+ of the various forms of the enzymes envisioned in the model described in the Discussion Section are sufficiently low that even when the concentrations of enzyme (monomers) and cofactor are equal at 1 μM, only about 20-25% of monomers are occupied by cofactor at the end of the experiment, so that roughly first-order kinetics are observed in this case, and more rigorously as the concentration of cofactor rises (Fig. 2.3).

2.3.4. Partition between fast and slow binding of NAD^+ to Hs-SAHH and Tc-SAHH as a function of $[NAD^+]$.

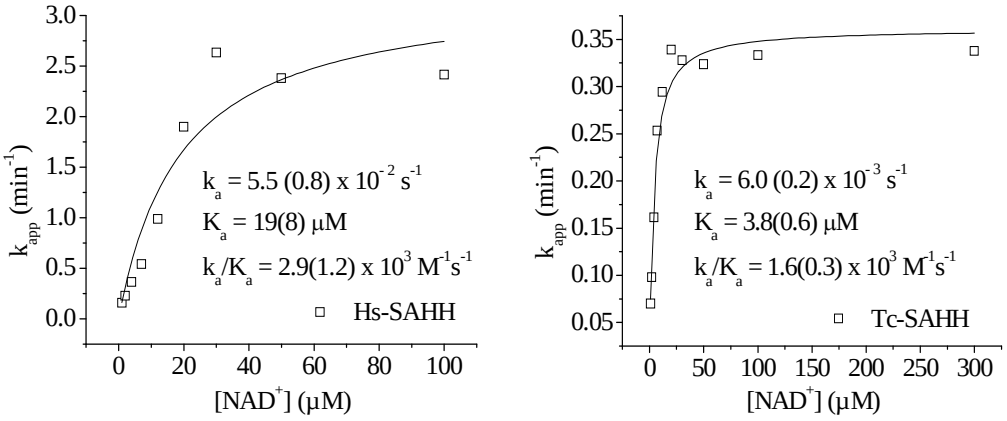

Figure 2.4. The dependence on the concentration of NAD^+ of the rate constants for the slow-binding phase of the association of NAD^+ with the apo-forms of Hs-SAHH and Tc-SAHH at 23 °C and pH 7.4. Some obvious signs of cooperativity for Hs-SAHH have been neglected and the data in both cases have been fitted to the simple hyperbolic saturation function of eq (9c). The parameters are shown in the figures with the standard deviations of fit in parentheses.

Fig. 2.5. shows the fractional activity produced in the fast-binding phase (as measured by A_o, the activity at the apparent zero of time), in the slow-binding phase (as measured by $[A_f - A_o]$), and the total fractional activity produced in both phases (A_f), all as a function of the cofactor concentration. The total fractional activity saturates at close to unity in the range of 10-20 μM cofactor for both enzymes. The slow-binding reaction dominates at low cofactor concentrations, increasingly so until it accounts for about 80-85% of the total activity at about 10 μM cofactor for both enzymes. Thereafter the fast-binding reaction increases in relative importance until the two processes each account for half the total activity above about 50 μM cofactor for Hs-SAHH and above about 300 μM cofactor for Tc-SAHH.

For Hs-SAHH, the fast-binding component shows extraordinary cooperativity as evidenced by the sigmoid appearance of the fast-binding curve in Fig. 2.4. To account approximately for this characteristic, the Hill equation [eq (9a)] was employed to fit the data in Fig. 2.4. Slow binding was described by eqs [(9b) - (9a)]. For total binding, the simple hyperbolic form of eq (9b) was adequate and was therefore employed. Although the sigmoid character of the fast-binding curve for Tc-SAHH is less pronounced, the same three equations (eqs (9a), (9b), and (9c)) were also used for these data.

For Hs-SAHH, the fast-binding data yield $K_o = 35 \pm 1$ μM, $n = 2.7 \pm 0.2$, $A_t = 1.27 \pm 0.04$. The total-binding data with n effectively fixed at 1.0 yield $K_f = 1.4 \pm 0.1$

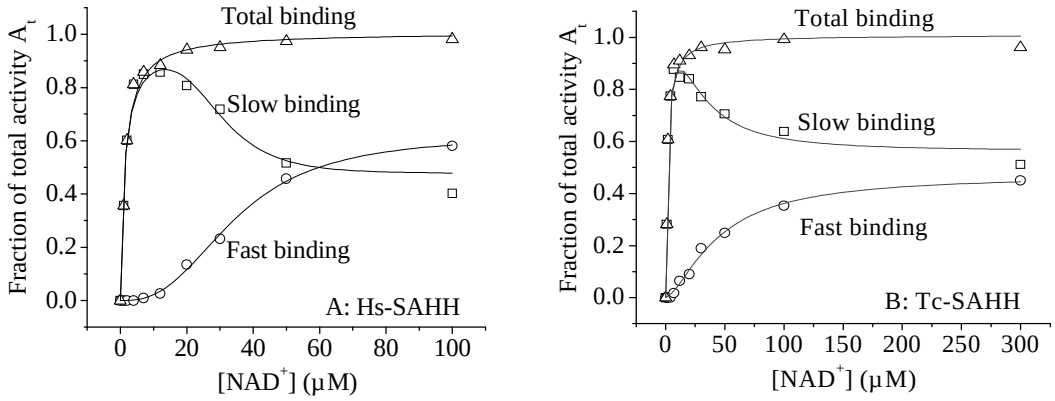

Figure 2.5. The dependence on [NAD^+] of the fractions of enzyme activity generated in the fast-binding phase (A_o in eq (8)), the slow-binding phase (A_f - A_o in eq (8)), and the total activity (A_f in eq (8)). The data were obtained in the kinetic experiments summarized in Fig. 2.3., with those at left (A) for Hs-SAHH and those at right (B) for Tc-SAHH. For each enzyme, the data for fast binding, total binding, and slow binding were independently fitted to eq (9a), eq (9b), and [eq (9b)-eq (9a)], respectively, to obtain the parameters given in the text. Eq. (9a) was used for fast binding in place of a hyperbolic function because of the distinctly sigmoid appearance of the data for Hs-SAHH; eq (9a) was then also used for consistency in treating the data for Tc-SAHH, where the sigmoid character is less pronounced.

μM, A_t = 1.01 ± 0.02. The slow-binding data yield K_o = 30 ± 4 μM, K_f = 1.3 ± 0.3 μM, n = 3.8 ± 1.4, A_t = 0.97 ± 0.06. For Tc-SAHH, the fast-binding data yield K_o = 45 ± 4 μM, n = 1.5 ± 0.1, A_t = 0.94 ± 0.04. The total-binding data with n fixed at 1.0 yield K_f = 1.5 ± 0.2 μM, A_t = 1.01 ± 0.02. The slow-binding data yield K_o = 31 ± 9 μM, K_f = 2.0 ± 0.4 μM, n = 1.7 ± 0.4, A_t = 1.13 ± 0.09. Mean values of the parameters are shown in Table 2.5. of the Discussion Section.

2.3.5 Temperature dependence of the slow-binding kinetics of the association of NAD^+ with Hs-SAHH and Tc-SAHH.

The effect of temperature on the slow-binding rate constant for association of NAD^+ with Hs-SAHH and Tc-SAHH is shown by the Eyring plots in Fig. 2.6. The rate was measured at 5 μM NAD^+, where the reaction is approximately first-order in the cofactor for both enzymes (see Fig. 2.4.), and the first order rate constants k_{app} were divided by 5 μM to produce the second-order rate constants k_o plotted.

On the basis of a model, developed in more detail in the Discussion Section, in which a partial, reversible, and perhaps quite local unfolding at higher temperatures deprives both enzymes of the capacity for cofactor binding, the apparent second-order rate constant k_o for cofactor binding will be given by $k_{on}(1/[1 + K_{un}])$ where k_{on} is the second-order rate constant for cofactor binding to the native form of the enzyme and the factor in parentheses is the fraction of enzyme in the native form, K_{un} being the

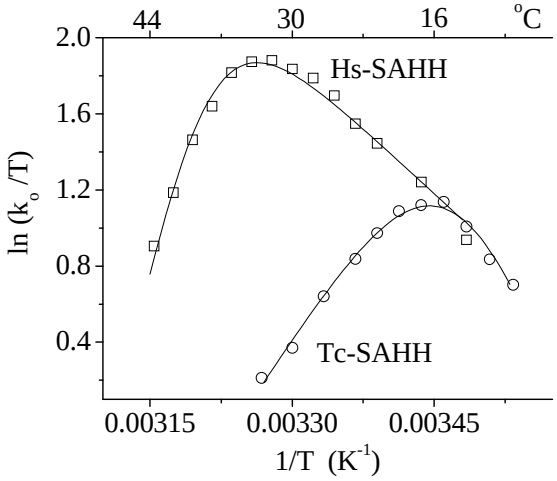

Figure 2.6. The temperature dependence of the rate constant for the slow-binding phase of the association of NAD^+ with the apo-forms of Hs-SAHH (upper curve) and Tc-SAHH (lower curve). The lines are plots of eq 10 with the parameters shown in Table 2.2. The rate constants were obtained in kinetic experiments of the kind summarized in Figure 2.3.

equilibrium constant for the unfolding. The temperature dependence of the apparent association constant k_o will then be described by eq (10), where we take the standard-state concentration of NAD^+, $[NAD^+]_{ss}$ = 1 M:

$$\ell n\,(k_o/T) = \Delta S^{\ddagger}_{on} / R - \Delta H^{\ddagger}_{on} / RT - \ell n\,[1 + \exp(\Delta S^{o}_{un} / R - \Delta H^{o}_{un} / RT)] - \ell n\,[NAD^+]_{ss} + \ell n\,(k/h) \qquad (10)$$

Here the subscript "on" denotes the quasi-thermodynamic parameters of activation for cofactor binding and the subscript "un" denotes the thermodynamic parameters of the reversible unfolding process. The values of these quantities are given in Table 2.2. The table also gives the ratio $\Delta H^{o}_{un}/\Delta S^{o}_{un}$, a rough measure of the "melting temperature" for the structural transition under observation.

2.3.6. Equilibrium dissociation constants of NAD^+ from Hs-SAHH and Tc-SAHH in the temperature range 30 – 37 ºC.

From the k_{on} and k_{off} values at temperatures between 30 ºC and 37 ºC (Fig. 2.2. and Fig. 2.6.), equilibrium dissociation constants K_d^{NAD+} for NAD^+ were calculated for Hs-SAHH and Tc-SAHH (Table 2.3.). The values are of the order of nanomolar for Hs-SAHH and micromolar for Tc-SAHH with the value of the ratio $(K_d^{NAD+})_{Tc} / (K_d^{NAD+})_{Hs}$ being about 600 at 37 ºC. Table 2.3. also shows the values of enthalpies and entropies of dissociation of NAD^+ from the two enzymes.

Table 2.2. Thermodynamic and quasi-thermodynamic parameters for NAD^+ association with Hs-SAHH and Tc-SAHH at temperatures in the interval 11-45 °C.

Enzyme	$\Delta S^{\ddagger}_{on}$ (J/K-mol)	$\Delta H^{\ddagger}_{on}$ (kJ/mol)	ΔS^{o}_{un} (J/K-mol)	ΔH^{o}_{un} (kJ/mol)	$\Delta H^{o}_{un}/\Delta S^{o}_{un}$ (K)
Hs-SAHH	-56 ± 9	38 ± 3	+788 ± 5	243 ± 2	308 ± 3 (35 °C)
Tc-SAHH	+225± 13	118 ± 4	+631 ± 8	182 ± 2	288 ± 5 (15 °C)

Table 2.3. Equilibrium dissociation constants for NAD^+ from its complexes with Hs-SAHH and Tc-SAHH at temperatures from 30 to 37 ˚C

Hs-SAHH, K_d^{NAD+}, nM (Temperature, °C)	9.6 ± 0.4 (30 ˚C)	13 ± 1 (32 ˚C)	17 ± 1 (34 ˚C)	31 ± 3 (37 ˚C)	ΔH^o = 130 ± 9 kJ/mol ΔS^o = 274 ± 9 J/mol-K
Tc-SAHH, K_d^{NAD+}, μM (Temperature, °C)	0.63 ± 0.04 (30 ˚C)	2.1 ± 0.2 (32 ˚C)	5.7 ± 0.6 (34 ˚C)	19 ± 2 (37 ˚C)	ΔH^o = 378 ± 24 kJ/mol ΔS^o = 1131 ± 83 J/mol-K.

2.3.7. Kinetics and thermodynamics at 37 ºC of the association with and dissociation from Tc-SAHH and Hs-SAHH of NADH.

The equilibrium constants K_d^{NADH} for dissociation of NADH from its complexes with Hs-SAHH and Tc-SAHH were measured by competition between NAD^+ (with dissociation constants given in Table 2.3.) and NADH, as described above. The values are 5.0 ± 0.1 nM for Hs-SAHH and 69 ± 6 nM for Tc-SAHH.

At concentrations of NADH below 7 μM, the association rate with Hs-SAHH is first-order in NADH so that the rate constant k_{on} could be measured as 1940 ± 90 $M^{-1}s^{-1}$ for Hs-SAHH and 930 ± 90 $M^{-1}s^{-1}$ for Tc-SAHH.

The dissociation of NADH from Hs-SAHH is too slow to allow measurement of the rate constant for dissociation k_{off} but k_{off} can be computed from $K_d^{NADH}k_{on}$ as 9.7 ± 2.0 x 10^{-6} s^{-1}. A similar calculation for Tc-SAHH yields 64 ± 10 x 10^{-5} s^{-1}, while a direct measurement, which is possible here, yields 69 ± 6 x 10^{-5} s^{-1}.

2.3.8. Thermal stability of the apo-forms of Hs-SAHH and Tc-SAHH.

Melting temperatures were determined both by DSC and CD for the thermal unfolding of the two proteins. The values for apo-Hs-SAHH are 44.9 ± 0.3 °C (DSC) and 44.2 ± 0.4 °C (CD) and for apo-Tc-SAHH are 53.0 ± 0.4 °C (DSC) and 52.8 ±

0.4 °C (CD). At temperatures below these values, apo-Hs-SAHH loses its capacity to bind NAD^+ (and thus become an active catalyst) more rapidly than does apo-Tc-SAHH (at 22 °C, Hs-SAHH loses this capacity completely within 30 hr, while Tc-SAHH still retains half of its capacity at 90 hr).

2.3.9. Evaluation of the NAD^+ and NADH analogs S-NAD^+ and S-NADH as selective inhibitors for Hs-SAHH and Tc-SAHH.

S-NAD^+ and S-NADH, the side-chain thione analogs of the natural cofactors, were tested for their ability to inhibit AdoHcy hydrolase activity. Hs-SAHH and Tc-SAHH, reconstituted with S-NAD^+, show about 1% of the activity of the NAD^+ form and the S-NADH forms of both enzymes show no measurable activity. The association and dissociation rate constants and equilibrium dissociation constants for S-NAD^+ and S-NADH with Hs-SAHH and Tc-SAHH at 37 ºC are summarized in Table 2.4. As a test of the relative efficacy of these substances as inhibitors of Hs-SAHH and Tc-SAHH, the enzymes (both in their active NAD^+ forms) were exposed to 50 µM S-NAD^+ or 20 µM S-NADH in the presence of 50 µM NAD^+ to simulate roughly the estimated [6] 70 µM levels of NAD^+ *in vivo* (Fig. 2.5.). Hs-SAHH was affected very little (2% inhibition with each inhibitor) in the first 5 min, during which Tc-SAHH lost 45% of its activity with S-NAD^+ or 52% with S-NADH. Apparent equilibrium was reached for Tc-SAHH at 10-20 min of exposure with all activity lost

Table 2.4. Rate and equilibrium constants for the association and dissociation of S-NAD^+ and S-NADH with Hs-SAHH and Tc-SAHH at 37 ˚C

Enzyme	Ligand	k_{on} [a] ($M^{-1}s^{-1}$)	$10^6 k_{off}$ (s^{-1})	K_d (nM)
Hs-SAHH	S-NAD^+	4153 ± 303	162 ± 11	39 ± 1
	S-NADH	4000 ± 712	148 ± 26	37 ± 1
Tc-SAHH	S-NAD^+	356 ± 29	5450 ± 300	15,300 ± 9,000
	S-NADH	467 ± 59	304 ± 26	651 ± 60

[a] *Calculated as k_{off} / K_d*

in the presence of S-NADH and about half lost in the presence of S-NAD^+. The apparent equilibrium for Hs-SAHH is reached only after 12 h of incubation.

2.4. Discussion

2.4.1. Kinetics of the dissociation of NAD^+ from Hs-SAHH and Tc-SAHH.

The data presented in Fig. 2.1. and Table 2.1. show that the dissociation of four equivalents of NAD^+ from the four active sites of homotetrameric SAHH proceeds by a simple first-order reaction, making no distinction in rate of dissociation among the four active sites. The loss of cofactor thus exhibits no apparent cooperativity. The rate constants for dissociation are substantially larger for Tc-SAHH than for Hs-SAHH: for example, at 37 °C, dissociation from Tc-SAHH is approximately 90-fold faster (caption of Fig. 2.1.).

2.4.2. Temperature dependence of the kinetics of the dissociation of NAD^+ from Tc-SAHH and Hs-SAHH.

Figure 2.2. shows that the rate constants of NAD^+ dissociation in the cases of both Hs-SAHH and Tc-SAHH generate non-linear Eyring plots. The upward curvature or “bowl shape” of these two plots can arise from a number of sources. The possible explanations are not always practically or even theoretically distinguishable

but a reasonable hypothesis would be that a structural change in the enzyme as the temperature is changed affects the activation parameters for the dissociation reaction. Attempts to describe the temperature dependence simply by two parallel routes of dissociation with different activation parameters were unsuccessful. The data are too sparse to evaluate in detail the hypothesis of a thermally induced structural transition, but some comments on the activation parameters in the high-temperature and low-temperature regimes can be made.

As Table 2.1. shows, the value of $\Delta H^{\ddagger}$ along the low-temperature limb of the Eyring plots is 116 kJ/mol for Hs-SAHH and 154 kJ/mol for Tc-SAHH, so that if entropic contributions were equal the cofactor would dissociate from Hs-SAHH 4 x 10^6-fold faster than from Tc-SAHH at 300 K. In fact the values of $\Delta S^{\ddagger}$ along the low-temperature limb of the Eyring plots are +24 J/mol-K for Hs-SAHH and +170 J/mol-K for Tc-SAHH, a difference that, taken alone, would confer a rate advantage of 4 x 10^7-fold on dissociation from Tc-SAHH over Hs-SAHH. The entropic contribution thus more than overcomes the enthalpic contribution so that dissociation of NAD^+ from Tc-SAHH is faster than from Hs-SAHH by roughly 10-fold in the low-temperature regime.

Along the high-temperature limb of the Eyring plots, the values of $\Delta H^{\ddagger}$ and $\Delta S^{\ddagger}$ for the two enzymes are within experimental error of each other (but note the long extrapolation of a few points to obtain the values). Phenomenologically,

dissociation occurs from Tc-SAHH more rapidly than from Hs-SAHH by factors in the range of 10-100-fold, and indeed the mean values of both $\Delta H^{\ddagger}$ and $\Delta S^{\ddagger}$ favor a more rapid dissociation from Tc-SAHH by factors in this range. One feature of the data is that the conversion temperature between the thermal regimes, which is given by eq (7) above, is considerably higher for Hs-SAHH (about 41 °C) than for Tc-SAHH (about 29 °C). The result is that at 37 °C, Tc-SAHH has entered the high-temperature regime and the rate constant has been increasing rapidly with temperature while Hs-SAHH remains in the low-temperature regime, where the rate constant is not increased as much by the rising temperature. At 37 °C then, dissociation from Tc-SAHH is about 90-fold faster than from Hs-SAHH.

The large increase in the values of the entropies of activation for dissociation of NAD^+ from both enzymes as the temperature rises through the range of 30-40 °C may suggest that the faster dissociation rates at higher temperatures derive in part from an increased mobility in the apo-enzyme of the unoccupied binding site for NAD^+. The fact that the conversion temperature is lower for Tc-SAHH would then suggest that the ease with which the increased mobility can be thermally induced is greater for Tc-SAHH.

2.4.3. Observed kinetics of the association of NAD^+ with Tc-SAHH and Hs-SAHH.

The association process, in contrast to the dissociation process, appears kinetically complicated, as shown above in Figs. 2.3., 2.4., and 2.5. The association processes for Hs-SAHH and Tc-SAHH show qualitatively similar but quantitatively different characteristics, as measured by the appearance of enzyme activity when NAD^+ becomes bound in the active sites.

For each enzyme, there is a fraction of occupation A_o of the total binding that occurs during the dead-time of the experiment, and depends in a saturating manner on $[NAD^+]$. A first-order time-dependent fraction of binding with rate constant k_{app} then follows and k_{app} also depends in a saturating manner on $[NAD^+]$. The total fraction of binding A_f at the end of the slow-binding phase depends in a saturating manner on $[NAD^+]$ and corresponds to full occupancy of all active sites at high cofactor concentrations. All three kinetic parameters of binding, A_o, A_f, and k_{app}, thus exhibit saturation behavior with cofactor concentration but the half-saturation concentrations of cofactor are different in each case (Figs. 2.4. and 2.5.).

Fig. 2.5. also shows that the fraction of activity generated by the slow-binding phenomenon ($A_f - A_o$) exhibits a particularly complex dependence on $[NAD^+]$. At low $[NAD^+]$, the slow-binding fraction rises sharply until it accounts for more than 80% of the total binding. Thereafter, it falls as the fast-binding fraction increases until at high $[NAD^+]$ (>60 μM for Hs-SAHH and >200 μM for Tc-SAHH), both the slow-binding and fast-binding phenomena account for roughly half of the enzyme activity.

2.4.4. A Model for the kinetics of association of NAD^+ with Hs-SAHH and Tc-SAHH.

A model that accommodates these observations is depicted in Fig. 2.7. Its basic assumption is that apo-SAHH from both species, before exposure to cofactor, contains two equally populated classes of active sites. Upon introduction of cofactor, all sites can and do bind NAD^+ rapidly, but in one class of sites (dissociation constant K_o) binding of NAD^+ generates a fully functional active site, while in the other class of sites (dissociation constant K_a) binding of NAD^+ generates no enzyme activity. Thus the initial activity A_o (see Figs. 3, 4, 5 and eqs (9) above) is given by the total population of potentially functional sites ($A_t/2$) multiplied by the fraction of these sites occupied at a given $[NAD^+] = N$, i.e., $N^n/(K_o^n + N^n)$. The Hill-equation formalism allows for the sigmoid character of the N-dependence of A_o visible in Fig. 2.5. In Fig. 2.7., the initial situation is portrayed by the left-hand box and the expression for A_o is given below the box.

Binding at the non-functional sites, although tighter than to the potentially functional sites, generates no activity. Binding of the cofactor in such a site does, however, initiate a time-dependent process (rate constant k_a) in which the non-functional sites, occupied to a fractional extent ($N/\{K_a + N$) of their total, are transformed - *along with their partner sites whether or not the latter are occupied* - into pairs of active sites both of which are potentially fully catalytically active when

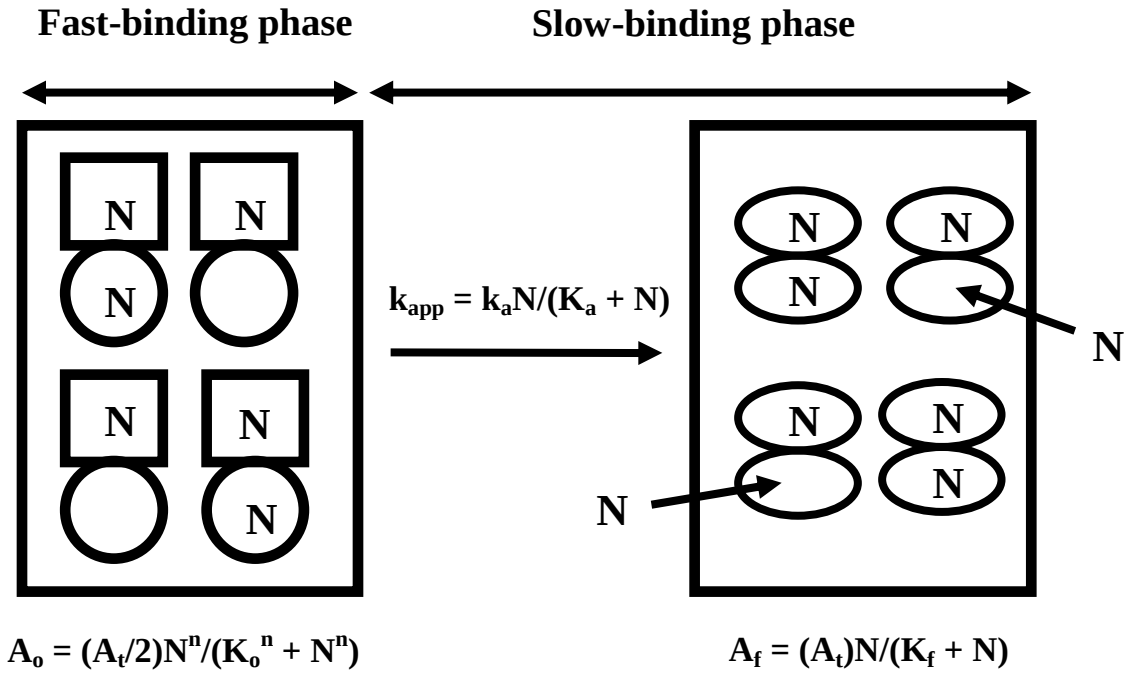

Figure 2.7. Speculative model for association and time-dependent activation of apo-SAHH by binding of NAD^+. The tetrameric apo-enzyme molecule is assumed to contain two classes of binding sites in equal amounts, the molecule thus being represented by a square-circle figure. The box at left represents the situation during the fast-binding phase. Upon introduction of the cofactor, represented by the letter N, both classes of sites are assumed to become wholly or partially occupied as shown in the box at left. The circle-sites are assigned a cofactor dissociation constant K_o, and are assumed fully capable of catalysis when occupied. The square-sites are assigned a cofactor dissociation constant K_a and they are assumed incapable of catalysis whether or not they are occupied by N or not. Equilibration of binding occurs within the dead-time of the experiment and constitutes the fast phase of generation of catalytic

activity, which arises solely from the occupied circle-sites. The initial activity is then equal to A_o as shown below the box at left. The box at right represents the situation following the slow-binding phase. During the slow phase, those species that contain N bound into a square-site undergo a reorganization in which the occupied square-site *and the adjacent circle site, whether occupied or not,* are converted to oval-sites as shown at right. Oval-sites have the same catalytic activity as circle-sites, but their substrate affinity is greater so that, as shown, more sites are rapidly occupied, as they become oval-sites. The reorganization is driven by the fraction of occupied square-sites, thus occurring with rate constant $k_aN/(K_a + N)$. Because the reorganization is irreversible, the entirety of the enzyme will be converted during the slow phase. The resulting enzyme equilibrates rapidly with free N, with all sites now having a dissociation constant K_f. The final activity is then given by the expression shown below the box at right. The three equations in the figure are eqs 9a-9c of the text.

occupied by cofactor. This slow-binding phase leads to a functionally homotetrameric enzyme with equilibrium constant K_f for dissociation of NAD^+ from any of the active sites. This form of the enzyme is in rapid, reversible cofactor-binding equilibrium at all active sites.

The situation at the end of the slow-binding phase is represented in Fig. 2.7. by the box on the right-hand side. Since binding at all sites is now rapid and reversible and because (a) $K_f < K_a < K_o$ so that all sites at the end of the slow phase have greater cofactor affinity than any site before the slow phase, and (b) the slow phase leads to the generation of two potentially functional sites of high affinity where only the non-functional partner was occupied initially, the overshoot phenomenon results at low cofactor levels. At low NAD^+ levels, the occupancy of the initially functional sites is low (especially as a consequence of the cooperativity in their occupation), and the occupancy of non-functional sites is relatively high. The highly occupied non-functional sites then transform along with their partner sites into fully functional sites of still higher affinity. These factors combine to generate the overshoot characteristic.

The expression over the arrow describes the N-dependence of k_{app} (Fig. 2.4.) and the expression below the right-hand box describes the N-dependence of A_f (Fig. 2.5.).

The values of the parameters of the model, as can be understood from Fig. 2.7. and eqs (9), are given in Table 2.5. The values were obtained by fitting of the data of Figs. 3, 4, and 5 to eqs (9) as described in the Results section.

To put into quantitative terms the description given above, fast binding of NAD^+ within the dead-time of the experiment occurs to potentially functional sites from which the dissociation constant K_o is 33 μM (Hs-SAHH) to 38 μM (Tc-SAHH). At the same time, sites with no catalytic capacity but greater affinity (K_a = 19 μM for Hs-SAHH, about 4 μM for Tc-SAHH) are rapidly occupied. A time-dependent conversion then ensues of these sites (and their partner sites whether occupied or not) to fully active sites (k_a about 10-fold larger for Hs-SAHH and corresponding to characteristic times of about 20 s for Hs-SAHH and 3 m for Tc-SAHH). At the end of the time-dependent phase, all active sites have the same activity and dissociation constant (1.4-1.5 μM for both enzymes).

The qualitative character of the cofactor-association process is the same for both enzymes, and some quantitative features are similar. For example, the non-functional sites of the apo-enzyme bind cofactor about twice as tightly as the functional active sites for Hs-SAHH and 10-fold as tightly for Tc-SAHH. This feature contributes to the overshoot of the slow-binding reaction (Fig. 2.5.), because more of the non-functional than the functional sites are initially occupied. More important, however, is the fact that each occupied non-functional site leads to *two* functional

Table 2.5. Values of rate and equilibrium constants in the kinetics of the fast and slow binding phases of the association reaction of NAD^+ with Hs-SAHH and Tc-SAHH at 23 °C and pH 7.4, according to the model of Figure 2.7.

Enzyme	K_o, μM binding to fully functional sites of apo-SAHH	K_a, μM binding to non-functional sites of apo-SAHH	K_f, μM binding to fully functional sites of holo-SAHH	k_a, s^{-1} transformation of apo-sites to functional holo-sites	k_a/K_a, $M^{-1}s^{-1}$ binding and transformation of apo-sites to holo-sites
Hs-SAHH	33 ± 4 n = 3.3 ± 1.4	19 ± 8	1.4 ± 0.3	$5.5 \pm 0.8 \times 10^{-2}$	$2.9 \pm 1.2 \times 10^{3}$
Tc-SAHH	38 ± 9 n = 1.6 ± 0.4	3.8 ± 0.6	1.8 ± 0.4	$6.0 \pm 0.2 \times 10^{-3}$	$1.6 \pm 0.3 \times 10^{3}$

sites of high affinity in the final enzyme, and thus the slow phase comes to account for 80-85% of the final activity at [NAD^+] below the saturation values for the functional active sites.

These qualitative features apply to both enzymes but quantitative distinctions exist. The achievement of final full activity occurs about 10 times faster for Hs-SAHH, as already noted. Furthermore, the rates of cofactor dissociation are quite different for the two enzymes, as will be discussed below, and both of these distinctions may be of some importance.

It should be noted as well that the values of K_f, the apparent dissociation constants of NAD^+ corresponding to a period about 30 to 60 min after mixing of apo-enzymes with cofactor, are of the order of 1-2 μM (23 °C) for both Hs-SAHH and Tc-SAHH (Table 2.5.). When the dissociation constants of NAD^+ are instead calculated as the ratio of dissociation and association rate constants, the dissociation rate constants obtained from fully reconstituted enzyme that has not only completed both phases of binding but thereafter undergone further maturation for some hours or more, K_d^{NAD+} for Tc-SAHH remains about the same (0.6 μM at 30 °C: Table 2.3.). In contrast, the K_d^{NAD+} for Hs-SAHH is around 10 nM at 30 °C, roughly 100-fold smaller than K_f. These results seem to indicate that the loose binding observed for Tc-SAHH after 30 to 60 min persists and represents the final thermodynamic equilibrium binding, while with Hs-SAHH, a further change in the strength of binding occurs over

some hours, resulting in a further 100-fold increase in the strength of cofactor association with Hs-SAHH.

2.4.5. Temperature dependence of the slow-binding kinetics of the association of NAD^+ with Hs-SAHH and Tc-SAHH.

The data of Fig. 2.6. were obtained at 5 μM NAD^+ so that for Hs-SAHH (K_a = 19 μM at 23 °C: Table 2.5.) the apparent second-order rate constant k_o is roughly equal to k_a/K_a, a constant similar to k_{cat}/K_M in enzyme catalysis. For Tc-SAHH (K_a = 4 μM at 23 °C: Table 2.5.), the situation is not so simple; the phenomenological observation that k_o in the neighborhood of 5 μM NAD^+ remains proportional to [NAD^+] for Tc-SAHH leads us to treat it as roughly equal to k_a/K_a. Fig. 2.6. shows that at low temperatures the observed k_o is about the same for the two enzymes. Extrapolating to 23 °C gives a value near 1500 $M^{-1}s^{-1}$, not so different from k_a/K_a (2900 $M^{-1}s^{-1}$ for Hs-SAHH, 1600 $M^{-1}s^{-1}$ for Tc-SAHH: Table 2.5.)

As already noted, the "dome-shaped" temperature dependences in Fig. 2.6. can arise from a model in which rising temperature on the one hand increases the value of the rate constant k_a/K_a while at the same time increasing the fraction of protein that has undergone an at least partial, reversible unfolding to a form that can no longer bind the cofactor (equilibrium constant K_{un} so that, as above, $k_o = k_{on}(1/[1 + K_{un}])$ with k_{on} being approximately equal to k_a/K_a.

As can be seen both from Fig. 2.6. and Table 2.2., the quasi-thermodynamic parameters of activation for k_{on} are different for Hs-SAHH and Tc-SAHH The values of $\Delta H^{\ddagger}$ (kJ/mol) are approximately 38 and 118, respectively, and the values of $\Delta S^{\ddagger}$ (J/mol-K) being about -56 and +225, respectively. The low-temperature limbs of the temperature dependences for the two enzymes do nearly superimpose, but only because the enzyme with the more favorable enthalpy of activation (Hs-SAHH) also has the less favorable entropy of activation. The combination of a small enthalpic barrier with a negative entropy of activation for Hs-SAHH would be consistent with a transition state for Hs-SAHH that comes after the development of a considerable part of the binding interactions between cofactor and protein (low enthalpy from liberation of binding energy, negative entropy from rigidification of segments of protein and cofactor structures). The combination of a larger enthalpic barrier with a positive entropy of activation for Tc-SAHH would be consistent with a transition state for Tc-SAHH that comes at a point where desolvation of the cofactor has advanced to some degree (thus high enthalpy from loss of solvation energy, positive entropy from liberation of water molecules) but few protein-cofactor interactions have developed, and thus the liberation of binding energy and rigidification of structure cannot cancel the contributions just described.

The thermodynamic values for the equilibrium constant of the postulated unfolding phenomenon are not extremely different for Hs-SAHH and Tc-SAHH [ΔH^{o}_{un} (kJ/mol) about 243 and 182, respectively, and ΔS^{o}_{un} (J/mol-K) near +788 and

+631, respectively: Table 2.2.]. The ratios $\Delta H^{o}_{un}/\Delta S^{o}_{un}$ of these values lead to "melting" temperatures for the corresponding unfolding process of 35 °C (Hs-SAHH) and 15 °C (Tc-SAHH), not far from the temperatures at which the two Eyring plots exhibit maxima (34 °C for Hs-SAHH, 17 °C for Tc-SAHH: Fig. 2.6.). It should be noted that this "melting" does *not* correspond to global unfolding of the enzymes, which occurs around 44-45 °C (Hs-SAHH) and 52-53 °C (Tc-SAHH). This suggests a more local phenomenon is adversely affecting the capacity of the enzyme to bind the cofactor.

The maxima are not expected to occur at the global "melting" temperatures but rather at the temperature for which the local unfolding process begins to dominate the rate process in determining the value of k_o, i.e., the temperature T_{max} for which $d[\ell n(k_o/T)]/d(1/T) = 0$. From this requirement, it emerges that at T_{max}, the fraction of locally unfolded protein $[K_{un}^{max}/(1 + K_{un}^{max})] = \Delta H^{\ddagger}_{on}/\Delta H^{o}_{un}$. This fraction is 0.19 for Hs-SAHH and 0.61 for Tc-SAHH, yielding values of K_{max} of 0.23 (Hs-SAHH) and 1.6 (Tc-SAHH), whence T_{max} (= $[\Delta H^{o}_{un}/(\Delta S^{o}_{un} - R\ell n[K_{max}])]$) is found as 34 °C (Hs-SAHH) and 16 °C (Tc-SAHH) in good agreement with the observations of 34 °C for Hs-SAHH and 17 °C for Tc-SAHH.

2.4.6. Equilibrium dissociation constants of NAD^+ from Hs-SAHH and Tc-SAHH in the temperature range 30 – 37 ºC.

In this limited temperature range where the on-rate constants and off-rate constants for both enzymes exhibit linear Eyring plots, effective equilibrium dissociation constants can be calculated for NAD^+ (Table 2.3.). They are substantially larger for Tc-SAHH than for Hs-SAHH, the ratio ranging from 66 at the low end to 613 at the high end of the temperature range. The lower relative affinity of Tc-SAHH for the oxidized cofactor derives from the cancellation of enthalpic and entropic factors. There is a much greater enthalpy cost of dissociation from Tc-SAHH (greater by 248 ± 25 kJ/mol) but this is combined with a larger entropic advantage for dissociation of NAD^+ from Tc-SAHH (greater by 263 ± 25 J/mol-K). The increased affinity of several hundred fold shown by Hs-SAHH thus arises from this cancellation of two very large and opposite contributions.

For both enzymes, the enthalpy of dissociation of NAD^+ is positive and the entropy of dissociation of NAD^+ is positive. This result is expected for the enthalpy because the attractive interactions of the cofactor with its binding site must be ruptured upon dissociation. The observed result is also expected for the entropy because two particles are generated from one (a minor contribution) and because rupture of the binding interactions allows increased freedom of motion within both cofactor and enzyme molecules. One interpretation of the much larger values of both the enthalpy and entropy terms for Tc-SAHH than for Hs-SAHH would be that a substantially greater mobility of the unoccupied cofactor-binding site in apo-TcSAHH would require a larger entropy loss to fix in place the enzyme structural

elements that bind to the cofactor (thus a larger entropy gain on dissociation) but that the same mobility would permit the development of a more favorable set of binding interactions, producing a larger release of energy upon binding and a larger energy cost of dissociation. This subject will be addressed in later papers in this series.

2.4.7. Kinetics and thermodynamics at 37 ºC of the association with and dissociation from Tc-SAHH and Hs-SAHH of NADH.

The association rate constant for NADH is about twice as large for Hs-SAHH (1940 $M^{-1}s^{-1}$) as for Tc-SAHH (930 $M^{-1}s^{-1}$), while the dissociation rate constant is smaller by about six-fold, resulting in a lower NADH-affinity for Tc-SAHH relative to Hs-SAHH by about 14-fold. This difference is somewhat smaller than was true for NAD^+ (600-fold tighter with Hs-SAHH), which results from the fact that the affinity of Hs-SAHH for cofactor is roughly the same whether the cofactor is oxidized or reduced (in the range of nanomolar in both cases), while the affinity of Tc-SAHH for cofactor is much greater for the reduced form (a bit over nanomolar) than for the oxidized form (roughly micromolar).

2.4.8. Thermal stability of the apo-forms of Hs-SAHH and Tc-SAHH.

As has already been mentioned, the global unfolding of apo-Hs-SAHH occurs at a temperature approximately 10 °C lower than for apo-Tc-SAHH. Combined with

the observations above that the two enzymes have differing affinities for both oxidized and reduced cofactors, and that in the case of the oxidized cofactor, these difference arise from large and opposing differences in enthalpies and entropies of association and dissociation, the difference in overall thermal stability favoring Tc-SAHH may signal differences in the dynamics of the cofactor binding sites. Since we can detect no structural differences in this region of the enzymes (unpublished data, which refer to the enzyme with NADH and oxidized substrate-analog as ligands) the dynamical differences may allow the nucleation of the global unfolding process in the cofactor-binding region, at a lower temperature for Hs-SAHH than for Tc-SAHH. This could reflect a greater thermal mobility for the cofactor site in Hs-SAHH, allowing it to adapt to the cofactor as it binds, leading to stronger affinity. This would conflict, however, with the larger entropy of dissociation shown by Tc-SAHH, so the matter is almost certainly more complicated than this view.

2.4.9. Evaluation of the NAD^+ and NADH analogs S-NAD^+ and S-NADH as selective inhibitors for Hs-SAHH and Tc-SAHH.

The comparative inhibitory effect of S-NAD^+ and S-NADH on Hs-SAHH and Tc-SAHH (Fig. 2.8., Table 2.4.) does not depend only on their relative affinity for the two enzymes, which is nearly 400-fold greater for Hs-SAHH in the case of S-NAD^+ and nearly 20 times greater for Hs-SAHH in the case of S-NADH. Instead the major factor is the exposure of an empty cofactor binding site to the environment, which

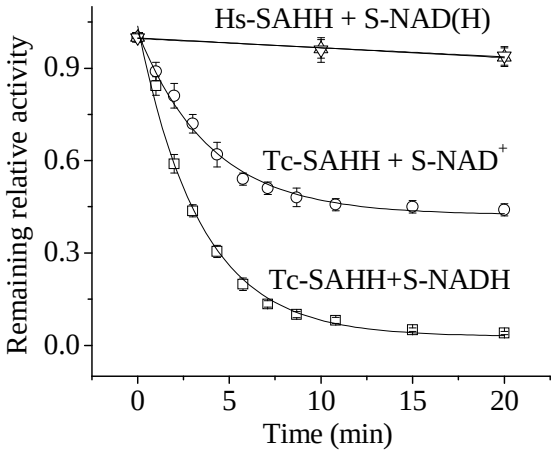

Figure 2.8. Loss of activity of Hs-SAHH (top curve, for 50 μM S-NAD^+ and for 20 μM S-NADH) and of Tc-SAHH (middle curve, 50 μM S-NAD^+, and lower curve, 20 μM S-NADH) in solutions containing 4 μM enzyme and 50 μM NAD^+ at 37 ºC, pH 7.4. Errors were calculated from two independent measurements.

occurs by dissociation of NAD^+ with a rate constant at 37 °C for Hs-SAHH of 5.8 x 10^{-5} s^{-1} and for Tc-SAHH of 4.7 x 10^{-3} s^{-1}, a factor (as noted above) of about 90-fold faster for Tc-SAHH. The exposed site is then competitively trapped by the inhibitor and the cofactor. The dissociation is probably the rate-limiting step and the half-life of dissociation (about 2.5 min from Fig. 2.2.) should match the half-life of inhibitor binding as is found, the latter being (Fig. 2.8.) about 2.5 min for binding of both S-NAD^+ and S-NADH. As Fig. 2.8. shows, the difference between the two inhibitors is that S-NADH is capable of displacing NAD^+ and generating complete loss of activity. This is consistent with the substantially greater affinity of Tc-SAHH for S-NADH than for S-NAD^+ (nearly 25-fold from Table 2.4.).

These data thus suggest that the faster off-rate of cofactor from Tc-SAHH could be exploited to design inhibitors that bind rapidly to the cofactor site of Tc-SAHH but only far more slowly to Hs-SAHH. Such inhibitors could be highly selective for the parasitic enzyme on the basis of the kinetic properties of the parasitic and human enzymes even if, as seen here, the human enzyme has a much larger equilibrium affinity for the inhibitor (greater by 400-fold in this case).

2.5. Conclusions.

The equilibrium and kinetic properties of association and dissociation of cofactor by Hs-SAHH and Tc-SAHH are qualitatively similar. Both enzymes bind

NAD^+ in a complex scheme that behaves as if the apo-enzyme has two numerically equal classes of sites that bind cofactor and generate catalytic activity either very rapidly (less than a minute) or quite slowly (over 30 min). Both enzymes undergo dissociation of NAD^+ from all four sites in a single first-order reaction. Both enzymes exhibit the "dimer of dimers" structure (*1, 11*) in which the homotetramer is made up of two pairs of monomers, and within each pair of monomers, a C-terminal segment from each partner penetrates into the other partner subunit and forms part of the cofactor binding site. These two communicating active sites may thus correspond to the two classes of active sites required in the kinetic model for binding cofactor that is discussed above.

The quantitative properties for cofactor association and dissociation of Hs-SAHH and Tc-SAHH are very different. The equilibrium affinity of Hs-SAHH for NAD^+ and NADH are both in the nanomolar range, while the equilibrium affinity of Tc-SAHH for NAD^+ is in the micromolar range and its affinity for NADH is in the nanomolar range, not far from the NADH affinity of Hs-SAHH. The slow binding of NAD^+ by both enzymes exhibits saturation kinetics with respect to the cofactor concentration but binding to Hs-SAHH has a maximum rate constant around 0.06 s^{-1}, while the rate constant for binding to Tc-SAHH levels out at 0.006 s^{-1}.

The dissociation rate constants for NAD^+ show a complex temperature dependence with both enzymes, but the cofactor always dissociates more rapidly from

Tc-SAHH than from Hs-SAHH, the ratio being around 80-fold at 37 °C. This feature presents an opening for selective inhibition of Tc-SAHH over Hs-SAHH, demonstrated with the thioamide analogs of NAD^+ and NADH, which inactivated Tc-SAHH to the extent of 60% (NAD^+ analog) or 100% (NADH analog) within 30 min, while inhibition of Hs-SAHH approached 30% only after 12 h. The following chapters in this series will present information that illuminates the structural features of Hs-SAHH and Tc-SAHH that are responsible for these differences.

2.6. References

1. Parker, N.B., et al., *Trypanosoma cruzi: molecular cloning and characterization of the S-adenosylhomocysteine hydrolase.* Exp Parasitol, 2003. **105**(2): p. 149-58.
2. Yang, X. and R.T. Borchardt, *Overexpression, purification, and characterization of S-adenosylhomocysteine hydrolase from Leishmania donovani.* Arch Biochem Biophys, 2000. **383**(2): p. 272-80.
3. Yuan, C.S., et al., *Mechanism of inactivation of S-adenosylhomocysteine hydrolase by (Z)-4',5'-didehydro-5'-deoxy-5'-fluoroadenosine.* J Biol Chem, 1993. **268**(23): p. 17030-7.
4. Yuan, C.S., D.B. Ault-Riche, and R.T. Borchardt, *Chemical modification and site-directed mutagenesis of cysteine residues in human placental S-adenosylhomocysteine hydrolase.* J Biol Chem, 1996. **271**(45): p. 28009-16.
5. Gomi, T., Y. Takata, and M. Fujioka, *Rat liver S-adenosylhomocysteinase. Spectrophotometric study of coenzyme binding.* Biochim Biophys Acta, 1989. **994**(2): p. 172-9.
6. Fjeld, C.C., W.T. Birdsong, and R.H. Goodman, *Differential binding of NAD^+ and NADH allows the transcriptional corepressor carboxyl-terminal binding protein to serve as a metabolic sensor.* Proc Natl Acad Sci U S A, 2003. **100**(16): p. 9202-7

Chapter 3

The Role of the Differential Stability of Helix α-18 in Comparative Kinetics of Cofactor Association and Dissociation for Hs-SAHH and Tc-SAHH.

3.1. Introduction

The X-ray crystallographic structures of Hs-SAHH [1], Pf-SAHH [2] and Tc-SAHH [3] indicate a unique binding site for the cofactor, composed in part by elements of a penetrating C-terminal extension from an adjacent subunit. The C-terminal extension is crucial in maintaining the activity and quaternary structure of SAHH [4, 5].

Although direct interactions between the cofactor and polypeptide that would normally be considered key interactions, including the interactions with the C-terminal extension of the adjacent monomer, are generally conserved in the human and parasitic enzymes, significant differences in the kinetics and thermodynamics of NAD^+ binding among the human and parasitic enzymes have been observed [6-8]. Our previous work indicated that there may be some local elements near the cofactor binding site which play an important role in NAD^+ binding [8]. Helix 18 (Fig. 3.1.), for example, terminates in a loop containing residues that interact with NAD^+. In this

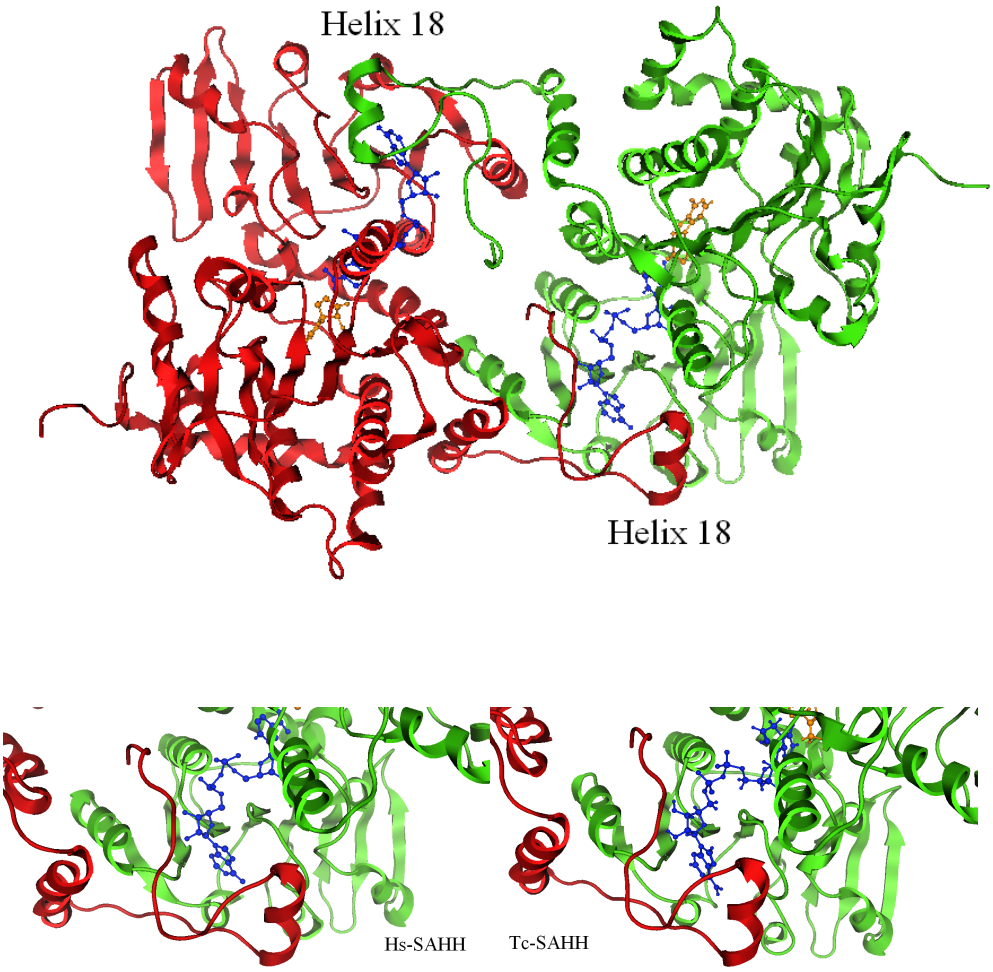

Figure 3.1. Above: the dimeric assocation of two monomeric subunits (red and green) within the tetrameric structure of Hs-SAHH (PDB 1A7A), showing the C-terminal extensions containing helix 18 which penetrate into the adjacent subunit. Helix 18 is relatively near the cofactor (blue) and relatively distant from the substrate (yellow substrate-analog structure). Below: Detail of the helix-18 region in Hs-SAHH and Tc-SAHH (PDB 1XBE), showing the C-terminal loop that proceeds from helix 18 and interacts with the cofactor.

paper, we present information that supports the hypothesis that helix 18 is an important element for human-parasitic distinctions in cofactor binding to SAHHs.

3.2. Methods

3.2.1. Site-directed mutagenesis.

All mutants were created by site-directed mutagenesis PCR. Each amplification reaction contained the following in a volume of 50 µL: 25 pmol of each primer, 20 nmol of each deoxynucleoside triphosphate, 20 ng of template DNA, 6 µL of 10x Pfu DNA ploymerase buffer and 3U Pfu DNA polymerase (Stratagene). Sequences of primers used for site-directed mutagenesis were:
5'-GCTAACTGATAACCAATGCCAGTACCTGGG-3' and
5'-CCCAGGTACTGGCATTGGTTATCAGTTAGC-3' for Hs-SAHH,
5'GACGAAGCTCACCGAGAAGCAGGCGCAGTACCTCGGCTGCCCCGT-3'&
5'-ACGGGGCAGCCGAGGTACTGCGCCTGCTTCTCGGTGAGCTTCGTC-3'for Tc-SAHH.

After 4 min of heat start step at 92 ˚C, 25 cycles of the following program were initiated: 20 second at 92 ˚C, 30 second at 55 ˚C and 20 min at 68 ˚C. PCR products were purified with PCR purification kit (Qiagen). After treated with Dpn I

(Biolab), the PCR products were transformed into BL21(DE3) *E. coli* (Stratagene). The sequences of mutant genes were confirmed by DNA sequencing.

3.2.2. Expression and purification of Hs-SAHH, Tc-SAHH and their mutants.

The expression of Hs-SAHH, Tc-SAHH and their mutants was basically the same as previously described [6, 7]. The transformed *E. coli* cells grew in 1 L of 2×YT medium containing ampicillin (100 mg/L) at 37 ^{o}C. At OD_{600} = 0.4 ~ 0.8, 1 mM isopropyl-1-thio-β-D-galactopyranoside was added to induce the protein expression at 37 ^{o}C for 8 h for Hs-SAHH and its mutant, and at 25 ^{o}C for 12 h for Tc-SAHH and its mutant. The procedures for purification of these enzymes were the same except that 50 μM NAD^{+} was added to the buffer in the case of purification of Tc-SAHH and its mutant.

3.2.3. Temperature-dependent fluorescence spectroscopy of Tc-SAHH and Tc-18Hs-SAHH in the presence of 8-anilino-1-naphthalene sulfonic acid.

Fluorescence emission spectra of holo-Tc-SAHH and its mutant holo-Tc-18Hs-SAHH (5.15 μM) in a solution containing a molar ratio of 12:1 ([dye]: [monomer]) of 8-anilino-1-naphthalene-sulfonic acid over protein were obtained

using a QuantaMaster™ spectrofluorometer (PTI, Monmouth Junction, NJ). The excitation wavelength was 372 nm and the emission was monitored at 480 nm over a range of temperature from 15 to 77.5 °C at 2.5 °C intervals.

3.3. Results

3.3.1. The stability of helix 18 in SAHHs, estimated from helix propensities, is greater for Hs-SAHH than for Tc-SAHH, Ld-SAHH, and Pf-SAHH.

The helix propensity of each helix 18 is the sum of the helix propensities of all residues in the helix (Fig. 3.1., Table 3.1.). A good measure of the helix propensity of a residue is the relative frequency with which the residue is present in helices, as calculated by Kallberg, et al, from a non-redundant set of protein sequences with known three-dimensional structures (1324 proteins, total of 269,058 amino acid residues) by PHD (profile network from HeiDelberg) [8, 9]. Helix-propensity values are typically used to predict secondary structure. Here, however, we presume that a helix with a higher total helix-propensity value may be more stable and therefore show less mobility and flexibility. As shown in Table 3.1., the helix propensities of helix 18 in Hs-SAHH and Pf-SAHH are the highest and the lowest, respectively.

3.3.2. Generation of SAHH mutants with altered structures of helix 18.

Table 3.1. The sequences and total helix propensity values for helix 18 of Hs-SAHH, Tc-SAHH, Ld-SAHH, and Pf-SAHHs. Individual sequence ranges for the helix are shown beneath the species identifier at left and the residue helix propensities are shown as subscripts.

SAHH	Sequences $_{(\text{propensity value})}$	Total helix propensity
Hs- (411-417)	$E_{(1.37)}K_{(1.14)}Q_{(1.34)}A_{(1.46)}Q_{(1.34)}Y_{(0.95)}L_{(1.36)}$	8.96
Tc- (416-422)	$A_{(1.46)}R_{(1.24)}Q_{(1.34)}A_{(1.46)}D_{(0.83)}Y_{(0.95)}I_{(1.07)}$	8.35
Ld- (416-422)	$P_{(0.40)}K_{(1.14)}Q_{(1.34)}A_{(1.46)}\ E_{(1.37)}Y_{(0.95)}I_{(1.07)}$	7.73
Pf- (459-465)	$D_{(0.83)}N_{(0.72)}Q_{(1.34)}C_{(0.75)}Q_{(1.34)}F_{(0.97)}L_{(1.36)}$	7.31

With guidance from the total helix propensities in Table 3.1., three mutant enzymes were created and compared to Hs-SAHH and Tc-SAHH. The mutants are (1) a Hs-SAHH mutant with its original helix 18 replaced with the one from Tc-SAHH and denoted Hs-18Tc-SAHH (E411A/K412R/Q415D), (2) a Tc-SAHH mutant with its original helix 18 replaced with the one from Hs-SAHH and denoted Tc-18Hs-SAHH (A416E/R417K/D420Q/I422L), and (3) a Hs-SAHH mutant with its original helix 18 replaced with the one from Pf-SAHH and denoted Hs-18Pf-SAHH (E411D/K412N/A414C/Y416F). The set of helix-18 mutants thus includes the "trypanosomized" human enzyme, the "humanized" trypanosomal enzyme, and a "plasmodiumized" human enzyme. This last mutant, Hs-18Pf-SAHH, represents the human enzyme modified to have the helix 18 of lowest total helical propensity present in any of the parasitic enzymes.

The mutant enzymes as well as the two wild type enzymes Hs-SAHH and Tc-SAHH were expressed, purified and characterized under very similar conditions. In all cases, it was determined by CD that the secondary structure was not detectably changed, and by size-exclusion chromatography that the tetrameric quaternary structure was intact. All enzymes were fully reconstituted with oxidized cofactor.

3.3.3. Catalytic kinetic constants of helix-18 mutant enzymes differ little from those of the wild-type enzymes.

Results of kinetic studies of Hs-SAHH, Tc-SAHH, and their helix-18 mutants are shown in Table 3.2. All enzymes exhibit nearly the same values for both the synthesis and hydrolysis of AdoHcy, minor exceptions being (1) the K_m for AdoHcy of Hs-SAHH is twice of Tc-SAHH; (2) K_m values for Hcy and AdoHcy of Tc-18Hs-SAHH are about half and four times, respectively, those of Tc-SAHH. The indication is thus that these mutations, relatively remote from the center of catalysis, have no major effects on catalysis.

3.3.4. The kinetics of the dissociation of NAD^+ from Hs-18Pf-SAHH and Tc-18Hs-SAHH show the same biphasic temperature dependences observed with Hs-SAHH and Tc-SAHH.

Eyring plots of the first-order rate constants k_{off} for dissociation of the cofactor NAD^+ from Hs-18Pf-SAHH (31 °C to 45.5 °C) and from Tc-18Hs-SAHH (21 °C to 45.5 °C) are similar to the ones for the two wild type enzymes (Fig. 3.2.): the dependences are non-linear for both enzymes, consisting of a linear low-temperature regime and a linear high-temperature regime. Data for the two temperature regimes were independently fitted by the Eyring equations eqs (2a) and (2b) as before [8].

$$k_{off} / (\mathbf{k}T/h) = \{\exp [(\Delta S^{\ddagger}_{\ell} / R) - (\Delta H^{\ddagger}_{\ell} / RT)]\} \quad (2a)$$

$$k_{off} / (\mathbf{k}T/h) = \{\exp [(\Delta S^{\ddagger}_{h} / R) - (\Delta H^{\ddagger}_{h} / RT)]\} \quad (2b)$$

Table 3.2. Kinetic parameters[a] for Hs-SAHH, Hs-18Tc-SAHH, Tc-SAHH, Tc-18Hs-SAHH and Hs-18Pf-SAHH measured in 50 mM phosphate buffer, pH 7.4, 1 mM EDTA at 37°C.

kinetic parameter	Hs-SAHH	Hs-18Tc-SAHH	Hs-18Pf-SAHH	Tc-18Hs-SAHH	Tc-SAHH
[Ado] varied for synthesis of AdoHcy					
k_{cat} (s^{-1})	12.5 ± 0.2	13.2 ± 0.4	11.8 ± 0.2	15.0 ± 0.5	15.5 ± 0.3
K_m (μM)	1.5 ± 0.1	1.4 ± 0.1	1.1 ± 0.1	2.0 ± 0.2	1.2 ± 0.1
[Hcy] varied for synthesis of AdoHcy					
k_{cat} (s^{-1})	16.2 ± 0.9	16.9 ± 1.1	14.6 ±1.2	15.6 ± 0.6	16.7 ± 1.1
K_m (μM)	160 ± 28	171 ± 24	188 ± 27	100 ± 12	219 ± 26
[AdoHcy] varied for hydrolysis of AdoHcy					
k_{cat} (s^{-1})	3.2 ± 0.1	3.3 ± 0.1	3.2 ± 0.1	3.2 ± 0.2	3.7 ± 0.1
K_m (μM)	6.4 ± 0.4	6.2 ± 0.4	5.8 ± 0.4	14.3 ± 0.3	3.2 ± 0.3

[a]*Standard deviations were obtained from least-squares fitting with Origin software, version 7.5. The fit was carried out with mean values from three experiments.*

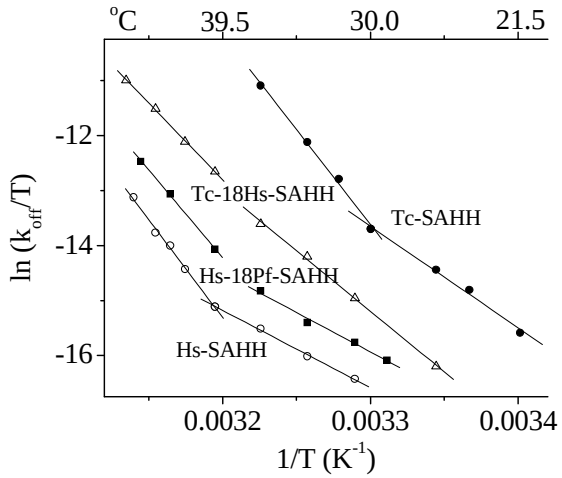

Figure 3.2. The temperature dependence of the rate constant k_{off} for dissociation of NAD^+ from Hs-SAHH, Hs-18Pf-SAHH, Tc-18Hs-SAHH, and Tc-SAHH. The lines are intersecting Eyring plots with the parameters given in Table 3.3.

Here, the subscript ℓ denotes the quasi-thermodynamic parameters of activation for the low-temperature regime and the subscript h denotes those for the high-temperature regime. The values of the quasi-thermodynamic parameters of activation are given in Table 3.3. The conversion temperature T_o for passage from the low-temperature regime to the high-temperature regime was calculated from eq (3) [8] and values are also given in Table 3.3.

$$T_o = [(\Delta H^{\ddagger}_h) - (\Delta H^{\ddagger}_\ell)] / [(\Delta S^{\ddagger}_h) - (\Delta S^{\ddagger}_\ell)] \quad (3)$$

Fig. 3.2. shows that the mutants Hs-18Pf-SAHH and Tc-18Hs-SAHH produce behavior that is intermediate between those of the two wild-type enzymes from which they derive. Table 3.3. shows that, as with the wild-type enzymes, a low-enthalpy, small positive entropy dependence at low temperatures is replaced by a high-enthalpy, large positive entropy change at high temperatures (the data are not persuasively biphasic for Tc-18Hs-SAHH, but a break is visually detectable).

3.3.5. The slow-binding kinetics of the association of NAD^+ with apo-Hs-18Pf-SAHH and apo-Tc-18Hs-SAHH show the same biphasic temperature dependences observed with Hs-SAHH and Tc-SAHH.

The wild-type enzymes were earlier found [8] to exhibit both a fast-binding phase (within the instrumental dead-time) and a slow-binding phase for the association of the apo-enzymes with NAD^+. The fast-binding phase was negligible at

Table 3.3. Quasi-thermodynamic parameters of activation for the low-temperature and high-temperature regimes, and conversion temperatures[a] T_o between the regimes for NAD^+ dissociation from Tc-SAHH (21 °C to 37 °C), Tc-18Hs-SAHH (26 °C to 46.5 °C), Hs-18Pf-SAHH (29 °C to 45.5 °C), and Hs-SAHH (31 °C to 45.5 °C) at pH 7.4.

Enzyme	**ΔS‡ℓ (J/mol-K)**	**ΔH‡ℓ (kJ/mol)**	**ΔS‡h (J/mol-K)**	**ΔH‡h (kJ/mol)**	**To, K**
Tc-SAHH	170 ± 15	154 ± 8	610 ± 30	287 ± 8	302 ± 34 (29 °C)
Tc-18Hs-SAHH	274 ± 1	181 ± 1	438 ± 9	232 ± 4	309 ± 11 (36 °C)
Hs-18Pf-SAHH	64 ± 7	119 ± 8	533 ± 18	265 ± 8	311 ± 19 (38 °C)
Hs-SAHH	50 ± 2	116 ± 4	600 ± 25	297 ± 9	314 ± 21 (41 °C)

[a]*Temperature of intersection of the high-temperature and low-temperature limbs of the temperature dependence and thus the apparent temperature of conversion between the two regimes.*

concentrations of NAD^+ of 5 μM and lower. Here the mutant enzymes were studied at 5 μM NAD^+. The first order rate constants k_{app} for association of NAD^+ with Hs-18Pf-SAHH and Tc-18Hs-SAHH were measured at 5 μM NAD^+ and used to calculate the second-order rate constants $k_{o,}$ as $k_{app}/[NAD^+]$ [8]. Fig. 3.3. presents the Eyring plots of the slow-binding rate constants k_o measured over a range of temperatures. A few representative points (not shown) were measured for Hs-18Tc-SAHH but were found to lie directly on the line for Hs-SAHH. We conclude that at least this property and perhaps others of Hs-SAHH are not altered by the 18Tc mutation. We therefore turned to Hs-18Pf-SAHH for further studies. The association kinetics and their temperature dependences for both Hs-18Pf-SAHH and Tc-18Hs-SAHH are distinctly different from the two wild-type enzymes and from each other (Fig. 3.3.).

A model developed previously [8] from similar data for the wild-type enzymes ascribes the decrease in association rate at higher temperatures to a (perhaps local) reversible unfolding phenomenon. The temperature dependence of the apparent association constant k_o is then described by eq (4), where we take the standard-state concentration of NAD^+, $[NAD^+]_{ss}$ = 1 M:

$$\ell n\,(k_o/T) = (\Delta S^{\ddagger}_{on} / R) - (\Delta H^{\ddagger}_{on} / RT) - \ell n\,\{1 + \exp[(\Delta S^{o}_{un} / R) - (\Delta H^{o}_{un} / RT)]\} - \ell n\,[NAD^+]_{ss} + \ell n\,(k/h) \qquad (4)$$

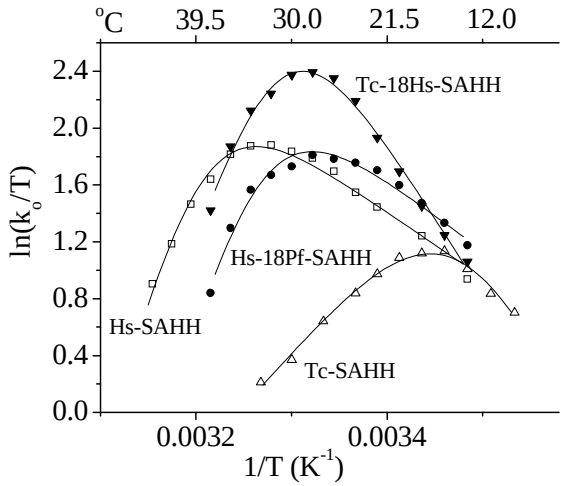

Figure 3.3. The temperature dependence of the rate constant for the slow-binding phase of the association of NAD^+ with the apo-forms of Hs-SAHH, Hs-18Pf-SAHH, Tc-18Hs-SAHH, and Tc-SAHH. The lines are plots of eq (4) with the parameters shown in Table 3.4.

Here the subscript “on” denotes the quasi-thermodynamic parameters of activation for cofactor binding and the subscript “un” denotes the thermodynamic parameters of the reversible unfolding process (thus $k_o = k_{on}/[1 + K_{un}]$). The values of the enthalpies and entropies are given in Table 3.4. The table also gives the ratio $\Delta H^o_{un}/\Delta S^o_{un}$, as a rough measure of the “melting temperature” for the presumed local structural transition.

3.3.6. Thermal structural perturbation of wild-type enzymes and helix-18 mutants analyzed by DSC and CD.

Fig. 3.4. presents thermograms obtained from DSC studies of wild-type and mutant enzymes as apo-enzymes, holo-enzymes, and holo-enzyme in the presence of 20 mM NAD^+. All the proteins showed an irreversible thermal unfolding process. A sharp reduction in heat capacity indicated that aggregation ensued rapidly after unfolding. Therefore, thermodynamic analysis by fitting data to models for reversible phase-transition processes is not possible. Thus, we hereafter use the term “stability” in this connection in a casual, non-thermodynamic sense simply to reflect changes in response of the protein to temperature variation, as detected by DSC and the spectroscopic techniques described below. Light-scattering measurements (data not shown) confirmed that aggregation followed unfolding.

Table 3.4. Thermodynamic and quasi-thermodynamic parameters[a] for NAD^+ association with Tc-SAHH, Tc-18Hs-SAHH, Hs-18Pf-SAHH, and Hs-SAHH at temperatures in the interval 11 - 45 °C, pH 7.4.

Enzyme	$\Delta S^{\ddagger}_{on}$ (J/K-mol)	$\Delta H^{\ddagger}_{on}$ (kJ/mol)	ΔS^{o}_{un} (J/K-mol)	ΔH^{o}_{un} (kJ/mol)	$\Delta H^{o}_{un}/\Delta_{Soun}$ (K)
Tc-SAHH	225 ± 13	118 ± 4	631 ± 8	182 ± 2	288 ± 5 (15 °C)
Tc-18Hs-SAHH	119 ± 19	89 ± 6	815 ± 5	247 ± 1	303 ± 2 (30°C)
Hs-18Pf-SAHH	- 42 ± 16	42 ± 5	765 ± 7	234 ± 2	306 ± 4 (33 °C)
Hs-SAHH	- 56 ± 9	38 ± 3	788 ± 5	243 ± 2	308 ± 3 (35 °C)

[a]*Parameters were obtained by least-squares fitting to eq 4 (Origin version 7.5). The subscript "on" identfies the quasi-thermodynamic parameters of activation for the binding rate constant of the slow-binding phase of cofactor binding. The subscript "un" identfies the equilibrium thermodynamic parameters for local unfolding in or near the cofactor binding site.*

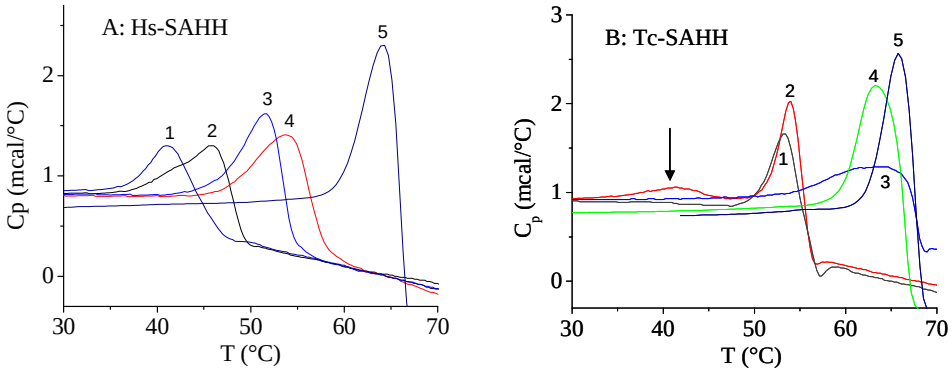

A:
1. apo-Hs-18Pf-SAHH
2. apo-Hs-SAHH
3. holo-Hs-18Pf-SAHH
4. holo-Hs-SAHH
5. holo-Hs-SAHH, 20 mM NAD^+.

B:
1. apo-Tc-SAHH
2. holo-Tc-SAHH
3. holo-Tc-18Hs-SAHH
4. holo-Tc-SAHH, 20 mM NAD^+
5. holo-Tc-18Hs-SAHH, 20 mM NAD^+.

Figure 3.4. DSC thermograms from 30 to 70 °C of the apo- and holo-forms (purified from E. coli cells, fully bound with cofactors: approximately 95 % of NAD^+ and 5 % of NADH) of Hs-SAHH, Hs-18Pf-SAHH, Tc-18Hs-SAHH, and Tc-SAHH.

Table 3.5. shows the apparent melting temperatures, which were taken to be the temperatures at which a maximum heat capacity was observed (Fig. 3.4A and 3.4B). In addition, data for CD observations are included in Table 3.5. and these agree with the DSC results in all cases.

Table 3.5. shows apo-Hs-SAHH is somewhat less thermally stable than apo-Tc-SAHH but that this difference is erased in the holo-enzymes and excess cofactor raises the melting temperatures of both enzymes further, either by assuring full cofactor-occupancy or by non-specific binding and stabilization. The observation that holo-Tc-SAHH melts at the same temperature as apo-Tc-SAHH is the result of an artifact: the DSC thermogram (Fig. 3.4.) shows that the cofactor dissociates at about 42 °C, so that the melting event at 53 °C reflects, in fact, the melting of the apo-enzyme (see also Fig. 3.5.).

The mutant Tc-18Hs-SAHH does not produce evidence in the data of Fig. 3.5. for such an anomaly, but the single peak in the thermogram of Fig. 3.4. is very broad, consistent with dissociation of the cofactor simultaneously with the larger structural changes. Consistent with this explanation, addition of excess cofactor produces a sharp peak in the thermogram, presumably by maintaining a high population of bound cofactor during global unfolding. The mutant Hs-18Pf-SAHH melts at slightly lower temperatures than the parent Hs-SAHH but is otherwise unremarkable with respect to more extensive unfolding.

Table 3.5. Apparent melting temperatures (˚C)[a] from differential scanning calorimetry (DSC, Fig. 3.4.) for the apo-enzyme and holo-enzyme forms (the latter also in the presence of 20 mM NAD^+) of Tc-SAHH, Tc-18Hs-SAHH, Hs-18Pf-SAHH, and Hs-SAHH, and similar data for apo-enzymes and holo-enzymes from circular dichroism (CD), determined from the midpoints of thermal unfolding curves.

	DSC			CD	
Enzyme	**Apo**	**Holo**	**Holo + 20 mM NAD^+**	**Apo**	**Holo**
Tc-SAHH	53.0 ± 0.2	53.2 ± 0.2	62.1 ± 0.4	54.0 ± 0.2	54.0 ± 0.2
Tc-18Hs-SAHH	53.0 ± 0.1	63.4 ± 0.2	65.2 ± 0.3	54.1 ± 0.2	62.0 ± 0.3
Hs-18Pf-SAHH	41.3 ± 0.2	51.4 ± 0.1	62.8 ± 0.5	41.2 ± 0.3	52.4 ± 0.5
Hs-SAHH	44.2 ± 0.1	55.2 ± 0.3	63.6 ± 0.4	44.4 ± 0.2	55.4 ± 0.3

[a]*Errors were obtained from the range of two independent measurements.*

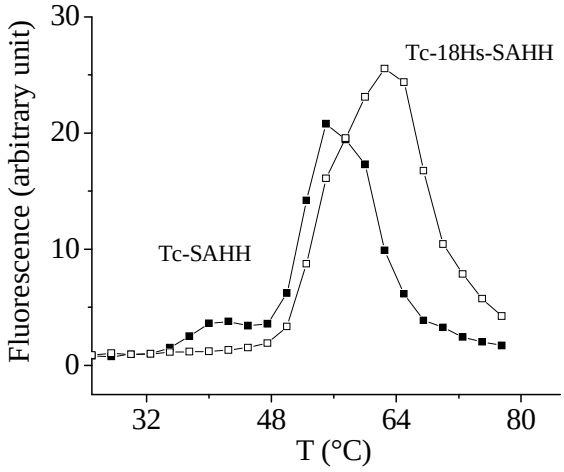

Figure 3.5. Thermally induced fluorescence changes for Tc-SAHH and Tc-18Hs-SAHH in the presence of the dye 8-anilino-1-naphthalene-sulfonate, which fluoresces when bound in a non-polar environment. At 42 °C, the cofactor dissociates from Tc-SAHH and the dye occupies the cofactor site. No such dissociation is seen with Tc-18Hs-SAHH. The large maxima result from global unfolding of apo-Tc-SAHH and of holo-Tc-18Hs-SAHH.

All holo-enzymes exhibit, in the presence of excess NAD^+, very similar apparent melting temperatures of around 62 - 65 °C as expected for their high sequence similarity and consistent with the composition of helix-18 having little or no influence on global unfolding.

The apo-enzymes apo-Hs-SAHH and apo-Hs-18Pf-SAHH show similar melting temperatures of 44 and 41 °C, respectively, while the apo-Tc-SAHH and apo-Tc-18Hs-SAHH both melt at 53 °C, consistent with a somewhat greater global stability for Tc-SAHH than for Hs-SAHH, with the mutated helix-18 producing no change in the thermal behavior of the wild-type enzyme. The holo-enzymes uniformly melt about 10 - 11 °C higher than do the apo-enzymes, consistent with thermal stabilization by the cofactor, except for the anomalous holo-Tc-SAHH (see above).

3.4. Discussion

3.4.1. The total helix propensities of helix 18 and structures for human and parasitic SAHHs suggest lower stability and perhaps larger mobility for the parasitic helices.

Helix 18 in the structure of SAHHs is relatively distant from the substrate-binding region and the surrounding catalytic residues [10] of the active site but

relatively close to the cofactor binding site (Fig. 3.1.). Helix 18 therefore seemed an attractive possibility for a significant contribution to the distinct kinetics and thermodynamics of cofactor association and dissociation observed for Hs-SAHH and Tc-SAHH, while at the same time conserving the catalytic kinetic properties of the two enzymes. We explored this hypothesis initially by use of helix propensities, supported by X-ray structures.

Table 3.1. shows the sequences in the helix-18 regions of Hs-SAHH, Tc-SAHH, Ld-SAHH, and Pf-SAHH, together with the total helix propensity for helix-18 in each of the enzymes. As predictors that a peptide segment will assume a helical conformation in a statistically averaged protein environment [9], helix propensities are limited by the omission of effects from nearby residues and their side chains in the primary sequence and the effect of environmental factors not accounted for in the statistical average. X-ray crystallographic structural data, now available [1, 2] for Hs-SAHH, Pf-SAHH, and Tc-SAHH, however, indicate some mitigating factors. Helix 18 in all of these SAHHs is located on the enzyme surface and makes few interactions with other parts of the protein (Fig. 3.6.).

All of the interactions identified in Fig. 3.6. suggest a greater stability for Hs-SAHH, and secondarily for Tc-SAHH, than for the other enzymes. Furthermore, the negatively charged E411, near the N-terminus of helix 18 in Hs-SAHH, should interact favorably with the helix dipole [11, 12] but is replaced by electrically neutral

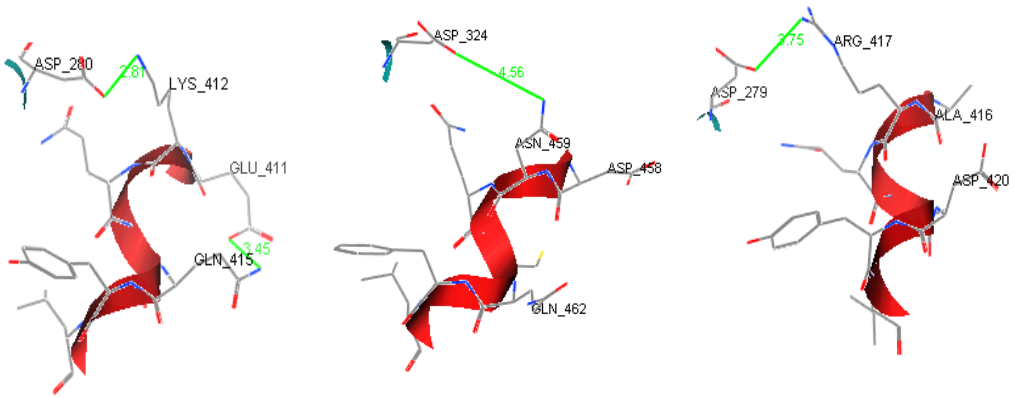

Hs PF TC

Figure 3.6. Hydrogen bonds formed between residues of helix 18 and nearby residues of the enzyme and among the residues within helix 18 for Hs-SAHH, Tc-SAHH, and Pf-SAHH.

residues in two of the three parasitic enzymes (Table 3.1.). The electrically neutral Q415 toward the C-terminus of the helix in Hs-SAHH is replaced by destabilizing [11, 13] negatively charged residues in two of the three parasitic enzymes.

The helix-propensity prediction (Table 3.1.) of a stability order for helix 18 of Hs-SAHH > Tc-SAHH > Ld-SAHH > Pf-SAHH appeared sufficiently supported by structural data to encourage further investigation of the effects of helix-18 sequences on cofactor binding and other properties of the human and parasitic enzymes. In addition to serving as indicators of helix stability, the helix propensities seemed possible indicators of the subtler property of helix mobility or flexibility. If it is assumed that a more stable or immobile helix-18 would provide a more stable cofactor binding site, then the results are consistent with the observation that the human enzyme binds NAD^+ more tightly than the parasitic enzymes [6-8].

3.4.2. Catalytic properties of wild-type and mutant enzymes.

Investigations of the role of helix 18 in the distinct properties of human and parasitic enzymes were pursued through construction of three mutants for comparison with wild-type enzymes: (1) Hs-18Tc-SAHH, the human enzyme bearing the helix 18 of Tc-SAHH in place of its own, (2) Tc-18Hs-SAHH, the trypanosomal enzyme containing the helix 18 of Hs-SAHH, and (3) Hs-18Pf-SAHH, the human enzyme with the helix 18 of Pf-SAHH. As will be described below, the properties of Hs-

18Tc-SAHH were found at an early point in this work to be essentially indistinguishable from those of Hs-SAHH. Therefore Hs-18Pf-SAHH was prepared with the sequence of helix 18 corresponding to that of lowest helix propensity; indeed the properties of this mutant were different from those of Hs-SAHH and further studies made use of this mutant. As expected, mutations in helix 18, quite distant from the catalytic site, produced no major changes in the catalytic properties of the wild-type enzymes, which are very similar to each other in this regard (Table 3.2.).

3.4.3. Helix 18 is stabilized by the binding of NAD^+ and a thermally induced structural change in or near helix 18 accelerates the dissociation of NAD^+.

The dissociation of NAD^+ from Hs-SAHH and Tc-SAHH was earlier found [8] to occur in a simple first-order fashion. For both enzymes, the rate constants increased with temperature biphasically, a transition occurring at 29 °C for Tc-SAHH and at 41 °C for Hs-SAHH. The transition altered a linear Eyring dependence with low enthalpy of activation and small positive entropy of activation (low temperatures) to a linear Eyring dependence with high enthalpy of activation and large positive entropy of activation (high temperatures). The sharpness of the transition from a low-temperature to high-temperature regime suggests a structural transition as the origin of this relatively abrupt change. As elaborated below, changes in helix 18 seem a likely source of this behavior.

If the conversion between the two temperature regions is caused by a thermal perturbation of helix 18, then the activation parameters of Table 3.3. appear consistent with a view that the altered structure at higher temperatures binds the cofactor more tightly but generates substantially more entropy upon its release. A second point is that the apparent unfolding in the presence of the cofactor results in an accelerated dissociation of the cofactor. This involves a large positive entropy of activation that more than compensates for an increased enthalpy of activation. This finding would also be consistent with a greater mobility of the enzyme following the unfolding of helix 18 and dissociation of the cofactor.

3.4.4. Helix 18 (and/or its neighborhood) is the site of local structural perturbation that attenuates the association of NAD^+ with apo-SAHHs at higher temperatures.

As described above, NAD^+ associates with Hs-SAHH and Tc-SAHH in a relatively complex manner that, in contrast to the catalytic properties, is quantitatively different for the two enzymes. Binding occurs in two phases, a fast-binding phase that occurs within the dead-time of the measurement method and a slow-binding phase that occurs over some minutes and exhibits saturation with respect to the cofactor [8], with the results in Fig. 3.3. and Table 3.4. referring to the slow-binding phase.

A striking difference in the wild-type enzymes is the local-unfolding temperature of about 35 °C for Hs-SAHH and about 15 °C for Tc-SAHH, as noted earlier [8]. It was also earlier realized [8] that the structural alteration cannot correspond to global unfolding of the enzyme since that occurs in the range of 62-65 °C (Table 3.5.).

The data for the two mutants, Hs-18Pf-SAHH and Tc-18Hs-SAHH, lend strong support to the hypothesis that the site of this local alteration is, in fact, helix 18. Introduction of the plasmodial helix 18 into the human enzyme shifts the perturbation temperature from 35 to 33 °C (although this shift is within the considerable error of the curve fit to the model, the phenomenological shift in the rate-constant maxima is clearly visible in Fig. 3.3.). More dramatically, introduction of the human helix 18 into the trypanosomal enzyme shifts this transition temperature in the opposite direction, from 15 to 30 °C, clearly beyond the errors of curve fitting and also readily visible in the temperature-dependent kinetic data of Fig. 3.3. These results are consistent with the concept that helix 18 of Hs-SAHH is, as indicated by helix propensities and structural information, a more stable and perhaps rigid entity than is helix 18 of Tc-SAHH and Pf-SAHH.

Furthermore, the data suggest that the general context of helix 18 is more dynamic in Tc-SAHH than in Hs-SAHH. Thus, introduction of the more rigid human helix-18 into the presumably flexible environment of Tc-SAHH results in a large rise

in the transition temperature, while introduction of the presumably most flexible plasmodial helix 18 into the rigid Hs-SAHH environment results in only a small downward shift of the transition temperature. The same idea can also explain the observation that the introduction of the trypanosomal helix 18 into the rigid Hs-SAHH matrix produces little or no effect.

It should be noted that the approximate order of the transition temperatures of helix 18 in the apo-enzymes, as here estimated from the cofactor association kinetics (Table 3.4.), namely, Hs-SAHH (35 °C) > Hs-18Pf-SAHH (33 °C) > Tc-18Hs-SAHH (30 °C) > Tc-SAHH (15 °C) is the same as the order of the estimated conversion temperatures from the low-temperature to the high-temperature regime of the cofactor-dissociation kinetics (Table 3.3.) discussed above, namely: Hs-SAHH (41 °C) > Hs-18Pf-SAHH (38 °C) > Tc-18Hs-SAHH (36 °C) > Tc-SAHH (29 °C). Admittedly, in some cases such comparisons fall well within the computed errors, but visual analysis of the figures lends support to their validity.

Most simply, the conversion temperatures for dissociation of cofactor are larger (29 °C to 41 °C) than the transition temperatures for its association (15 °C to 35 °C). This result would indicate that the helix has significantly greater thermal stability in the presence of the cofactor. Scheme 3.1. summarizes the situation. At left, the apo-enzyme consists of an equilibrium mixture of two forms: a high-temperature form incapable of binding the cofactor C and a low-temperature form capable of

Scheme 3.1. Temperature effects on the cofactor on-rates and off-rates.

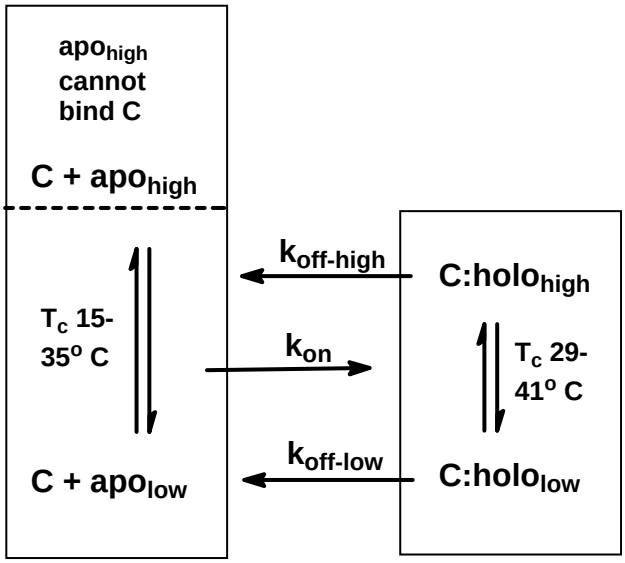

binding C, so that the on-reaction (rate constant k_{on}) proceeds from the fraction of apo-enzyme in the low-temperature form. The conversion temperature between the two forms is 15-35 °C and we suspect the conversion is a local structural change in or near helix 18. The holo-enzyme at right likewise consists of an equilibrium mixture of low-temperature and high-temperature forms. Each releases the cofactor C but the high-temperature form does so more rapidly, with a steeper temperature dependence. The conversion temperatures here are larger, around 29-41 °C. Again we suppose the conversion to be caused by local structural changes in or near helix 18. Conceivably the structural changes involved in the on-reaction and off-reaction are the same or similar but the conversion temperatures tend to be higher for the off-reaction because the cofactor stabilizes helix 18 and its neighborhood.

3.4.5. Helix 18 has only a minor role in the global stability of SAHHs.

The global unfolding temperatures given in Table 3.5. show that, for all forms of the wild-type and mutant enzymes, global unfolding occurs for apo-enzymes in the range 41-65 °C and for holo-enzymes in the range 51-65 °C. This is beyond the temperature range of 15-41 °C for which structural alterations of helix 18 are proposed as the cause of the biphasic transitions observed in the kinetics of association and dissociation of the cofactor from SAHHs. This strongly suggests that the phenomenon involved in the cofactor association-dissociation kinetics is not due

to the onset of global unfolding, but rather results from the proposed conformational changes in helix 18.

3.5. Conclusion

Previous studies [8] showed that the human enzyme Hs-SAHH and the parasitic enzyme Tc-SAHH have similar catalytic properties but differ distinctly in the on- and off-rates of the tightly bound NAD^+ cofactor. Structural information and calculations of helix propensities suggest that differences in the stability and possible mobility of helix 18, near the C-terminus and embedded into the cofactor binding site of the partner subunit, might account for these observations. Mutants were therefore constructed of the wild-type enzymes Hs-SAHH and Tc-SAHH in which the human helix 18 (predicted to be more stable and perhaps more rigid than the parasitic helices) has been replaced by a plasmodial helix 18 (predicted to be less stable), Hs-18Pf-SAHH, and in which the trypanosomal helix 18 (predicted to be of lower stability) has been replaced by the human helix 18 (Tc-18Hs-SAHH). These wild-type and mutant enzymes (1) exhibited essentially the same catalytic kinetic constants; (2) showed biphasic temperature dependences of the dissociation rate constants for NAD^+, with a thermal inflection reflecting structural changes in or near the cofactor binding sites, and the transition temperatures sytematically varying from 29 °C (Tc-SAHH) to 41 °C (Hs-SAHH), the two mutants falling between these limits; (3) showed biphasic temperature dependences of the association rate constants for

NAD^+, with a thermal maximum reflecting local changes in or near the cofactor binding sites, and the transition temperatures sytematically varying from 15 °C (Tc-SAHH) to 35 °C (Hs-SAHH), the two mutants again falling between these limits; (4) underwent more global unfolding at temperatures in the range 62 °C to 65 °C, indicating that helix 18 has little direct role in global thermal stability, and that the thermal transitions at considerably lower temperatures involved in the on-off rate alterations for NAD^+, indeed reflect local, reversible structural changes, probably within helix 18 itself.

Helix 18 and other nearby structures may therefore identify critical sites at which inhibitory ligands that have the capacity to distinguish between human and parasitic enzymes could be designed to bind. Such compounds have the potential to function as specific antiparasitic drugs. Figure 3.6. shows some of the details of the structures of helix 18 in Hs-SAHH, Tc-SAHH, and Pf-SAHH.

3.6. References

1. Yang, X., et al., *Catalytic strategy of S-adenosyl-L-homocysteine hydrolase: transition-state stabilization and the avoidance of abortive reactions.* Biochemistry, 2003. **42**(7): p. 1900-9.
2. Tanaka, N., et al., *Crystal structure of S-adenosyl-L-homocysteine hydrolase from the human malaria parasite Plasmodium falciparum.* J Mol Biol, 2004. **343**(4): p. 1007-17.
3. Li, Q.-S., Huang, W. , *The x-ray structure of S-adenosylhomocysteine hydrolase from Trypanosoma cruzi bound with Neplanocin A.* PDB code 1XBE, 2004.
4. Ault-Riche, D.B., C.S. Yuan, and R.T. Borchardt, *A single mutation at lysine 426 of human placental S-adenosylhomocysteine hydrolase inactivates the enzyme.* J Biol Chem, 1994. **269**(50): p. 31472-8.
5. Komoto, J., et al., *Effects of site-directed mutagenesis on structure and function of recombinant rat liver S-adenosylhomocysteine hydrolase. Crystal structure of D244E mutant enzyme.* J Biol Chem, 2000. **275**(41): p. 32147-56.
6. Yang, X. and R.T. Borchardt, *Overexpression, purification, and characterization of S-adenosylhomocysteine hydrolase from Leishmania donovani.* Arch Biochem Biophys, 2000. **383**(2): p. 272-80.
7. Parker, N.B., et al., *Trypanosoma cruzi: molecular cloning and characterization of the S-adenosylhomocysteine hydrolase.* Exp Parasitol, 2003. **105**(2): p. 149-58.

8. Li, Q.-S., et al., *Comparative kinetics of cofactor association and dissociation for the human and trypanosomal s-adenosylhomocysteine hydrolases. 1. Basic features of the association and dissociation processes.* Biochemistry, 2007. **46**(19): p. 5798-809.

9. Kallberg, Y., et al., *Prediction of amyloid fibril-forming proteins.* J Biol Chem, 2001. **276**(16): p. 12945-50.

10. Elrod, P., et al., *Contributions of active site residues to the partial and overall catalytic activities of human S-adenosylhomocysteine hydrolase.* Biochemistry, 2002. **41**(25): p. 8134-42.

11. Facchiano, A.M., G. Colonna, and R. Ragone, *Helix stabilizing factors and stabilization of thermophilic proteins: an X-ray based study.* Protein Eng, 1998. **11**(9): p. 753-60.

12. Marshall, S.A., C.S. Morgan, and S.L. Mayo, *Electrostatics significantly affect the stability of designed homeodomain variants.* J Mol Biol, 2002. **316**(1): p. 189-99.

13. Richardson, J.S. and D.C. Richardson, *Amino acid preferences for specific locations at the ends of alpha helices.* Science, 1988. **240**(4859): p. 1648-52.

Chapter 4

The Role of the Conserved Hydrophobic Residues in β-Sheet A of the Rossmann Motif in Comparative Kinetics of Cofactor Association and Dissociation for Hs-SAHH and Tc-SAHH.

4.1. Introduction

This chapter has focused on the NAD^+ binding motif (Rossmann motif) and its contribution to the kinetics and thermodynamics of NAD^+ dissociation and association for SAHH. It emerges as useful, as will be apparent, to include the properties of the wild-type enzyme from *Plasmodium falciparum.*

The Rossmann motif (Fig. 4.1.), a βαβαβ unit, is found in most $NAD(P)^+$ binding proteins [1, 2]. The motif that binds $NAD(P)^+$ usually has a second repeated βαβαβ unit that is structurally related to the first one by approximately a two fold rotation, with the more N-terminal β-sheets adjacent to each other. Among the 30-35 amino acids of the fingerprint sequences of the Rossmann motif, there are six small, generally conserved, hydrophobic residues, distributed with two each on the first β-sheet (βA in SAHH), the first α-helix (αB in SAHH), and the second β-sheet (βB in SAHH). These six residues form the hydrophobic core of the motif, and are

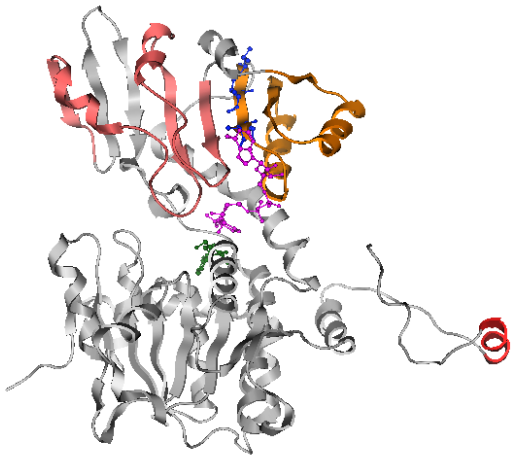

Figure 4.1. The monomeric-subunit structure of Hs-SAHH (pdb file 1LI4). The N-terminus is at bottom left and the large N-terminal domain is the substrate-binding or catalytic domain (substrate in green ball-and-stick representation), while the large upper domain is the cofactor-binding domain (cofactor in purple ball-and-stick representation). The Rossmann motif [2] consists of β-sheet A (residues 215-219 in blue ball-and-stick representation), followed by α-helix B (223-234), β-sheet B (238-242), α-helix C (246-254), and β-sheet C (258-260), all of which along with intervening loops are shown in gold ribbon representation [3]. The C-terminal extension is at right; it protrudes into the partner subunit where helix 18 (red) forms part of the cofactor-binding site of that subunit. A similar extension from the partner subunit also contributes its helix 18 to the binding site shown here. Helix 18 (red) was the locus of mutational studies reported in the preceding publication [4] and β-sheet A (blue) is the locus of mutational studies reported in the present paper. A second repeat of the Rossmann motif (residues 271-322) is shown in pink ribbon representation: no alterations in this region were made in the present work.

commonly considered necessary for proper steric relationships in the packing of the β-sheets against the α-helices [1].

SAHH exhibits two classical Rossmann motifs in each monomeric subunit: one is in the substrate-binding domain (recall that the substrate is a nucleoside) and the other in the cofactor-binding domain. In this study, only the Rossmann motif in the NAD^+ binding domain (which consists of residues 215 through 260 in Hs-SAHH; Fig. 4.1.) was subjected to systematic alteration. A second repeated Rossmann motif, shown in pink in Fig. 4.1. (residues 271-322), was not altered.

Alignment of the 30-35 amino acids of the fingerprint sequences of the Rossmann motif in the NAD^+-binding domain of human and parasitic (*Trypansoma cruzi*, *Plasmodium falciparum*, and *Leishmania donovani*) SAHHs reveals that the two small, generally conserved, hydrophobic residues on β-sheet A are conserved as hydrophobic residues in Hs-SAHH and Pf-SAHH, but are replaced by two hydrophilic residues in Tc-SAHH and Ld-SAHH (Table 4.1.). The replacement of the hydrophobic residues by two hydrophilic residues would seem likely to weaken the stabilizing hydrophobic interactions and thus increase the flexibility of the hydrophobic core region formed by the six hydrophobic residues and other residues. Such an increased flexibility could influence the kinetics and thermodynamics of NAD^+ association and dissociation. To examine this hypothesis, a Tc-SAHH mutant (Tc-βAHs-SAHH [Tc-(T214V, C216V)-SAHH], a partially "humanized" parasite enzyme) was constructed with the two hydrophilic residues of β-sheet A replaced by

Table 4.1. The sequences and β-sheet-propensity values for β-sheet A (Fig. 4.1.) of the Rossmann motif in the NAD^+ binding domain of Hs-SAHH, Hs-βATc-SAHH, Tc-βAHs-SAHH, Tc-SAHH, Pf-SAHH and Ld-SAHH. Individual sequence ranges for β-sheet A are shown beneath the species identifier at left and the β-sheet propensities [5] of the individual residues are shown as subscripts.

SAHH	**Sequences (propensity value)**	**Total β-sheet-propensity**
Hs- (215-219)	$V_{(1.89)}A_{(0.78)}V_{(1.89)}V_{(1.89)}A_{(0.78)}$	7.23
Hs-βATc- (215-219)	$T_{(1.21)}A_{(0.78)}C_{(1.26)}V_{(1.89)}A_{(0.78)}$	5.92
Tc-βAHs- (214-218)	$V_{(1.89)}A_{(0.78)}V_{(1.89)}V_{(1.89)}C_{(1.26)}$	7.71
Tc- (214-218)	$T_{(1.21)}A_{(0.78)}C_{(1.26)}V_{(1.89)}C_{(1.26)}$	6.40
Pf- (259-263)	$I_{(1.65)}V_{(1.89)}V_{(1.89)}I_{(1.65)}C_{(1.26)}$	8.34
Ld- (214-218)	$T_{(1.21)}C_{(1.26)}C_{(1.26)}V_{(1.89)}C_{(1.26)}$	6.88

the two hydrophobic residues present at the corresponding positions in Hs-SAHH. A Hs-SAHH mutant (Hs-βATc-SAHH [Hs-(V215T, V217C)-SAHH], a partially "parasitized" human enzyme) was created with the two hydrophobic residues of β-sheet A replaced by the two hydrophilic residues present in β-sheet A of Tc-SAHH. The kinetics and thermodynamics of NAD^+ association and dissociation were investigated and the results compared with those for the wild type enzymes, Hs-SAHH, Tc-SAHH, and Pf-SAHH.

4.2. Methods

4.2.1. Site-directed mutagenesis.

All mutants were created by site-directed mutagenesis using PCR. Each amplification reaction contained the following in a volume of 50 µL: 25 pmol of each primer, 20 nmol of each deoxynucleoside triphosphate, 20 ng of template DNA, 6 µL of 10x Pfu DNA ploymerase buffer and 3U Pfu DNA polymerase (Stratagene). The sequences of the primers used for site-directed mutagenesis were

5'-GGCAAGACAGCGTGTGTAGCAG-3' and

5'-CTGCTACACACGCTGTCTTGCC-3' for Hs-SAHH, and

5'-GCTGGAAAGGTTGCCGTTGTTTGTGG-3' and

5'-CCACAAACAACGGCAACCTTTCCAGC-3'for Tc-SAHH. After 4 min of a heat-start step at 92˚C, 25 cycles of the following program were initiated: 20 sec at

92˚C, 30 sec at 55˚C and 20 min at 68˚C. PCR products were purified with a PCR purification kit (Qiagen). After treatment with Dpn I (Biolab), the PCR products were transformed into BL21(DE3) *E. coli* (Stratagene). The sequences of mutant genes were confirmed by DNA sequencing.

4.2.2. Determination of rate constants for association of NAD^+ with apo-enzymes (apparent first-order rate constant k_{app} and apparent second-order rate constant k_o).

This process was executed as described previously [6]. Typically, except for Pf-SAHH and Tc-βAHs-SAHH, a 50 μL solution (50 mM phosphate buffer, pH 7.4, 1 mM EDTA) containing 2 μM apo-enzyme was added to a pre-incubated 50 μL aliquot of NAD^+ solution with a concentration in the range from 2 to 600 μM. Samples were taken for activity assay at measured times during incubation at the desired temperature. The measured activities A were either converted to the amount of enzyme:NAD^+ complex or used directly in eq. 1.

$$A = A_f + (A_o - A_f)[\exp(-k_{app}t)] \quad (1)$$

Here, A is the activity measured at time t, A_o is the activity at the apparent time zero (reflecting reaction during the dead-time of the experiment), A_f is the activity at the end of the experiment, and k_{app} is a first-order rate constant for association that generally will be a function of $[NAD^+]$. At $[NAD^+]$ = 5 μM, A_o is

quite small and k_{app} is approximately proportional to [NAD^+]; an apparent second-order rate constant for the association reaction k_o was therefore calculated from data at this concentration as $k_o = k_{app}/[NAD^+]$.

For Pf-SAHH and Tc-βAHs-SAHH, the method is the same as described above except that apo enzyme concentration was 10 μM, NAD^+ concentration was in the range from 0.1 to 20 mM and the k_o was calculated from data at 2 mM NAD^+ concentration as $k_o = k_{app}/[NAD^+]$.

4.2.3. Determination of the rate constants (k_{off}) for dissociation of NAD^+ from Hs-βATc-SAHH, Pf-SAHH, and Tc-βAHs-SAHH.

Briefly, NAD^+ was allowed to dissociate from fully reconstituted enzyme in the presence of excess NADH which irreversibly traps each vacated binding site. The decrease in enzyme activity occurred in a first-order fashion with a rate constant $k_{obs} = k_{off} + k_{ina}$, where k_{ina} is the first-order rate constant for thermal inactivation, determined in control experiments. The dissociation rate constants k_{off} were calculated as $k_{off} = k_{obs} - k_{ina}$. The measurements for Pf-SAHH reconstituted *in vitro* and Tc-βAHs-SAHH reconstituted *in vitro* were carried out on a much shorter time scale and thus, in contrast to the above, NADH, alcohol dehydrogenase, and 2-propanol were not added; no measurement of k_{ina} was made; and the dissociation process was carried out at 4 ^oC, instead of at 37 ^oC.

4.2.4. Notation for cofactor-association rate constants and calculation of the cofactor dissociation constant (K_d).

Binding of NAD^+ occurs on both a fast time-scale, for which rate constants are not obtained, and a slow time-scale with an apparent first-order rate constant $k_{app.}$ The rate constant k_{app} exhibits saturation kinetics with [NAD^+] according to eq. (2c) below, yielding a second-order rate constant for slow binding k_a/K_a. At sufficiently low [NAD^+], the ratio $k_{app}/[NAD^+]$ yields a good approximation to k_a/K_a, which we denote k_o. As the temperature is increased, a local, reversible unfolding phenomenon inhibits association of NAD^+, such that the temperature dependence of k_o is described by $k_o = k_{on}/(1 + K_{un})$, where K_{un} is the equilibrium constant for the local, reversible unfolding process. Here k_{on} is the approximate second-order rate constant for association of [NAD^+] with fully folded enzyme. The value of the equilibrium dissociation constant of NAD^+ can be calculated as the ratio of off-rate constant k_{off} to the on-rate constant k_a/K_a or approximated as k_{off}/k_{on} or, at temperatures where unfolding is negligible, k_{off}/k_o.

4.3. Results

4.3.1. The mutant enzymes Tc-βAHs-SAHH and Hs-βATc-SAHH have secondary and quaternary structure unaltered from the wild-type enzymes.

The sequences of β-sheet A of the Rossmann motifs in Hs-SAHH, Pf-SAHH and Tc-SAHH are listed in Table 4.1. To generate Tc-βAHs-SAHH, the hydrophilic residues T214 and C216 of Tc-SAHH were replaced by the valines present at the corresponding positions (V215, V217) of Hs-SAHH (thus mutations T214V/C216V of Tc-SAHH). To generate Hs-βATc-SAHH, mutations V215T and V217C were introduced in Hs-SAHH. Studies of the CD spectra and size-exclusion chromatography showed that the mutations had no significant effects on secondary or quaternary structure (data not shown; the methods and results were very similar to those exemplified in reference [7]).

4.3.2. Catalytic properties of mutant enzymes differ from those of the wild-type enzymes only by small factors.

Table 4.2. shows the steady-state kinetic parameters obtained from a partial kinetic characterization of Pf-SAHH, Hs-βTc-SAHH, and Tc-βHs-SAHH. The parameters consist, for the hydrolysis of AdoHcy, of the values of k_{cat}, K_m, and their ratio (the full kinetics) and, for the synthesis of AdoHcy, the values of k_{cat} and K_m from variation of [Hcy] at a single concentration of Ado (ca. $250K_{mAdo}$) and from

Table 4.2. Kinetic parameters[a] for Hs-SAHH, Hs-βATc-SAHH, Pf-SAHH, Tc-βAHs-SAHH and Tc-SAHH measured in 50 mM phosphate buffer, pH 7.4, 1 mM EDTA at 37°C.

kinetic parameter	Hs-SAHH[b]	Hs-βATc-SAHH	Pf-SAHH	Tc-βAHs-SAHH	Tc-SAHH[b]
[Ado] varied for synthesis of AdoHcy at [Hcy] = 1mM = ca. 5K_{mHcy}					
k_{cat} (s^{-1})	12.5 ± 0.2	6.5 ± 0.2	2.1 ± 0.2	1.4 ± 0.1	15.5 ± 0.3
K_m (μM)	1.5 ± 0.1	3.5 ± 0.1	2.0 ± 0.3	0.7 ± 0.1	1.2 ± 0.1
$10^6 k_{cat}/K_m$ ($M^{-1}s^{-1}$)	8.3 ± 0.6	1.9 ± 0.08	1.1 ± 0.2	2.0 ± 0.3	12.9 ± 1.1
[Hcy] varied for synthesis of AdoHcy at [Ado] = 1 mM = ca. 250K_{mAdo}					
k_{cat} (s^{-1})	16.2 ± 0.9	6.2 ± 0.3	2.0 ±0.1	1.4 ± 0.1	16.7 ± 1.1
K_m (μM)	160 ± 28	135 ± 18	68 ± 5	40 ± 6	219 ± 26
$10^6 k_{cat}/K_m$ ($M^{-1}s^{-1}$)	0.10 ± 0.02	0.05 ± 0.01	0.03 ± 0.003	0.04 ± 0.01	0.08 ± 0.01
[AdoHcy] varied for hydrolysis of AdoHcy					
k_{cat} (s^{-1})	3.2 ± 0.1	3.1 ± 0.1	0.5 ± 0.1	0.8 ± 0.1	3.7 ± 0.1
K_m (μM)	6.4 ± 0.4	10.8 ± 0.4	2.1 ± 0.1	6.2 ± 0.4	3.2 ± 0.3
$10^6 k_{cat}/K_m$ ($M^{-1}s^{-1}$)	0.50 ± 0.03	0.29 ± 0.01	0.24 ± 0.05	0.13 ± 0.02	1.2 ± 0.5

[a]Standard deviations were obtained from least-squares fitting of specific velocities to the Michaelis-Menten equation by Origin version 7.5. The fit was carried out with the mean of values from three experiments. [b]Data for Tc-SAHH and Hs-SAHH from reference [6].

variation of [Ado] at a single concentration of Hcy (ca. $5K_{mHcy}$). Corresponding values for Hs-SAHH and Tc-SAHH from a previous study are also included in Table 4.2. Although the kinetic information on the synthetic reaction is incomplete (a complete characterization with simultaneous variation of [Ado] and [Hcy] would have yielded precise values of K_{mAdo}, K_{mHcy}, and K_{iAdo} [8]), the results are adequate to demonstrate that these mutations in β-sheet A produce no large effects on the catalytic properties of either parent enzyme. All properties of Hs-βATc-SAHH are within 4-fold of the corresponding properties of Hs-SAHH. All properties of Tc-βAHs-SAHH are within about 12-fold of the corresponding properties of Tc-SAHH.

4.3.3. The dissociation of NAD^+ from Hs-βATc-SAHH is slightly faster than from Hs-SAHH and the dissociation of NAD^+ from Tc-βAHs-SAHH is 13 times slower than from Tc-SAHH.

As previously observed with Hs-SAHH, Tc-SAHH and their mutants in the helix-18 region [6, 9], the dissociation of cofactor from the holoenzymes leads to a simple mono-exponential decay of the enzyme activity from its initial value to zero. The same is true with the β-sheet A mutants and Pf-SAHH examined here (Fig. 4.2.). Hs-βATc-SAHH, with the two hydrophobic residues in β-sheet A replaced by two hydrophilic residues (see Table 4.1.), showed a slightly faster NAD^+ dissociation rate than the wild type Hs-SAHH enzyme. Tc-βAHs-SAHH, having the two hydrophilic residues in β-sheet A replaced by two hydrophobic residues, showed a NAD^+

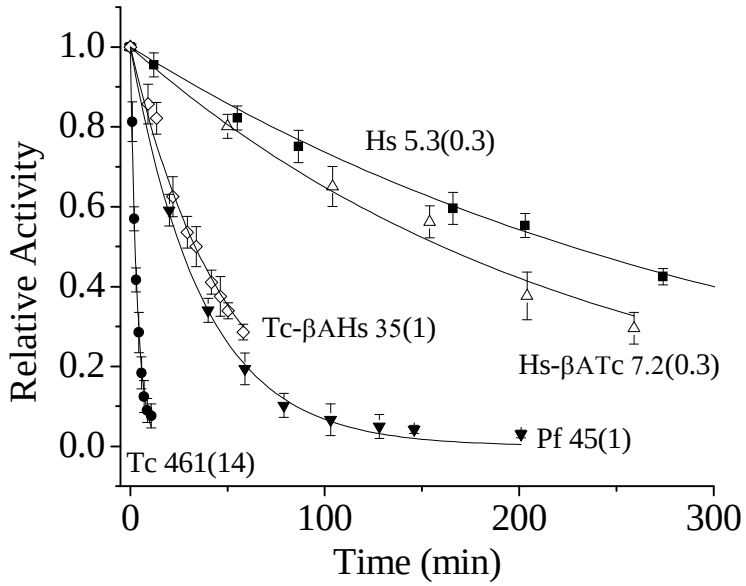

Figure 4.2. The rate of dissociation NAD^+ from Hs-SAHH, Hs-βATc-SAHH, Tc-βAHs-SAHH, Pf-SAHH, and Tc-SAHH at 37 °C in 50 mM phosphate buffer, pH 7.4. Data were calculated from three independent measurements. The rate constants ($10^5 k_{off}$, s^{-1}) with standard deviations in parentheses are shown next to each curve. The curves correspond to an exponential decay of relative activity from unity to zero activity.

dissociation rate constant 13 times smaller than that for Tc-SAHH, similar in magnitude to the rate constant for NAD^+ dissociation from Pf-SAHH.

4.3.4. The association of NAD^+ with apo-Hs-βATc-SAHH is qualitatively and semi-quantitatively similar to the cofactor-association processes of Hs-SAHH and Tc-SAHH.

The process of NAD^+ association with apo-Hs-βATc-SAHH is qualitatively similar to that of the two wild-type enzymes, apo-Hs-SAHH and apo-Tc-SAHH. The association of NAD^+ with the three apo-enzymes leads to a time-dependent rise in activity that can be described by three constants: A_o, the initial enzyme activity at time zero; k_{app}, an exponential relaxation constant; and A_f, the final enzyme activity [6]. A_o is a measure of the amount of *fast binding of the cofactor*, occurring within the dead time of the experiment. The parameter k_{app} is the rate constant for *slow binding of the cofactor*, with A_f measuring the amount of total binding (fast plus slow) and $A_f - A_o$ measuring the amount of slow binding. The constants A_o, A_f, and k_{app} (and thus the fraction of fast binding, the fraction of slow binding, and the rate constant of slow binding) are all dependent on $[NAD^+]$. Figure 4.3.A shows the dependence of the fractions of fast and slow binding as a function of $[NAD^+]$ for Hs-βATc-SAHH, and Fig. 4.3.B shows the dependence of k_{app} on $[NAD^+]$.

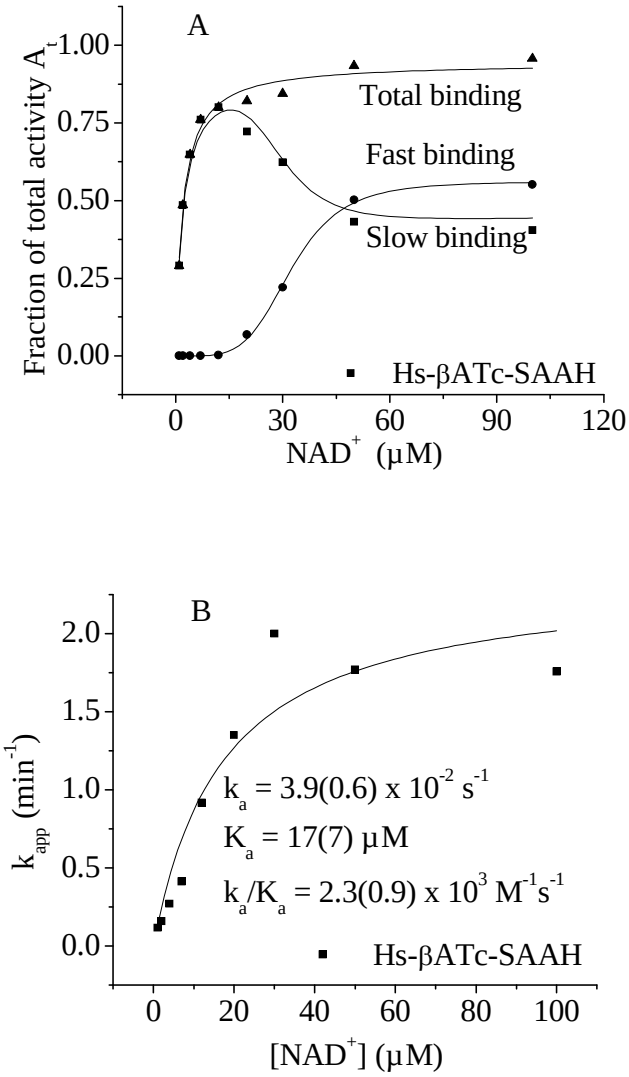

Figure 4.3. A: The dependence on [NAD^+] of the fractions of enzyme activity generated with Hs-βATc-SAHH in the fast-binding phase, the slow-binding phase, and the total activity. B: The dependence on the concentration of NAD^+ of the rate constant for the slow-binding phase of the association of NAD^+ with the apo-forms of Hs-βATc-SAHH at 23 °C and pH 7.4. The curves show the best fit of the data to eqs 2 with the parameters given in Table 4.3. (also shown on Fig. 4.3.B).

Table 4.3. Values of rate and equilibrium constants in the kinetics of the fast and slow binding phases of the association reaction of NAD^+ with Hs-SAHH, Hs-βATc-SAHH, Tc-βAHs-SAHH, Pf-SAHH at 23 °C and pH 7.4, from reference [6] and from fits of the data in Figs. 3-5 to eqs. 2.

Enzyme	K_o, μM binding to fully functional sites of apo-SAHH	K_a, μM binding to non-functional sites of apo-SAHH	K_f, μM binding to fully functional sites of holo-SAHH	k_a, s^{-1} transformation of non-functional apo-sites to functional holo-sites	k_a/K_a, $M^{-1}s^{-1}$ binding and transformation of apo-sites to holo-sites
Hs-SAHH	33 ± 4 n = 3.3 ± 1.4	19 ± 8	1.4 ± 0.3	5.5 ± 0.8 x 10^{-2}	2.9 ± 1.2 x 10^3
Hs-βATc-SAHH	30 ± 2 n = 4.5 ± 0.8	17 ± 7	2.0 ± 0.2	3.9 ± 0.6 x 10^{-2}	2.3 ± 0.9 x 10^3
Tc-SAHH	38 ± 9 n = 1.6 ± 0.4	3.8 ± 0.6	1.8 ± 0.4	6.0 ± 0.2 x 10^{-3}	1.6 ± 0.3 x 10^3
	K_o	K_a, mM	K_f	k_a, s^{-1}	k_a/K_a, $M^{-1}s^{-1}$
Tc-βAHs-SAHH	a	5.8 ± 0.5	a	2.1 ± 0.1 x 10^{-3}	0.36 ± 0.04
Pf-SAHH	a	7.9 ± 1.7	a	1.6 ± 0.2 x 10^{-3}	0.20 ± 0.05

[a] The data for total binding to Tc-βAHs-SAHH and Pf-SAHH in Fig. 4.5.AB show anomalies: a poor fit for total binding to a saturation function and, for Tc-βAHs-SAHH, a decrease in binding at higher $[NAD^+]$, so that estimates of the constant K_f (either from total binding or slow binding) are likely to be erroneous. The data for fast binding to either enzyme, even at levels approaching 10 mM $[NAD^+]$, are insufficient to contain any information on the saturation constant K_o. Thus we omit estimates of K_f and K_o.

A model that accounts for such results [4, 6] envisions an apo-enzyme with two classes of active sites, equal in number: one which generates full activity when occupied by cofactor, but which binds cofactor relatively weakly; another which generates no activity when occupied by cofactor, but which binds cofactor relatively strongly. The binding occurs rapidly on the time scale of the experiment. The activity at time zero A_o is given by eq 2a, allowing for the activity-generating half of the sites to become saturated with NAD^+ with dissociation constant K_o and Hill coefficient n. Here, A_t represents the total enzyme activity at a saturating $[NAD^+]$ after completion of slow binding. Occupancy of the second class of sites produces no activity, but their binding of the cofactor (dissociation constant K_a) stimulates the slow conversion of these sites (rate constant k_a to sites of full activity *and* simultaneous conversion of all sites to ones of higher affinity for cofactor (dissociation constant K_f) than either class of binding sites in the apo-enzyme. The dependence of A_f and k_{app} on $[NAD^+]$ are thus given by eqs 2b and 2c, where the treatment is simplified by the omission of possible cooperativity (n = 1).

$$A_o = (A_t/2)\{[NAD^+]^n/(K^n_o + [NAD^+]^n)\} \quad (2a)$$

$$A_f = (A_t)\{[NAD^+]/(K_f + [NAD^+])\} \quad (2b)$$

$$k_{app} = k_a\{[NAD^+]/(K_a + [NAD^+])\} \quad (2c)$$

The curves shown in Fig. 4.3.A are plots of A_o/A_t (fast binding), $[A_f - A_o]/A_t$ (slow binding), and A_f/A_t (total binding) with the parameters K_o, n, and K_f shown in

Table 4.3. The curve shown in Fig. 4.3.B is a plot of eq 2c with the parameters k_a and K_a shown in Table 4.3.

4.3.5. The association of NAD^+ with apo-Tc-βAHs-SAHH is quantitatively similar to the cofactor-association process of apo-Pf-SAHH and very different from those of either apo-Hs-SAHH or apo-Tc-SAHH.

In contrast to Hs-SAHH, Hs-βATc-SAHH, and Tc-SAHH, all of which undergo fast and slow binding of cofactor with initial and final cofactor-dissociation constants K_o, K_a, and K_f in the micromolar range, the levels of cofactor required for association with apo-Tc-βAHs-SAHH are in the millimolar range (Fig. 4.4.A). This behavior emerges as very similar to that of Pf-SAHH (Fig. 4.4.B).

Application of the model leading to eqs. 2 then produces the results shown in Fig. 4.5.A for the cofactor-concentration dependence of the fractions of fast binding and slow binding, and in Fig. 4.5.B for the cofactor-concentration dependence of the rate constant for slow binding. The curves plotted in Fig. 4.5. correspond to the parameters shown for Tc-βAHs-SAHH and Pf-SAHH in the lower part of Table 4.3.. As expected, the initial and final equilibrium cofactor-dissociation constants for these two species are larger than those for Hs-SAHH, Hs-βATc-SAHH, and Tc-SAHH by 3-4 orders of magnitude. The rate constant for slow binding, however, remains in the same range for all enzymes.

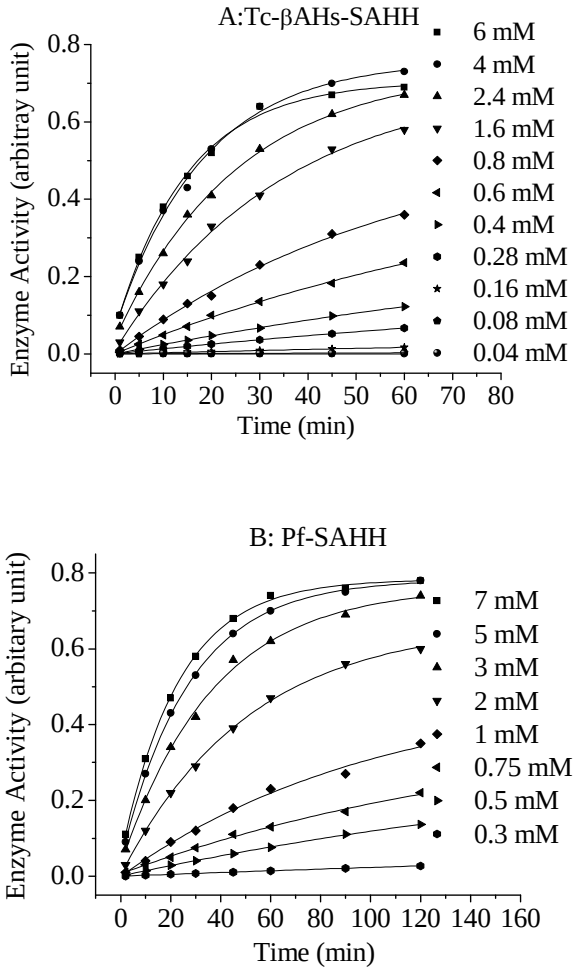

Figure 4.4. Time dependence of NAD^+ binding to Tc-βAHs-SAHH (A) and to Pf-SAHH (B) as measured by the development of catalytic activity. As the concentration of cofactor increases, the intercept at zero time increases (fast binding, within the dead-time of the experiment), the final activity increases, and the rate of approach to the final level (slow binding) increases. Note that in both cases, the cofactor levels required to reach final binding that approaches complete saturation within the two-hour period are of millimolar magnitudes.

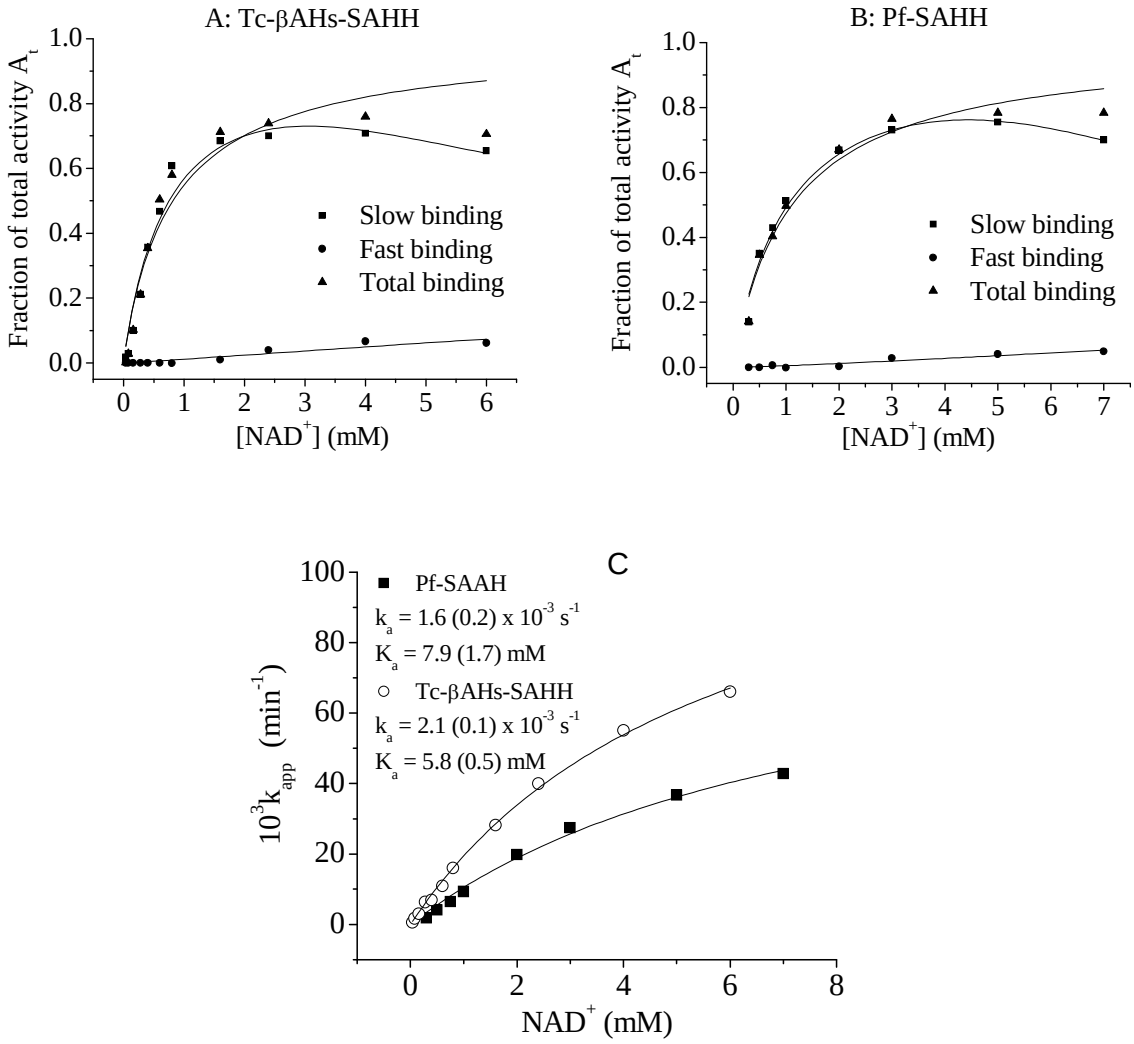

Figure 4.5. The dependence on [NAD^+] of the fractions of enzyme activity generated with Tc-βAHs-SAHH (A) and Pf-SAHH (B) in the fast-binding phase, the slow-binding phase, and the total activity. C: The dependence on the concentration of NAD^+ of the rate constants for the slow-binding phase of the association of NAD^+ with the apo-forms of Tc-βAHs-SAHH and Pf-SAHH at 23 °C and pH 7.4. The curves show the best fit of the data to eqs 2 with the parameters given in the lower

part of Table 4.3. (also shown on Fig. 4.5.C). increasing with temperature at low temperatures and decreasing with temperature at high temperatures. This behavior was noted [6] to correspond to a model in which the normal rise in rate constant as temperature rises is opposed by a local, reversible unfolding phenomenon such that the cofactor binding site becomes increasing disabled as temperature rises. Thus $k_o = k_{on}(1/[1 + K_{un}])$, where K_{un} is the equilibrium constant for local unfolding and the factor in parentheses gives the fraction of still folded enzyme.

4.3.6. The Temperature dependence of the association reaction of NAD^+ with apo-Hs-βATc-SAHH is little changed from that of apo-Hs-SAHH while cofactor association with apo-Tc-βAHs-SAHH is far slower than cofactor association with apo-Tc-SAHH.

For association of NAD^+ with Hs-SAHH and Tc-SAHH, it was previously established that at $[NAD^+] = 5\ \mu M$, the fraction of fast-binding was negligible and the dependence of the slow-binding rate constant k_{app} on $[NAD^+]$ was linear. Thus a phenomenological second-order rate constant for slow binding, which we denote k_o, can be obtained as $k_{app}/[NAD^+]$. The measurements were possible over a range of temperatures [6]. Figure 4.6.A presents the effect of temperature on k_0 in the form of Eyring plots for Hs-SAHH, Hs-βATc-SAHH, and Tc-SAHH. The curves in all cases are biphasic, with k_o.

The temperature dependence of the apparent association constant k_o is then described by eq (3), where we take the standard-state concentration of NAD^+, $[NAD^+]_{ss} = 1\ M$:

$$\ell n\ (k_o/T) = (\Delta S^{\ddagger}_{on} / R) - (\Delta H^{\ddagger}_{on} / RT) - \ell n\ \{1 + \exp [(\Delta S^{o}_{un} / R) - (\Delta H^{o}_{un} / RT)]\}$$
$$- \ell n\ [NAD^+]_{ss} + \ell n\ (k/h) \qquad (3)$$

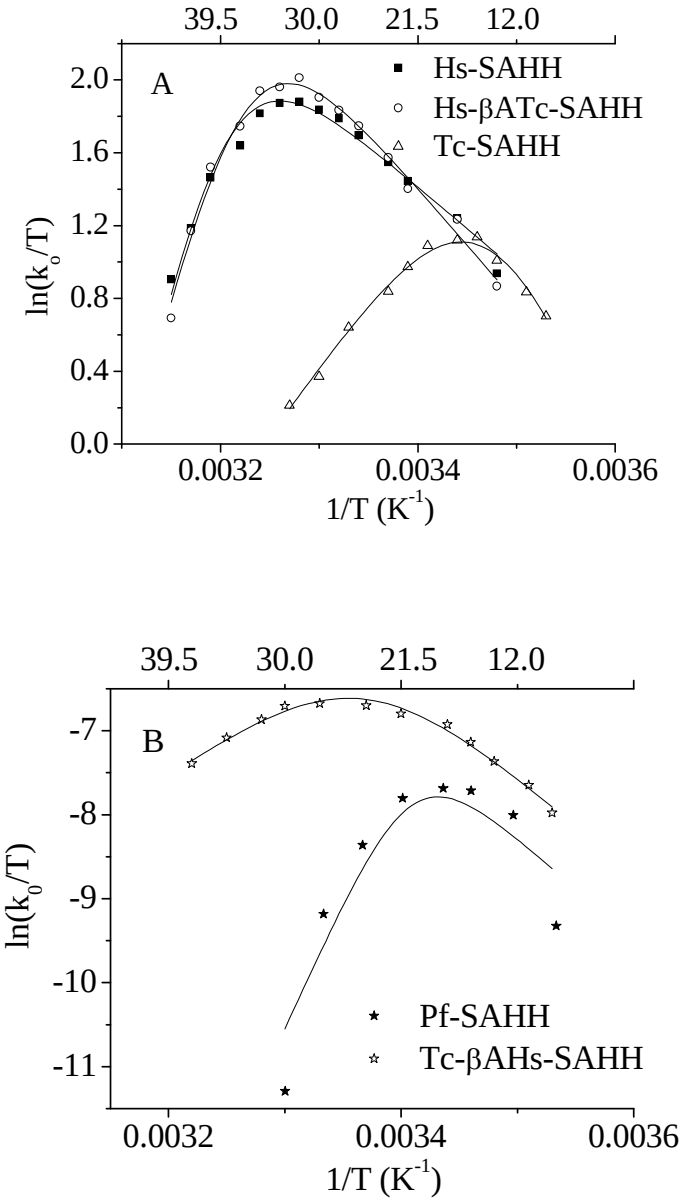

Figure 4.6. Temperature dependence of the rate constant for the slowing-binding phase of the association of NAD^+ with apo forms of Hs-SAHH, Hs-βATc-SAHH, Tc-SAHH (A), Pf-SAHH and Tc-βAHs-SAHH (B). The curves are plots of eq (3) with the parameters listed in Table 4.4.

Table 4.4. Thermodynamic and quasi-thermodynamic parameters[a] for NAD^+ association with Tc-SAHH, Pf-SAHH, Tc-βAHs-SAHH, Hs-βATc-SAHH, and Hs-SAHH at temperatures in the interval 10 - 45 °C, pH 7.4.

Enzyme	$\Delta S^{\ddagger}_{on}$ **(J/K-mol)**	$\Delta H^{\ddagger}_{on}$ **(kJ/mol)**	ΔS^{o}_{un} **(J/K-mol)**	ΔH^{o}_{un} **(kJ/mol)**	$\Delta H^{o}_{un}/\Delta S^{o}_{un}$ **(K)**
Hs-SAHH	- 56 ± 9	38 ± 3	788 ± 5	243 ± 2	308 ± 3 (35 °C)
Hs-βATc-SAHH	-8 ± 12	52 ± 4	752 ± 6	233 ± 2	310 ± 4 (37 °C)
Tc-SAHH	225 ± 13	118 ± 4	631 ± 8	182 ± 2	288 ± 5 (15 °C)
Tc-βAHs-SAHH	83 ± 33	98 ± 9	599 ± 8	178 ± 2	297 ± 5 (24 °C)
Pf-SAHH	83 ± 318	100 ± 91	1205 ± 34	354 ± 10	294 ± 12 (21°C)

[a]Parameters were obtained by least-squares fitting to eq 3 (Origin version 7.5). The subscript "on" identfies the quasi-thermodynamic parameters of activation for the binding rate constant of the slow-binding phase of cofactor binding. The subscript "un" identfies the equilibrium thermodynamic parameters for local unfolding in or near the cofactor binding site.

In eq (3), the subscript “on” denotes the quasi-thermodynamic parameters of activation for cofactor binding and the subscript “un” denotes the thermodynamic parameters of the reversible unfolding process. The values of the enthalpies and entropies are given in Table 4.4. The table also gives the ratio $\Delta H^{o}_{un}/\Delta S^{o}_{un}$, as a rough measure of the “melting temperature” for the presumed local structural transition.

4.3.7. The temperature dependence of the dissociation reaction of the mutant enzymes is qualitatively similar to the biphasic dependence for the wild-type enzymes.

Figure 4.7. presents Eyring plots of the first-order rate constants k_{off} for dissociation of the cofactor NAD^+ from the mutant enzymes, Hs-βATc-SAHH (29 °C to 45.5 °C) and Tc-βAHs-SAHH (23 °C to 43.5 °C). Previously measured dependences [6] are shown for the wild-tpe enzymes, Hs-SAHH and Tc-SAHH. The Eyring plots for all enzymes are nonlinear, consisting of a linear low-temperature regime and a linear high-temperature regime. As before [6], two Eyring equations (4a and 4b) were used for fitting of the data.

$$k_{off} / (\mathbf{k}T/h) = \{\exp [(\Delta S^{\ddagger}_{l} / R) - (\Delta H^{\ddagger}_{l} / RT)]\} \qquad (4a)$$

$$k_{off} / (\mathbf{k}T/h) = \{\exp [(\Delta S^{\ddagger}_{h} / R) - (\Delta H^{\ddagger}_{h} / RT)]\} \qquad (4b)$$

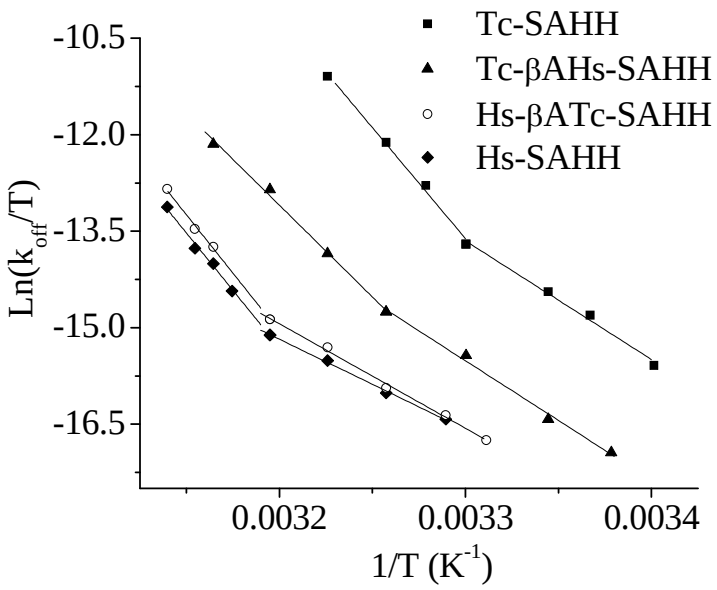

Figure 4.7. Temperature dependence of the rate constant k_{off} for dissociation of NAD^+ from Hs-SAHH, Hs-βATc-SAHH, Tc-βAHs-SAHH, and Tc-SAHH. The lines are intersecting Eyring plots with the parameters given in Table 4.5.

Table 4.5. Quasi-thermodynamic parameters of activation for the low-temperature and high-temperature regimes, and conversion temperatures[a] T_o between the regimes for NAD^+ dissociation from Tc-SAHH (21 °C to 37 °C), Tc-βAHs-SAHH (23 °C to 43.5 °C), Hs-βATc-SAHH (29 °C to 45.5 °C), and Hs-SAHH (31 °C to 45.5 °C) at pH 7.4.

Enzyme	$\Delta S^{\ddagger}_{\ell}$ **(J/mol-K)**	$\Delta H^{\ddagger}_{\ell}$ **(kJ/mol)**	$\Delta S^{\ddagger}_{h}$ **(J/mol-K)**	$\Delta H^{\ddagger}_{h}$ **(kJ/mol)**	**T_o, K**
Tc-SAHH	170 ± 15	154 ± 8	610 ± 30	287 ± 8	302 ± 34 (29 °C)
Tc-βAHs-SAHH	183 ± 13	154 ± 8	453 ± 22	237 ± 10	307 ± 56 (34 °C)
Hs-βATc-SAHH	111 ± 6	135 ± 5	644 ± 24	302 ± 10	313 ± 25 (40 °C)
Hs-SAHH	50 ± 2	116 ± 4	600 ± 25	297 ± 9	314 ± 21 (41 °C)

[a]*Temperature of intersection of the high-temperature and low-temperature limbs of the temperature dependence and thus the apparent temperature of conversion between the two regimes.*

In above equations, the subscript ℓ denotes the quasi-thermodynamic parameters of activation for the low-temperature regime and the subscript h denotes those for the high-temperature regime. Table 4.5. summarizes the values of the quasi-thermodynamic parameters of activation. The conversion temperature T_o for passage from the low-temperature regime to the high-temperature regime was calculated from eq (5) and values are also listed in Table 4.5.

$$T_o = [(\Delta H^{\ddagger}_h) - (\Delta H^{\ddagger}_\ell)] / [(\Delta S^{\ddagger}_h) - (\Delta S^{\ddagger}_\ell)] \qquad (5)$$

The Eyring plots for the mutants Hs-βATc-SAHH and Tc-βAHs-SAHH are similar in character to the ones for Hs-SAHH and Tc-SAHH and lie between the latter. The values listed in Table 4.5. show that a low-enthalpy, small positive entropy dependence at low temperatures is replaced by a high-enthalpy, large positive entropy change at high temperatures for both wild-type enzymes and mutant enzymes.

4.4. Discussion

4.4.1. Mutants at sites in β-sheet A of the Rossmann motif of Hs-SAHH and Tc-SAHH, the "parasitized" human enzyme Hs-βATc-SAHH and the "humanized" parasitic enzyme Tc-βAHs-SAHH, exhibit intact secondary and quaternary structure and catalytic properties little changed from those of Hs-SAHH and Tc-SAHH.

The loci and character of the mutations V215C/V217C in Hs-SAHH and T214V/C216V in Tc-SAHH are not expected to cause changes in secondary or quaternary structure, given the strong similarity of these structures in the two wild-type enzymes, Hs-SAHH (11-15) and Tc-SAHH (16), and indeed the circular dichroism spectra are near-identical and size-exclusion chromatography shows both mutant enzymes to be homotetrameric. Little effect is also expected on the catalytic properties as the mutational loci are quite distant from the site of chemical changes in catalysis (Fig. 4.1.) and the catalytic properties of Hs-SAHH and Tc-SAHH are themselves not very different. Indeed all four enzymes are very similar in their catalytic properties (Table 4.2.).

4.4.2. The complete dissociation of the cofactor NAD^+ from all four subunits of the mutant enzymes Hs-βATc-SAHH and Tc-βAHs-SAHH is a simple first-order reaction with rate constant intermediate in magnitude between those of Hs-SAHH and Tc-SAHH.

It was established in previous work that dissociation of the four bound cofactor molecules from the tetrameric Hs-SAHH and Tc-SAHH enzymes [6] and enzymes mutated at sites in helix-18 [4] was in each case a simple single-exponential relaxation process. In contrast to the very similar catalytic properties of Hs-SAHH and Tc-SAHH, Hs-SAHH underwent cofactor dissociation at 37 °C nearly 100-fold

more slowly than Tc-SAHH (these data are also shown in Fig. 4.2.). The dissociation rates for the mutant enzymes Hs-βATc-SAHH and Tc-βAHs-SAHH fall between the rates for Hs-SAHH and Tc-SAHH, in a pattern that was also true for the helix-18 mutants [4]. Cofactor dissociates from the "parasitized" human enzyme, Hs-βATc-SAHH, more rapidly than from Hs-SAHH, but only by less than a factor of two (Fig. 4.3.). Cofactor dissociates from the "humanized" parasitic enzyme, Tc-βAHs-SAHH, more slowly than from Tc-SAHH but here by a more substantial factor of 13 (Fig. 4.2.).

This pattern was previously seen [4] with mutations in helix-18 of Hs-SAHH and Tc-SAHH: "parasitizing" mutations of Hs-SAHH tended to produce small shifts of enzyme properties in the direction of the properties of Tc-SAHH, while "humanizing" mutations of Tc-SAHH produced larger shifts of enzyme properties in the direction of the properties of Hs-SAHH. It was noted that Hs-SAHH had a larger total helix propensity for helix-18 than was the case for Tc-SAHH, and that Hs-SAHH might therefore have a more robust or rigid and less easily perturbed helix-18 than Tc-SAHH. The mutational effects for Tc-SAHH would then be larger than those for Hs-SAHH, as observed. A similar case could also be made here: the total β-sheet propensity of β-sheet A of the Rossmann motif is about 7.2 for Hs-SAHH and 6.4 for Tc-SAHH. Thus β-sheet A may be more robust and less easily perturbed in Hs-SAHH, giving rise to smaller mutational effects, then in Tc-SAHH, where larger mutational effects are observed.

4.4.3. Association of NAD^+ with the "parasitized" human enzyme apo-Hs-βATc-SAHH resembles association of NAD^+ with apo-Hs-SAHH and apo-Tc-SAHH, both qualitatively and quantitatively.

Cofactor association with the apo-enzymes of Hs-SAHH, Tc-SAHH, and their mutants at helix-18 sites exhibits a kinetic pattern similar to that for association with apo-Hs-βATc-SAHH (Fig. 4.3.). This pattern is consistent with a model having the following properties [4, 6]:

(a) The tetrameric apo-enzyme has four cofactor-binding sites that fall into two classes, equal in number.

(b) Half of the sites exhibit a relatively larger cofactor-dissociation constant K_o (ca. 33 μM for Hs-SAHH) and occupation of these sites by cofactor produces a full complement of catalytic activity. These sites are rapidly occupied (within the dead-time of the experiment), and give rise to an initial *fast-binding* activity A_o which increases with cofactor concentration according to eq 2a above. For Hs-SAHH and Tc-SAHH, fast binding is cooperative with Hill coefficients n around 2-3.

(c) Half of the sites exhibit a relatively smaller cofactor-dissociation constant K_a (ca. 19 μM for Hs-SAHH), are also rapidly occupied but generate no immediate catalytic activity. Instead, occupancy of these sites stimulates a time-dependent

conversion of all sites in the enzyme (rate constant k_{app}) to sites of full activity A_f with a still smaller cofactor-dissociation constant K_f. The cofactor-concentration dependences of A_f and k_{app} are given by eqs 2b and 2c, respectively. The *slow-binding* activity is $A_f - A_o$.

(d) Plots of the dependence on cofactor concentration of the fractions of fast-binding activity (A_o/A_t), of slow-binding activity ($[A_f - A_o]/A_t$), and of total binding activity (A_f/A_t), where A_t is the final activity after slow binding is complete of the fully saturated enzyme, give the appearance of Fig. 4.3.A. Briefly, the fast-binding curve tends to be sigmoidal, not hyperbolic, so that relatively little fast binding occurs at low cofactor concentrations. This gives rise to the steep increase of the slow-binding curve at low cofactor levels, with slow binding accounting for 80% or more of the total. As the fast binding mode begins to account for more binding, the slow-binding curve drops and both then level off at half of the total binding in accord with the equal populations of the two kinds of sites.

(e) Plots of k_{app} against cofactor concentration have in previous work, tended to present an appearance similar to Fig. 4.3.B.

Apparently, as Fig. 4.3. suggests, the same model can describe the association of NAD^+ with the "parasitized" human enzyme Hs-βATc-SAHH. Indeed, essentially all of the quantities determined in the analysis are nearly the same for Hs-SAHH and

Hs-βATc-SAHH and only slightly different for Tc-SAHH (upper part of Table 4.4.). This may indicate that the structural and dynamic phenomena underlying features (a), (b), and (c) of the association model described above are insensitive to structure in β-sheet A of the Rossmann motif.

4.4.4. Association of NAD^+ with the "humanized" parasitic enzyme apo-Tc-βAHs-SAHH differs radically from association of NAD^+ with apo-Hs-SAHH or apo-Tc-SAHH, but resembles association of NAD^+ with apo-Pf-SAHH.

Fig. 4.4. shows the time courses of the binding of NAD^+ to apo-Tc-βAHs-SAHH (Fig. 4.4.A) and to apo-Pf-SAHH (Fig. 4.4.B). These time courses resemble qualitatively the corresponding data for binding to apo-Hs-SAHH and apo-Tc-SAHH: the initial activity A_o, the final activity A_f, and the relaxation constant k_{app} all rise with increasing [NAD^+]. However, the range of [NAD^+] required to span a corresponding range of the parameters for apo-Hs-SAHH and apo-Tc-SAHH was 1 - 100 μM whereas in Fig. 4.4., the range for apo-Tc-βAHs-SAHH is 40 μM to 6 mM and the range for apo-Pf-SAHH is 300 μM to 7 mM.

Obviously the chemical potential of NAD^+ required to drive cofactor binding to these two enzymes is greater than the requirement for Hs-SAHH, Hs-βATc-SAHH, and Tc-SAHH by around 2 orders of magnitude. Indeed the complete kinetic profile

of association could not be explored except by use of cofactor levels approaching 20 mM, at which point anomalies (perhaps arising from self-association [10, 11] or inhibition of enzyme activity) are already appearing. Because the accessible data (Fig. 4.5., Table 4.3.) are limited and partly anomalous, it cannot be definitely shown that the model described for the other enzymes also holds for cofactor association with apo-Tc-βAHs-SAHH and apo-Pf-SAHH.

However, if it is assumed that the model holds, then the derived parameters (lower part of Table 4.3.) suggest that initial cofactor binding to the apo-enzyme occurs with dissociation constants K_a in the millimolar rather than the supra-micromolar range. The rate constant k_a for slow binding is not so different from that seen with Tc-SAHH, but the greatly increased dissociation constant makes the value of k_a/K_a smaller by nearly four orders of magnitude.

The structural basis for this phenomenon is currently unknown. It is being investigated by computational methods.

4.4.5. The temperature dependences of the slow-binding rate constants for association of NAD^+ are similar for apo-Hs-SAHH and apo-Hs-βATc-SAHH and four orders of magnitude faster than for apo-Pf-SAHH and apo-Tc-βAHs-SAHH.

It has already been noted and discussed [4, 6] that the local structural transition that impedes cofactor association occurs in apo-Tc-SAHH at a substantially lower temperature (15 °C) than is the case for apo-Hs-SAHH (35 °C). Mutations in helix-18 of the cofactor binding site that interchanged human/parasitic structures, analogous to the β-sheet A mutations reported here, gave rise to species with intermediate transition temperatures. Hs-α18Pf-SAHH showed a small shift (perhaps none) from 35 °C to 33 °C, while Tc-α18Hs-SAHH showed a dramatic shift from 15 °C to 30 °C. This and other evidence led to the tentative conclusion that the "site of this local alteration is, in fact, helix 18."

The results reported here require a more complex picture (Fig. 4.6., Table 4.4.). The mutant enzyme Hs-βATc-SAHH gives a temperature dependence (transition temperature 37 °C) scarcely distinguishable from that of Hs-SAHH, in agreement either with the locus of the transition being elsewhere (perhaps helix 18) or instead with the robustness of β-sheet A in the human enzyme, in common with the robustness of helix 18 in the human enzyme. The mutant enzyme Tc-βAHs-SAHH shows a transition temperature of 24 °C, dramatically shifted from the Tc-SAHH value of 15 °C in the direction of the human enzyme. This result would suggest a role for β-sheet A in controlling the transition or at least an interaction between structure at β-sheet A and at helix 18 during the transition.

Far more striking is the fact that the values of k_{on} are smaller by a factor around 40,000, a property that is shared by the wild-type plasmodial enzyme Pf-SAHH. These two enzymes, Pf-SAHH and Tc-βAHs-SAHH, also share the property of possessing a β-sheet A consisting of four hydrophobic residues followed by a cysteine (Table 4.1.) and they possess the two highest total β-sheet propensities (8.34 and 7.71, respectively) in Table 4.1. We hope that theoretical work may elucidate the molecular origins of this phenomenology.

4.4.6. The temperature dependences of the rate constants for dissociation of NAD^+ from Hs-βATc-SAHH and Tc-βAHs-SAHH are similar in character to and quantitatively intermediate between those for Hs-SAHH and Tc-SAHH.

The temperature dependences of the cofactor-dissociation rate constants (Fig. 4.7., Table 4.5.) can be seen from a far simpler perspective. The biphasic dependence with a shift to higher enthalpies of activation at temperatures from 29 °C (Tc-SAHH, with the fastest dissociation) to 41 °C (Hs-SAHH, roughly 10-30-fold slower dissociation) is reproduced by the mutants, with the properties of Hs-βATc-SAHH scarcely changed from those of Hs-SAHH, while Tc-βAHs-SAHH shows a large shift from Tc-SAHH in the direction of Hs-SAHH. Thus the indication of a robustness of the Hs-SAHH properties, contrasting with the malleability of Tc-SAHH, is maintained.

4.5. Summary and Conclusions.

The following generalizations may be advanced:

1. As with the helix-18 mutants [4] in chapter 3, the mutants here discussed in β-sheet A of human and trypanosomal SAHHs have negligible effects on the catalytic properties of the enzymes, as is expected, in one sense, for mutational sites so distant from the locus of the catalytic chemistry (see Fig. 4.1.). Although much evidence on hydride-transfer processes of exactly the kind that participate in the redox partial reaction of SAHHs [12] indicates the vibrational involvement of remote residues in catalysis, the present study has produced no such indications.

2. For the kinetics of dissociation of cofactor from the enzyme and their temperature dependence (Fig. 4.2., Fig. 4.7., Table 4.5.), the introduction of mutations in Hs-SAHH such that β-sheet A of the Rossmann motif more closely resembles the same structure in Tc-SAHH ("parasitizing" mutations, Hs-βATc-SAHH), the rate constants and their Eyring plot are moved away from the data for wild-type Hs-SAHH in the direction of the data for wild-type Tc-SAHH. Correspondingly, the introduction of "humanizing" mutations in β-sheet A of the Rossmann motif of Tc-SAHH (Tc-βAHs-SAHH) results in changes of the rate constants and their Eyring plots in the direction of the data for wild-type Hs-SAHH. Here as in other cases, the mutationally induced changes are larger in magnitude for Tc-SAHH than for Hs-

SAHH, in agreement with ascription of greater structural robustness or resilience to Hs-SAHH in contrast to Tc-SAHH. In a development (Fig. 4.2.) that presages other, more dramatic findings described below, the rate constant for cofactor dissociation at 37 °C, pH 7.4, for Tc-βAHs-SAHH (36×10^{-5} s^{-1} vs. 461×10^{-5} s^{-1} for Tc-SAHH) is very close to that for the wild-type plasmodial enzyme Pf-SAHH (45×10^{-5} s^{-1}).

3. The kinetics of NAD^+ association for the "parasitized" human enzyme Hs-βATc-SAHH are similar to and intermediate between the data for the wild-type human enzyme Hs-SAHH and the wild-type trypanosomal enzyme Tc-SAHH (Fig. 4.3., Table 4.3.; Fig. 4.6., Table 4.4.). In stark contrast, the "humanized" trypanosomal enzyme Tc-βAHs-SAHH exhibits an equilibrium dissociation constant for cofactor after slow binding that is 2-3 orders of magnitude weaker, roughly millimolar rather than micromolar, than for Hs-SAHH, Tc-SAHH, and Hs-βATc-SAHH (Figs. 4.4 and 4.5., Table 4.3.). The slow binding rate constants, however, are similar for all four enzymes. The data for Tc-βAHs-SAHH are extremely similar to those, where available, for Pf.-SAHH (Figs. 4.4 and 4.5, Table 4.3., Fig. 4.6., Table 4.4.).

4. The results reported here for mutations in β-sheet A of the Rossmann motif, like those reported earlier [4] for mutations in helix 18 of the cofactor binding site, support the proposal [4, 6] that design of inhibitory ligands for binding to the cofactor site, rather than in the catalytic site, is a promising approach to anti-parasitic therapy.

4.6. References

1. Bellamacina, C.R., *The nicotinamide dinucleotide binding motif: a comparison of nucleotide binding proteins.* Faseb J, 1996. **10**(11): p. 1257-69.
2. Brandén, C. and J. Tooze, *Introduction to Protein Structure.* Garland Publishing, Inc., New York and London,, 1991: p. pp 144-146.
3. Turner, M.A., et al., *Structure and function of S-adenosylhomocysteine hydrolase.* Cell Biochem Biophys, 2000. **33**(2): p. 101-25.
4. Li, Q.-S., et al., *Comparative kinetics of cofactor association and dissociation for the human and trypanosomal S-adenosylhomocysteine hydrolases. 2. The role of helix 18 stability.* Biochemistry, 2008. **47**(17): p. 4983-91.
5. Kallberg, Y., et al., *Prediction of amyloid fibril-forming proteins.* J Biol Chem, 2001. **276**(16): p. 12945-50.
6. Li, Q.-S., et al., *Comparative kinetics of cofactor association and dissociation for the human and trypanosomal s-adenosylhomocysteine hydrolases. 1. Basic features of the association and dissociation processes.* Biochemistry, 2007. **46**(19): p. 5798-809.
7. Elrod, P., et al., *Contributions of active site residues to the partial and overall catalytic activities of human S-adenosylhomocysteine hydrolase.* Biochemistry, 2002. **41**(25): p. 8134-42.
8. Cook, P.F. and W.W. Cleland, *Enzyme Kinetics and Mechanism.* Garland Sciences Publishing, New York and London, 2007: p. 196-204.

9. Yuan, C.S., D.B. Ault-Riche, and R.T. Borchardt, *Chemical modification and site-directed mutagenesis of cysteine residues in human placental S-adenosylhomocysteine hydrolase.* J Biol Chem, 1996. **271**(45): p. 28009-16.

10. Neurohr, K. and H. Mantsch, *Specific binding of phenylalanine and tryptophan to P-nicotinamide adenine dinucleotide.* Can. J. Chem. , 1979. **57**: p. 2297-2301

11. Gallego, E. and F. Peral, *Self-association of nicotinamide-adenine dinucleotides in aqueous solution.* . Journal of Molecular Structure 1993. **298**(1-3): p. 87-94.

12. Nagel, Z.D. and J.P. Klinman, *Tunneling and dynamics in enzymatic hydrogen transfer*. Chem. Rev. , 2006. **106**: p. 3095-3118. .

Chapter 5

The Role of Lysyl and Tyrosyl Residues of the C-terminal Extension in Comparative Kinetics of Cofactor Association and Dissociation for Hs-SAHH and Tc-SAHH.

5.1. Introduction

Several X-ray crystallographic structures of Hs-SAHH [1] and Tc-SAHH (unpublished data of Drs. Q.-S. Li and W. Huang) are available. Both SAHHs are homotetramers and each subunit contains a substrate-binding domain, a cofactor (NAD^+/NADH)-binding domain and a C-terminal tail which covers the cofactor-binding site of the neighboring subunit (Fig. 5.1.). A lysine and a tyrosine located on the C-terminal chain are very close to the NAD(H) cofactor in the x-ray structures and may make important contributions to the cofactor binding of the SAHHs. The studies of the kinetics and thermodynamics of the association and dissociation reactions of the nicotinamide cofactors study on cofactor binding of Hs-SAHH and Tc-SAHH, revealing significant differences in binding properties between these two enzymes. However, the atomic-level mechanism of the differential nicotinamide cofactor binding properties between Hs-SAHH and Tc-SAHH is not yet clear [4].

Figure 5.1. The "dimer" structure of SAHHs [1]. The contributing monomers are shown in red and green, with cofactor ligands in blue ball-and-stick representation and a substrate-analog ligand in a gold ball-and-stick representation. The C-terminal extension of each monomer, containing helix 18, can be seen penetrating into the partner monomer to form part of the cofactor binding site (top left, in green; bottom right, in red). K426 (yellow) and Y430 (purple) are located in the final coil between helix 18 and the C-terminus.

To analyze microscopic differences in NAD binding to Hs-SAHH and Tc-SAHH, we have performed calculations of cofactor binding free energies and computational alanine scanning (CAS) based on the Molecular Mechanics-Generalized Born Surface Area (MM-GBSA) approach. The free energy calculations allow the identification of residues which contribute the most to cofactor binding. CAS is a different approach, using computational mutagenesis to provide predictions of key residues in protein structure and/or function [5]. According to the increased binding free energy caused by alanine mutation, residues may be divided into hot spots (> 4.0 kcal/mol), warm spots (2.0 – 4.0 kcal/mol) and null spots (< 2.0 kcal/mol) [6]. The identified hot spots may then be used to guide further research on protein structure and function [5]. In present study, experimental mutagenesis was performed to test the computational calculations for two pairs of conserved residues: a lysine and a tryptophan in the C-terminal tail in both enzymes.

5.2. Methods:

5.2.1. Computational procedures:

The starting crystallographic structures of Hs-SAHH and Tc-SAHH were downloaded from the Protein Data Bank (PDB), entries 1A7A and 1XBE, respectively. Calculations for another crystal structure of Hs-SAHH (PDB code: 1IL4) yielded very similar results. Thus, only the data for the 1A7A structure are

shown in this study. The 1A7A structure was solved by incorporating selenium atoms (SE) in place of the sulfurs in Met residues. Assuming that this does not influence the structure, Se atoms were replaced by S atom and the residue names were changed from MSE to MET. After this modification, the 1A7A structure was ready for calculation. The simulation system was set up using the Xleap module of Amber 7 software. According to the SAHH's homotetramer structure, subunits A and B form a dimer, with the second dimmer formed by subunits C and D. To calculate the binding free energy of NADH to subunit A, our analysis includes the residues of subunit A as well as the C-terminal tail of neighboring subunit B, which forms close contacts with the NADH bound to A. In brief, the protein (AB dimer with two NADH bound) was solvated using a periodic truncated octahedral box of 29,419 water molecules, described by a TIP3P model [7], extended to a distance of 10 Å from any solute atom. The system was then neutralized by 16 sodium cations initially placed around the protein using a Coulombic potential on a grid. Then all minimization and MD were performed in the Amber 7 suite of programs. The ff99 force field (parm99) was used for proteins and NADH cofactor throughout the energy minimization and MD. The starting geometry of ligands was taken from the protein PDB files. The input files of ligands for MD simulation were prepared with the antechAmber program in Amber 7 which uses the General Amber Force Field (GAFF). Partial charges of the ligand atoms were calculated with the AM1-BCC method available in antechAmber [8].

5.2.1.1. Energy Minimization.

The energy minimization was performed using the sander module in the Amber 7 suite of programs with the particle - mesh Ewald method for inclusion of long-range electrostatic interactions [9]. There were two stages of energy minimization. In the first stage, only water molecules were minimized while the protein was fixed. The second stage minimized the entire system. Each stage was conducted with 500 cycles of steepest descent followed by 4500 conjugate steps of gradient minimization. The non-bonded cutoff was set to 12.0 Å.

5.2.1.2. Molecular Dynamics Simulations.

The equilibration process was carried out in two stages following the protocol suggested in the Amber manual. In the first stage, the system was heated gradually from a low temperature of 100 K to 300 K over 10 picoseconds (ps) simulation time with a time step of 2 femtoseconds (fs). A cutoff distance of 12 Å was used for the non-bonded interaction. The SHAKE algorithm was used to constrain the bonds involving hydrogen atoms and the force evaluations for these bonds were omitted. A periodic boundary with a constant volume and without pressure control was used. Then a second 10 ps equilibration was continued under a constant pressure and a constant temperature with isotropic position scaling to adjust the density of water to experimental values. After that, the whole system was equilibrated for 100 ps under a constant temperature of 300 K and a constant pressure of 1 bar. The SHAKE algorithm and 2 fs time steps were employed through all MD stages.

A 500 ps production run was performed with the same protocol as in the final stage of equilibration. After the simulation was completed, the ptraj module in Amber 7 was used to re-image the whole trajectory (including all equilibration and production runs), and to remove the waters and Na^+ from the trajectory file, and to calculate the root-mean-square deviations (rmsd) of backbone atoms from the starting structure over the whole course. Fifty snapshots were taken at 2-ps intervals from the section of the MD trajectory where the rmsd reached a plateau were used for further analysis. These sections corresponded to a rmsd of about 1.7 Å for Hs-SAHH and a rmsd of about 1.3 Å for Tc-SAHH.

5.2.1.3. Calculation of binding free energy by MM-GBSA.

MM-GBSA was used in evaluating binding free energies of the cofactor NADH to SAHH. In this method, the thermodynamic cycle shown in Scheme 5.1. was used to calculate the binding free energy:

Scheme 5.1.:

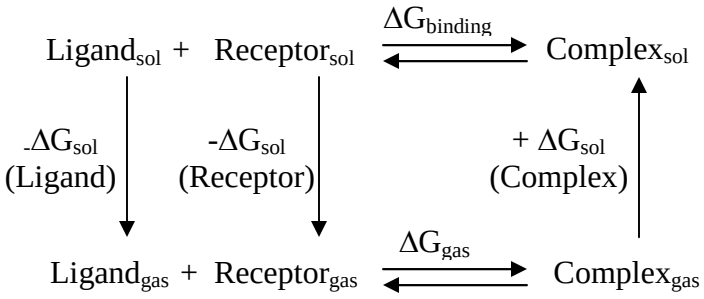
Ligand$_{sol}$ + Receptor$_{sol}$
$\Delta G_{binding}$
Complex$_{sol}$
$-\Delta G_{sol}$ (Ligand)
$-\Delta G_{sol}$ (Receptor)
$+\Delta G_{sol}$ (Complex)
Ligand$_{gas}$ + Receptor$_{gas}$
ΔG_{gas}
Complex$_{gas}$

The free energy of a molecule (ligand or receptor or complex), which is a sum of the internal energy, the electrostatic interaction energy, the van der Waals interactions, the free energy of polar solvation, the free energy of nonpolar solvation and the entropic contribution to the molecular free energy, is calculated as:

$$G_{molecule} = \langle E_{internal} \rangle + \langle E_{electrostatic} \rangle + \langle E_{vdW} \rangle + \langle G_{polar\text{-}solvation} \rangle + \langle G_{nonpolar\text{-}solvation} \rangle - T\Delta S \quad (1)$$

Here, the symbol < > denotes an average over a set of snapshots along an MD trajectory. $E_{internal}$ includes the bond, angle and torsional angle energies. $G_{polar\text{--}solvation}$ was calculated with the GB model of Sander. It describes the difference in electrostatic free energy between charging up the solute in vacuum and the solvent modeled as a dielectric continuum. The polar solvation process is equivalent to the transfer of a protein from one medium whose dielectric constant is equal to that of the interior of the protein to another medium whose dielectric constant is equal to that of the exterior of the protein. $G_{nonpolar\text{-}solvation}$ includes cavity creation in water and van der Waals interactions between the modeled nonpolar protein and water molecules. $\Delta G_{nonpolar\text{-}solvation} = \gamma A + b$, where A is the solvent-accessible surface area calculated by Paul Beroza's *molsurf* program with the values of the constant $\gamma = 0.00542$ kcal/mol · Å and the constant $b = 0.92$ kcal/mol [10].

The free energy of ligand (Cofactor) binding to receptor (Apoenzyme) to form the complex (Enzyme-cofactor) was calculated using the following equation:

$$\Delta G_{binding} = G_{complex} - (G_{cofactor} + G_{apoenzyme}) \quad (2)$$

The above ΔG_{gas} is the interaction energy between ligand and receptor in the gas phase and ΔG_{sol}(ligand), ΔG_{sol}(receptor), ΔG_{sol}(complex) are the solvation free energies of ligand, receptor, and complex, which are estimated using a continuum approach.

Normal-mode analysis was used to estimate conformational entropy $-T\Delta S$. Because this analysis requires extensive computer time, only six snapshots were taken in this study to estimate the order of magnitude of the conformational entropy. Also the total number of atoms of the SAHH dimer (~16000) made calculations on the whole system impossible, so only one subunit was considered.

5.2.1.4. Calculation of energy decomposition by MM-GBSA.

MM-GBSA calculations were performed using the mm_pbsa.pl script in the Amber package. A single-trajectory approximation was used to estimate the free energy of NADH binding from trajectories of the SAHH:NADH complexes only and what approximations this entails, which was assumed to provide reliable information on the residues responsible for differential cofactor binding in human and parasitic

SAHHs and in the calculation of the binding free energy of NADH to subunit A. The SAHHs used in analysis includes subunit A and its neighboring residues, the C-terminal tail of subunit B, which forms close contacts with the NADH bound to subunit A. The simulated complexes include inhibitor-bound enzyme [closed-form Hs-SAHH with DHCeA (pdb code: 1A7A) and closed-form Tc-SAHH with NepA (pdb code: 1XBE)] as well as cofactor NADH. Our assumption is that enzyme has the same conformation before and after cofactor binding, which may not be true. This assumption simplifies the calculation and focuses on the role of the residues in the experimentally determined complex structure on the binding free energy of cofactor to enzyme. Based on this assumption, the snapshots for enzyme and cofactor were extracted from the MD trajectory projections.

5.2.1.5. Computational alanine scanning by MM-GBSA.

For alanine scanning, alanine was used to replace selected protein residues one at each time. This alanine mutation was assumed not to cause a significant conformation change from wild type enzyme, so snapshot of the wild type trajectory were used in these calculations. The 38 residues within 5 Å of the NAD(H) binding site in SAHHs were used in the binding free energy calculation. The binding free energy differences between the mutant and wild type complexes are defined as:

$$\Delta\Delta G_{binding} = \Delta G_{binding\text{-}mutant} - \Delta G_{binding\text{-}wild\ type} \quad (3)$$

5.2.2. Experimental procedures:

5.2.2.1. Construction of the mutants of Hs-SAHH and Tc-SAHH.

The wild type genes of Hs-SAHH and Tc-SAHH were inserted in the pPROK-1 vector (Clonetech, CA), respectively. Three alanine mutants (HsY430A, TcK431A, TcY435A) were prepared by the site-directed mutagenesis PCR. The primer sequences are listed below:

HsY430A: 5'-- CAAGCCGGATCACGCCCGCTACTGAGA -- 3'

5' -- TCTCAGTAGCGGGCGTGATCCGGCTTG -- 3'

TcK431A: 5' – ACGGCCCATTCGCGCCGGACCACTACC – 3'

5' – GGTAGTGGTCCGGCGCGAATGGGCCGT – 3'

TcY435A: 5' – AAGCCGGACCACGCCCGCTACTAATCG – 3'

5' – CGATTAGTAGCGGGCGTGGTCCGGCTT – 3'

The amplification reactions of HsY430A, TcK431A and TcY435A were performed in a volume of 50 μL containing 20 ng template, 25 pmol of 5' and 3' primers, 12.5 nmol of each deoxynucleoside triphosphate, 3 U native Pfu DNA polymerase (Stratagene), 6 μL 10x Pfu buffer and 2.5 μL DMSO. The steps of the PCR program were set up as follows: 1) 92 °C for 4 mins; 2) 25 cycles of 92 °C for

30 sec, 52 °C for 30 sec and 68 °C for 20 mins; 3) 68 °C for 10 mins; 4) hold at 4 °C. The PCR products of HY430A and TcK431A were purified with a Qiagen PCR purification kit, while the PCR product of TcY435A contains two fragments of different sizes. The correct-size band (large size) was cut and collected from a 1 % DNA gel (low melting point) and then the PCR product was recycled by a Qiagen gel extraction kit. These three purified PCR products were digested by DpnI (Biolab) and transformed into *E. coli* competent cell stain JM109 (Sigma). The purified mutant genes were confirmed by DNA sequencing.

5.2.2.2. Determination of contents of NADH in isolated Hs-SAHH and Tc-SAHH mutants.

The mutant proteins (395 μg in 90 μL of 50 mM phosphate buffer, pH 7.2, 1 mM EDTA) were mixed with 10 μL of 1 M Na_2CO_3/$NaHCO_3$, pH 10.7. Then a volume of 700 μL of 95 % ethanol was added to denature the proteins and release NADH into solution. After centrifugation for 10 mins at 18,760 xg to remove precipitated proteins, the fluorescence intensity of NADH was measured by a photon technologies QM-3 scanning luminescence spectrophotometer. The excitation wavelength was 340 nm and the emission wavelength was 450 nm. NADH standards were prepared ranging from 0.1–10 μM. The NADH content of SAHH inactivated by NepA was used as a control (100 % NAD^+ reduced to NADH).

5.2.2.3. Determination of contents of NAD^+ in Hs -SAHH and Tc-SAHH mutants.

The mutant proteins (395 μg in 80 μL of 50 mM KPB, pH 7.2, 1 mM EDTA) were denatured by addition of 2 μL of 5 M $HClO_4$. Samples were centrifuged at 18760 xg for 10 mins at 4 °C to remove precipitated proteins. Supernatant was injected into a reversed-phase C18 column (Vydac 218TP54, 300 , 5 μm, 4.5x250 mm) to measure the concentration of NAD^+ at 258 nm. The NAD^+ standard curve was made for a range of 1-200 μM. NAD^+ was eluted from the HPLC column at ~ 5.9 min by a gradient of 2-10 % mobile phase B over 20 min with a flow rate of 1 mL/min. Mobile phase A contained 10 mM 1-heptanesulfatic acid, 50 mM sodium phosphate, pH 3.2 and mobile phase B 80 % acetonitrile and 20 % 2-propanol.

5.3. Results:

5.3.1. Computational Results

5.3.1.1. MM-GBSA calculation of the free energy of NADH binding indicates stronger binding to Hs-SAHH than to Tc-SAHH.

The calculated results are listed in Table 5.1. The free energy of binding of NADH to wild type Hs-SAHH is much more negative (-42.43 kcal/mol) than the free energy of binding of NADH to wild type Tc-SAHH (-26.75 kcal/mol).

5.3.1.2. Single-residue contributions to free energy of NADH binding to Hs-SAHH and Tc-SAHH.

Hs-SAHH and Tc-SAHH share about 70 % identity of their amino-acid sequences. In superimposed structures of Hs-SAHH and Tc-SAHH, with the superposition centered on the center of gravity of the cofactor ligand NADH, there are 38 protein residues within a spherical volume of 5-Å radius about the center of the cofactor. To identify protein residues with the largest contributions to differential cofactor binding of Hs-SAHH and Tc-SAHH, contributions to NADH binding free energy from every residue within 5Å of the cofactor binding site were calculated and the results are listed in Table 5.2. Thirty-four of these 38 residues (89 %) are identical in Hs-SAHH and Tc-SAHH. Four pairs of these identical residues (Hs#AaaTc#: 191ASN193; 243GLU242; 426LYS431; 430TYR435), which are shown in red, make significantly different free-energy contributions to the binding of NADH to Hs-SAHH and Tc-SAHH.

5.3.1.3. Hot spots of Hs-SAHH and Tc-SAHH identified by computational alanine scanning.

Table 5.1. Free energy calculation of NADH binding to the apo form of Hs-SAHH (pdb code: 1A7A) and Tc-SAHH (pdb code: 1XBE) using the Generalized Born (GB) method. The components are shown with the standard deviations of fit in parentheses.

$$\text{Cofactor + Apoenzyme} \xrightleftharpoons{\Delta G} \text{Enzyme-cofactor complex}$$

$$\Delta G = G(\text{complex})-[G(\text{receptor}) + G(\text{ligand})]$$

Contribution	**Apo-Tc-SAHH + NADH (kcal/mol)**	**Apo-Hs-SAHH + NADH (kcal/mol)**
$\Delta E_{electrostatic}$	122.95 (12.03)	174.88 (17.38)
ΔE_{vdW}	-87.00 (4.29)	-84.73 (5.46)
$\Delta E_{internal}$	0.01 (0.02)	0.02 (0.02)
ΔGAS	35.96 (11.50)	90.17 (15.54)
ΔGB_{SUR}	-10.49 (0.16)	-10.37 (0.18)
ΔGB	-86.56 (10.15)	-155.46 (13.43)
ΔGB_{SOL}	-97.05 (10.13)	-165.83 (13.45)
ΔGB_{ELE}	36.39 (5.42)	19.42 (7.64)
ΔGB_{TOT}	-61.09 (4.46)	-75.67 (6.81)
$T\Delta S^*$	-34.34	-33.24
$\Delta G_{binding}$	**-26.75**	**-42.43**

$T\Delta S^*$ was estimated for one chain bound with one substrate and one cofactor using normal mode because of the limitation of the software. All other numbers were estimated for dimer with two substrates and cofactors bound.

[Refer Amber Manual 7: GAS – $\Delta E_{electrostatic}$ + ΔE_{vdW} + $\Delta E_{internal}$; GB_{SUR} – hydrophobic contribution to slovation free energy for GB calculations; GB – reaction field energy calculation by GB; GB_{SOL} – GB_{SUR} + GB; GB_{ELE} – GB + $E_{electrostatic}$; GB_{TOT} – GB_{SOL} + GAS; $\Delta G_{binding}$ = ΔGBTOT -TΔS.]

Table 5.2. Free energy contribution of the 38 residues within 5 Å of the NAD(H) binding site in Hs-SAHH and Tc-SAHH. The unit of free energy is kcal/mol. Four pairs of non-identical residues are shown in bold, while four pairs of residues are colored in red due to their significant difference in free energy contribution.

Hs-SAHH Residues	157 THR	158 THR	159 THR	181 ASN	186 LYS	190 ASP	191 ASN	195 CYS	**219 ALA**	220 GLY
Free energy Contribution	-2.16	-6.26	-1.48	0.04	-0.72	0.10	-6.29	-0.60	**-0.90**	-1.55
Tc-SAHH residues	156 THR	157 THR	158 THR	180 ASN	185 LYS	189 ASP	190 ASN	194 CYS	**218 CYS**	219 GLY
Free energy Contribution	-3.00	-6.88	-1.54	-0.29	-1.36	0.45	-1.55	-0.16	**-0.86**	-1.30
Hs-SAHH Residues	221 TYR	222 GLY	223 ASP	224 VAL	225 GLY	242 THR	243 GLU	**244 ILE**	245 ASP	248 ASN
Free energy Contribution	-1.44	-5.23	-0.36	-5.19	-0.51	-0.15	-3.30	**-3.06**	0.27	-1.19
Tc-SAHH residues	220 TYR	221 GLY	222 ASP	223 VAL	224 GLY	241 THR	242 GLU	**243 VAL**	244 ASP	247 ASN
Free energy Contribution	-0.79	-3.61	0	-4.71	-0.12	-0.23	-9.68	**-2.42**	0.16	-0.11
Hs-SAHH Residues	275 THR	276 THR	277 GLY	**278 CYS**	281 ILE	299 ILE	300 GLY	301 HIS	305 GLU	344 LEU
Free energy Contribution	-0.26	-3.18	-0.27	**-0.34**	-1.23	-1.63	-1.41	-0.13	0.34	-0.60
Tc-SAHH residues	274 THR	275 THR	276 GLY	**277 ASN**	280 ILE	298 ILE	299 GLY	300 HIS	304 GLU	343 LEU
Free energy Contribution	-0.13	-3.56	-0.96	**-0.67**	-0.98	-1.85	-1.09	-1.96	0.50	-0.52
Hs-SAHH Residues	346 ASN	353 HIS	407* THR	409* LEU	413* GLN	**417* LEU**	426* LYS	430* TYR		
Free energy Contribution	-2.84	-0.46	-0.99	-0.63	0.02	**-0.17**	-10.01	-3.87		
Tc-SAHH residues	344 ASN	352 HIS	412* THR	414* LEU	418* GLN	**422* ILE**	431 * LYS	435* TYR		
Free energy Contribution	-2.08	0.06	-0.58	-0.19	0.12	**-1.06**	-2.65	-0.49		

*: These residues are from the tail of the second chain.

Based on the free energy contributions of the 38 pairs of residues, selected residues were replaced by alanine, computationally, one at a time. Comparing the difference from $\Delta G_{binging\text{-}mutant}$-$\Delta G_{binding\text{-}wildtype}$ ($\Delta\Delta G$) of Hs-SAHH and Tc-SAHH, residues contributing most to differential binding were identified. Table 5.3. lists four pairs of identical residues showing significant $\Delta\Delta G$ values (> 5.5 kcal/mol) and they are the same pairs of residues making significantly different free energy contributions of NADH to SAHH, which are highlighted in red in Table 5.2. However, only the two pairs of residues located on the tail of the second chain were focused on in the following experimental research.

5.3.2. Experimental Results

5.3.2.1. Y430 in the C-terminal extension of Hs-SAHH may slightly influence binding of NAD^+ and NADH to apo-Hs-SAHH.

The mutant HsY430A was purified and found to be of the correct molecular mass (190 kDa). It also possessed intact tetrameric structure (size exclusion chromatography). The enzyme is isolated from the expression system with 30 ± 5 % active-site occupancy by NAD^+ (HPLC) and 86 ± 5 % active-site occupancy by NADH (fluorescence). Denaturation of the isolated enzyme yielded 3.1 ± 0.1 % adenosine and 81 ± 1 % adenine. Reconstitution of apo-HsY430A with NAD^+ yielded

Table 5.3. Computational alanine scanning for the effect on cofactor binding affinity of four pairs of residues identical in Hs-SAHH and Tc-SAHH. The parameters are shown in the figures with the standard deviations of fit in parentheses. For the wild-type enzymes, $\Delta G_{binding\text{-}wildtype}$ = -75.67 ± 6.81 kcal/mol (Hs-SAHH); -61.09 ± 4.46 kcal/mol (Tc-SAHH). $\Delta G_{binding}$ is calculated from the 38 residues within 5 Å of the NAD(H) binding site in both enzymes.

Hs-SAHH	**N191A**	**E243A**	**K426A**	**Y430A**
$\Delta G_{binding\text{-}mutant}$ ($\Delta G_{binding}$ for the Ala mutant) kcal/mol	-67.92 ± 6.24	-64.38 ± 6.53	-53.72 ± 7.12	-69.29 ± 7.02
mutational effect on $\Delta G_{binding}$, $\Delta\Delta G$, kcal/mol	7.8 ± 9.2	11.3 ± 9.4	22.0 ± 9.9	6.4 ± 9.8
Tc-SAHH	**N190A**	**E242A**	**K431A**	**Y435A**
$\Delta G_{binding\text{-}mutant}$ ($\Delta G_{binding}$ for the Ala mutant) kcal/mol	-58.84 ± 4.29	-36.23 ± 3.85	-54.36 ± 4.58	-61.55 ± 4.39
mutational effect on $\Delta G_{binding}$, $\Delta\Delta G$, kcal/mol	2.3 ± 6.2	24.9 ± 5.9	6.7 ± 6.4	- 0.5 ± 6.3

Protein with 79 ± 1 % occupancy (HPLC) and 70 ± 1% catalytic activity. Reconstitution of apo-HsY430A with NADH yielded protein with 94 ± 1% occupancy (fluorescence).

5.3.2.2. K431 in the C-terminal extension of Tc-SAHH is required for the binding of NAD^+ and NADH to apo-Tc-SAHH.

The mutant TcK431A was purified and found to be of the correct molecular mass (194 kDa) and possessed an intact tetrameric structure (size exclusion chromatography). The enzyme was isolated from the expression system with no NAD^+ occupancy (detection limit 0.1 % active-site occupancy) and little NADH occupancy (1.30 ± 0.03 % active-site occupancy by fluorescence). Attempts at reconstitution with cofactor of apo-TcK431A yielded no detectable occupancy by either NAD^+ or NADH.

5.3.2.3. Y435 in the C-terminal extension of Tc-SAHH is required for tight binding of NAD^+ and NADH to apo-Tc-SAHH.

The mutant TcY435A was purified and found to be of the correct molecular mass (194 kDa) and possessed an intact tetrameric structure (size exclusion

chromatography). The enzyme is isolated from the expression system with 18 ± 1 % active-site occupancy by NAD^+ (HPLC) and 90 ± 1 % active-site occupancy by NADH (fluorescence). Denaturation of the isolated enzyme yielded 24 ± 1% adenosine and 65 ± 1 % adenine. Attempted reconstitution of apo-TcY435A with NAD^+ or NADH yielded protein with no detectable cofactor occupancy.

5.3.2.4. Rate constants for dissociation of NAD^+ from mutant SAHHs HsY430A and TcY435A are 20-fold and 255-fold larger, respectively, than those for the corresponding wild-type enzymes.

Cofactor dissociated from the mutant enzymes is a simple first-order relaxation process as previously observed in other cases ([2, 4, 11] and unpublished data of Dr. Qing-Shan Li) in which the enzymatic activity proceeded from full activity to zero. Mutant HsY430A released cofactor at 30 °C, pH 7.4, with k_{off} = 4.2 ± 0.1 x 10^{-4} s^{-1} while the wild-type enzyme Hs-SAHH released cofactor with k_{off} = 1.9 ± 0.3 x 10^{-5} s^{-1}. The mutation therefore increases the dissociation rate constant by a factor of about 20. Mutant TcY435A released cofactor at 24 °C, pH 7.4, with k_{off} = 2.8 ± 0.2 x 10^{-2} s^{-1} while the wild-type enzyme Tc-SAHH released cofactor with k_{off} = 1.1 ± 0.2 x 10^{-4} s^{-1}. The mutation therefore increases the dissociation rate constant by a factor of about 255. The values of these rate constants are included with other data in Table 5.4.

Table 5.4. Values of rate and equilibrium constants in the kinetics of the fast and slow binding phases of the association reaction of NAD^+ with Hs-SAHH, HsY430A, Tc-SAHH, and TcY435A at 23 °C and pH 7.4, from reference [4, 11] and from fits of the data in Fig. 5.2. to eqs. 1.

Enzyme	K_o, μM binding to fully functional sites of apo-SAHH	K_a, μM binding to non-functional sites of apo-SAHH	K_f, μM binding to fully functional sites of holo-SAHH	10^3k_a, s^{-1} Transformation of non-functional apo-sites to functional holo-sites	$10^{-3}k_a/K_a$, $M^{-1}s^{-1}$ binding and transformation of apo-sites to holo-sites	$10^{-3}k_{on}$ $M^{-1}s^{-1}$	10^6k_{off} s^{-1}	K_d, nM k_{off}/k_{on} $k_{off}/(k_a/K_a)$
Hs-SAHH	33 ± 4 n = 3.3 ± 1.4	19 ± 8	1.4 ± 0.3	55 ± 8	2.9 ± 1.2	1.9 ± 0.04	19 ± 3	10 ± 2 7 ± 3
HsY430A	432 ± 93 n = 0.9 ± 0.1	17 ± 2	2.0 ± 0.3	9.5 ± 0.4	0.56 ± 0.07	0.54 ± 0.04	420 ± 10	784 ± 64 750 ± 95
Tc-SAHH	38 ± 9 n = 1.6 ± 0.4	3.8 ± 0.6	1.8 ± 0.4	6.0 ± 0.2	1.6 ± 0.3	0.68 ± 0.02	110 ± 20	161 ± 30 69 ± 18
	K_o, mM	K_a, mM	K_f, mM	k_a, s^{-1}	k_a/K_a, $M^{-1}s^{-1}$	k_{on}, $M^{-1}s^{-1}$	10^3k_{off}, s^{-1}	K_d, mM
TcY435A	2.6 ± 1 n = 0.6 ± 0.2	0.39 ± 0.04	0.20 ± 0.03	11 ± 0.4	29 ± 9	18 ± 2	28 ± 2	1.6 ± 0.2 1.0 ± 0.3

5.3.2.5. Association kinetics of NAD^+ with mutant SAHHs HsY430A and TcY435A.

These mutant enzymes exhibited (Supporting information) association time courses like those seen with other SAHHs [[2, 4, 11] and unpublished data of Dr. Li]: fast binding occurred within the dead-time of the experiment giving rise to an initial enzyme activity A_o; slow binding ensued with an apparent first-order rate constant k_{app} and combined with A_o to give a final activity A_f. Each of these three parameters is a function of $[NAD^+]$. The expected dependences on the basis of a model to be described in the Discussion Section are given by eqs 1.

$$A_o = (A_t/2)\{[NAD^+]^n/(K^n_o + [NAD^+]^n)\} \quad (1a)$$

$$A_f = (A_t)\{[NAD^+]/(K_f + [NAD^+])\} \quad (1b)$$

$$k_{app} = k_a\{[NAD^+]/(K_a + [NAD^+])\} \quad (1c)$$

Here A_t is the total enzyme activity at saturating $[NAD^+]$ after completion of both phases of binding. Figure 5.2. shows (a) the dependences on $[NAD^+]$ of the fraction of fast binding A_o/A_t, the fraction of slow binding $(A_f - A_o)/A_t$, and the fraction of total binding A_f/A_t; (b) the dependence of k_{app} on $[NAD^+]$ for the mutants HsY430A and TcY435A. The curves in Fig. 5.2. represent least-squares best fits of eqs 1 to the data, with parameters K_o, n, K_f, k_a, and K_a as given in Table 5.4.

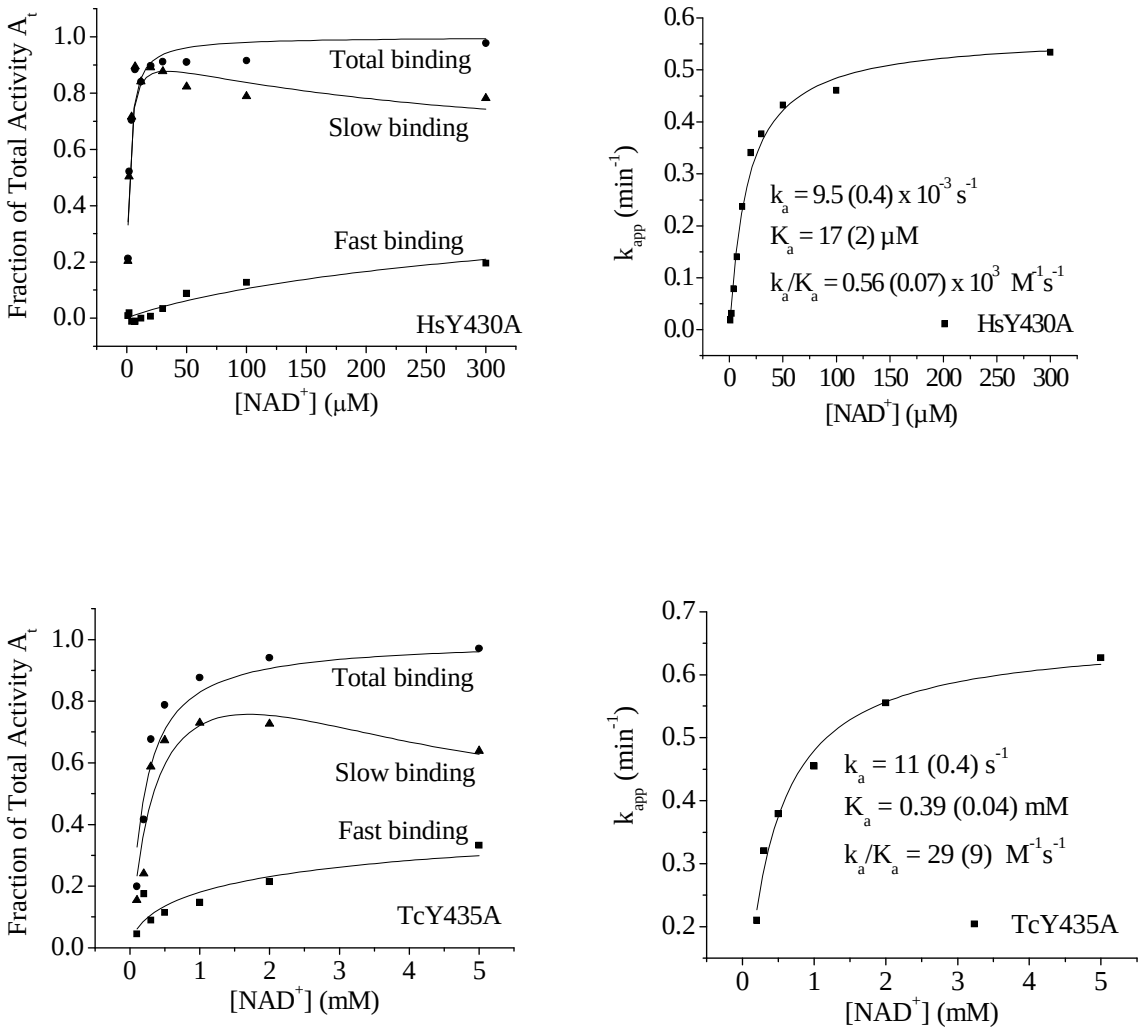

Figure 5.2. Above: The fractions of fast binding, slow binding, and total binding of NAD^+ to the mutant enzyme HsY430A (left) and the value of the slow-binding rate constant k_{app} (right), both as a function of [NAD^+]. Below: The fractions of fast binding, slow binding, and total binding of NAD^+ to the mutant enzyme TcY435A (left) and the value of the slow-binding rate constant k_{app} (right), both as a function of [NAD^+]. The curves are drawn from eqs 1 with the least-squares best-fit parameters given in Table 5.4. Note that the concentration scales for HsY430A are below 300 μM while those for TcY435A go up to 5 mM.

5.4. Discussion

5.4.1. MM-GBSA calculation of the free energy of cofactor NADH binding to SAHHs indicates stronger binding to Hs-SAHH than to Tc-SAHH.

Previous experimental data shows that cofactor NAD(H) binds to Hs-SAHH more tightly than to parasite SAHH [4, 11]. Detailed studies on the kinetic properties of cofactor NAD(H) association and dissociation for both Hs-SAHH and Tc-SAHH have recently been reported and determined in chapter 4 [4]. In this work, we attempt to explain the differential cofactor binding properties between the two enzymes, focusing on the contributions of individual residues to cofactor binding affinity. The calculated binding free energies $\Delta G_{binding}$ for NADH-Tc-SAHH (-26.75 kcal/mol) and for NADH-Hs-SAHH (-42.43 kcal/mol) (Table 5.1) indicate that cofactor NADH binds more favorably to the latter enzyme in qualitative agreement with the experimental results. Thus, reliable results on differential cofactor binding may be obtained from the single-trajectory approximation.

5.4.2. Computed free-energy contributions of individual residues to the cofactor affinities of Hs-SAHH and Tc-SAHH identify four conserved residues as the locus of differential cofactor affinities.

The 38 residues within 5 Å of the NAD(H) binding site, which may form strong interactions with cofactor NAD(H), were chosen for this study. The structures of Hs-SAHH and Tc-SAHH were overlaid and 34 out of the 38 residue pairs were found to be identical. The four pairs of non-identical residues were, HsA219, TcC218; HsI244, TcV243; HsC278, TcN277; HsL417, TcI422, shown in boldface font in Table 5.2.. However, none of these four non-identical residues makes a significant free-energy contribution to the differential in the free energy of cofactor binding between Hs-SAHH and Tc-SAHH (Table 5.2.). In fact, it is four pairs of *identical* residues (shown in red in Table 5.2: Hs/Tc N191/190; E243/242; K426/431; Y430/435) that show the most significant differential free-energy contributions (from about 3.4 to 7.4 kcal/mol) to the cofactor binding of Hs-SAHH and Tc-SAHH.

5.4.3. Computational alanine scanning allows selection of K426/435 and Y430/435 for experimental study of differential cofactor binding to Hs-SAHH and Tc-SAHH.

Computational alanine scanning replaces individual residues with alanines, assuming the conformation of the rest of the protein remains unchanged [12]. Computed from the equation $\Delta\Delta G_{binding} = \Delta G_{mutant} - \Delta G_{wild\ type,}$ the calculated binding free-energy changes can be seen in Table 5.3. for the mutant enzymes HsN191A, TcN190A; HsE243A, TcE242A; HsK426A, TcK431A; HsY430A, TcY435A. Table 5.3. also shows the mutational effect on the binding free-energy change, which

exceeds the probable error only for HsE243A, HsK426A, TcE242A, and TcK431A (slightly). In these cases, the mean values are all positive indicating that the mutation decreases affinity for the cofactor. Even where the probable error exceeds the prediction, the mean values are all positive except for TcY435A.

These findings confirm the computational results of residue free energy contribution (Table 5.2), which indicated these residues to play important roles in cofactor binding. In deciding which cases to address experimentally, we took note of the facts that Turner et al. [13] had identified HsK426 and HsY430 of special interest because they are "involved in interactions with the NAD bound predominantly to the other monomer," an unusual feature of cofactor binding in SAHHs, and that Ault-Riché et al [14] had prepared the mutant HsK426A and found it to be devoid of cofactor affinity and catalytic activity. We therefore decided to concentrate on HsK426, HsY430, and the corresponding residues of Tc-SAHH, TcK431 and TcY435.

5.4.4. Y430 in the C-terminal extension of Hs-SAHH only slightly influences binding of NAD^+ and NADH to apo-Hs-SAHH.

The mutant HsY430A continues to bind NAD^+ and NADH sufficiently strongly that the enzyme passes through the purification procedure from the expression system with essentially full occupancy of the cofactor sites (116 ± 7%). A

preponderance of the cofactor sites were occupied by NADH (86 ± 5%). Denaturation resulted in release of a small amount of adenine (ca. 3%) and a larger amount (81 ± 1%) of adenosine. One possible explanation of these observations is that at least part of the NADH arose by oxidation of adenosine in the active site to 3'-ketoadenosine, which can decompose to adenine, the fragments then remaining in the active site in the "closed" conformation [1, 3] of the enzyme. The isolated enzyme could be converted to the apo-enzyme and reconstituted to around 79 % occupancy by NAD^+, with the reconstituted enzyme exhibiting around 70 % of the activity of wild-type enzyme, which has full occupancy of NAD^+. The HsY430A mutation thus has no major effect on the effective affinity of the enzyme for NAD^+ or NADH, and little or no effect on the enzyme activity.

5.4.5. K431 in the C-terminal extension of Tc-SAHH is required for the binding of NAD^+ and NADH to apo-Tc-SAHH.

The mutant TcK431A is the equivalent of the mutant HsK426A, prepared in previous work [11] and shown to have lost both cofactor affinity and tetrameric structure. TcK431A maintains its tetrameric structure but is isolated from the expression system without cofactor and cannot be reconstituted under normal conditions with either NAD^+ or NADH. Thus, as with Hs-SAHH, this lysine residue is critical for cofactor affinity (it is thought to form hydrogen bonds to the 2'- or 3'-OH group of the nicotinamide-bearing ribose ring [1]). It is striking that the mutation

causes loss of tetrameric structure in Hs-SAHH but not in Tc-SAHH. Previous comparisons ([4, 11] and unpublished data of Dr. Qing-Shan Li) of Hs-SAHH, Tc-SAHH, and their mutants have suggested that Hs-SAHH possesses a structure more robust with respect to mutation, typically showing smaller changes in its properties upon mutation than does Tc-SAHH. The quaternary structure would seem to be an exception to the rule.

5.4.6. Y435 in the C-terminal extension of Tc-SAHH is required for tight binding of NAD^+ and NADH to apo-Tc-SAHH.

The mutant TcY435A is the equivalent of HsY430A described above. Like HsY430A, the Tc-mutant is isolated with high occupancy of cofactor (mostly NADH) and releases a mixture of adenosine and adenine upon denaturation. Unlike HsY430A, the apo-form of the Tc-mutant no longer exhibits sufficient effective affinity for cofactor to permit reconstitution. The kinetic experiments reported here were conducted with enzyme as isolated from the expression system.

5.4.7. Rate constants for dissociation of NAD^+ from mutant SAHHs HsY430A and TcY435A are 20-fold and 255-fold larger, respectively, than those for the corresponding wild-type enzymes.

The alanine-scanning calculations predicted a reduced affinity for NADH of HsY430A of around 6 kcal/mol (about a factor of 10^4) and an *increased* affinity for NADH of TcY435A of around 0.5 kcal/mole (about a factor of 2-3), although the estimated errors in both values were larger than the values themselves. The experimental results, related to NAD^+ rather than NADH, show that loss of the tyrosine in both enzymes increases the cofactor dissociation rate constant, but by a factor that is an order of magnitude larger than for the Tc-enzyme. This is consistent with the systematic observation cited above ([2, 4, 11] and unpublished data of Dr. Qing-Shan Li) that the human enzyme is less susceptible to mutational induced changes in its properties than the trypanosomal enzyme.

5.4.8. Association kinetics of NAD^+ with mutant SAHHs HsY430A and TcY435A.

Cofactor combination with these mutant enzymes follows a model previously observed with Hs-SAHH, Tc-SAHH and various mutants of both ([2, 4, 11] and unpublished data of Dr. Qing-Shan Li). The elements of this model are the following:

(1) The apo-enzyme possesses two equally numbered classes of active sites.

(2) Half of the sites are capable of binding cofactor rapidly (during the dead time of the experiment), with a relatively low affinity, and generating the full activity of these sites. This phenomenon accounts for the fast-binding activity A_o observed at time zero from sites with cofactor-dissociation constant K_o and Hill coefficient n.

(3) Half of the apo-enzyme sites (slow-binding sites) are capable of binding cofactor rapidly, with a relatively high affinity (dissociation constant K_a), but generating initially no enzymic activity. These events initiate a time-dependent reorganization with rate constant k_a in which the slow-binding sites acquire full enzymatic activity and all sites acquire a common cofactor-dissociation constant K_f, the final activity being A_f.

This model generates eqs 1 above, which were fit to the data as shown in Fig. 5.2, producing the values of K_o, K_a, K_f, k_a, and n given in Table 5.4. Table 5.4. also gives these values for Hs-SAHH and Tc-SAHH as determined previously [4]. Finally Table 5.4. gives values of the "on" rate constant for NAD^+, estimated as described in the Materials and Methods section by two different methods, and the "off" rate constant for NAD^+, obtained as described above. Together these allow the calculation of the equilibrium constant K_d for NAD^+.

Comparison of the association kinetics for the wild-type enzymes Hs-SAHH and Tc-SAHH show no dramatic differences. The value of k_{off} is about 5-fold larger for Tc-SAHH and values for k_{on} smaller by 2 or 3-fold; the result is a dissociation constant 10 or 20-fold larger.

The mutant HsY430A has lower affinity for the fast-binding sites and a smaller reorganization rate constant k_a than wild type Hs-SAHH, perhaps suggesting

that some of the binding and reorganization events involve Y430 or its neighbors. The mutant off-rate is over 20-fold larger and the on-rate 4-fold slower than for Hs-SAHH, resulting in a dissociation constant larger by about 100-fold.

The mutant TcY435A exhibits far more dramatic effects: the constants K_o, K_a, and K_f have all risen from the wild type Tc-SAHH values at approximately micromolar values to around millimolar values, indicating that these affinities are significantly damaged by the removal of the tyrosine residue. The rate constant for reorganization is unaffected but the off-rate of cofactor is increased by nearly 1000-fold, while the on-rates are smaller by about 100-fold. The result is cofactor binding with a millimolar dissociation constant in the mutant, as compared to a sub-micromolar dissociation constant for the wild-type Tc-SAHH.

This relationship is similar to that for the HsY430A mutation and for the Tc-SAHH/Hs-SAHH comparison: a somewhat smaller decrease in on-rate combines with a larger increase in off-rate to generate a weaker cofactor binding in the mutant enzyme compared to the wild-type enzyme or in Tc-SAHH compared to Hs-SAHH.

5.5. Conclusion.

Computational approaches and crystallographic structures of SAHHs suggest that a lysine residue and a tyrosine residue on a C-terminal extension of each subunit

that forms part of the NAD^+/NADH binding site in a partner subunit might be critical for full cofactor affinity. Earlier work [14] showed that the mutation HsK426A of the human enzyme Hs-SAHH destroyed both cofactor affinity and the terameric structure of the enzyme. Here we show that the corresponding mutation TcK431A of the trypanosomal enzyme Tc-SAHH reduces cofactor affinity strongly but leaves the tetrameric structure intact, a rare example in which the trypanosomal enzyme appears more robust to mutational change than the human enzyme. The residue HsY430 modulates the association-dissociation kinetics noticeably in the case of Hs-SAHH, generating by its mutation to Ala a decreased cofactor affinity of just under 100-fold. The corresponding mutation TcY435A decreased cofactor affinity by around 100,000-fold. Both effects arise from a larger increase in the cofactor off-rate, combined with a smaller decrease in on-rate.

5.6. References & Supporting Information

1. Turner, M.A., et al., *Structure and function of S-adenosylhomocysteine hydrolase.* Cell Biochem Biophys, 2000. **33**(2): p. 101-25.
2. Hu, Y., et al., *Crystal structure of S-adenosylhomocysteine hydrolase from rat liver.* Biochemistry, 1999. **38**(26): p. 8323-33.
3. Yang, X., et al., *Catalytic strategy of S-adenosyl-L-homocysteine hydrolase: transition-state stabilization and the avoidance of abortive reactions.* Biochemistry, 2003. **42**(7): p. 1900-9.
4. Li, Q.-S., et al., *Comparative kinetics of cofactor association and dissociation for the human and trypanosomal s-adenosylhomocysteine hydrolases. 1. Basic features of the association and dissociation processes.* Biochemistry, 2007. **46**(19): p. 5798-809.
5. Moreira, I.S., P.A. Fernandes, and M.J. Ramos, *Unraveling the Importance of Protein-Protein Interaction: Application of a Computational Alanine-Scanning Mutagenesis to the Study of the IgG1 Streptococcal Protein G (C2 Fragment) Complex.* J. Phys. Chem. B, 2006. **110**: p. 10962-69.
6. Pons, J., A. Rajpal, and J. Kirsch, *Energetic analysis of an antigen/antibody interface: alanine scanning mutagenesis and double mutant cycles on the HyHEL-10/lysozyme interaction.* Protein Sci., 1999. **8**: p. 958-68.
7. Jorgensen, W.L., et al., *Comparison of simple potential functions for simulating liquid water.* J. Chem. Phys. , 1983. **79**: p. 926-935.

8. Jakalian, A., et al., *Fast, efficient generation of high-quality atomic charges. AM1-BCC model: I. Method.* Journal of Computational Chemistry, 2000. **21**(2): p. 132-146.

9. Sugui, C. and T.A. Darden, *Molecular dynamics simulations of biomolecules: long-range electrostatic effects.* . Annu. Rev. Biophys. Biomol. Struct. , 1999. **28**: p. 155-179.

10. Sitkoff, D., K.A. Sharp, and B. Honig, *Accurate calculation of hydration free energies using macroscopic solvent modes.* J. Phys. Chem., 1994. **98**: p. 1978-1988.

11. Li, Q.-S., et al., *Comparative kinetics of cofactor association and dissociation for the human and trypanosomal S-adenosylhomocysteine hydrolases. 2. The role of helix 18 stability.* Biochemistry, 2008. **47**(17): p. 4983-4991.

12. Huo, S., I. Massova, and P.A. Kollman, *Computational Alanine Scanning of the 1:1 Human Growth Hormone–Receptor Complex.* Journal of Computational Chemistry, 2002. **23**(1): p. 15-27.

13. Turner, M.A., et al., *Structure determination of selenomethionyl S-adenosylhomocysteine hydrolase using data at a single wavelength.* Nat Struct Biol, 1998. **5**(5): p. 369-76.

14. Ault-Riche, D.B., C.S. Yuan, and R.T. Borchardt, *A single mutation at lysine 426 of human placental S-adenosylhomocysteine hydrolase inactivates the enzyme.* J Biol Chem, 1994. **269**(50): p. 31472-8.

Supporting information is available:

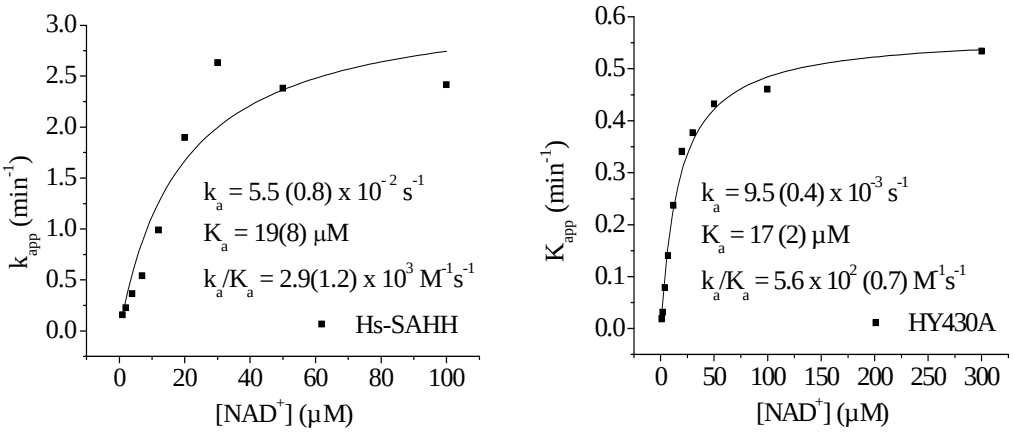

Figure 5.S1. The dependence on the concentrations of NAD^+ of the rate constants for the slow-binding phase of the association of NAD^+ with the apo-forms of mutant HY430A and wild type Hs-SAHH[a] at 23 °C and pH 7.4. Some obvious signs of cooperativity for Hs-SAHH have been neglected and the data in both cases have been fitted to the simple hyperbolic saturation function of equation $k_{app} = (k_a)([NAD^+]/\{K_a + [NAD^+]\})$. The parameters are shown in the figures with the standard deviations of fit in parentheses. [a] The figure of wild type Hs-SAHH is cited from reference [4].

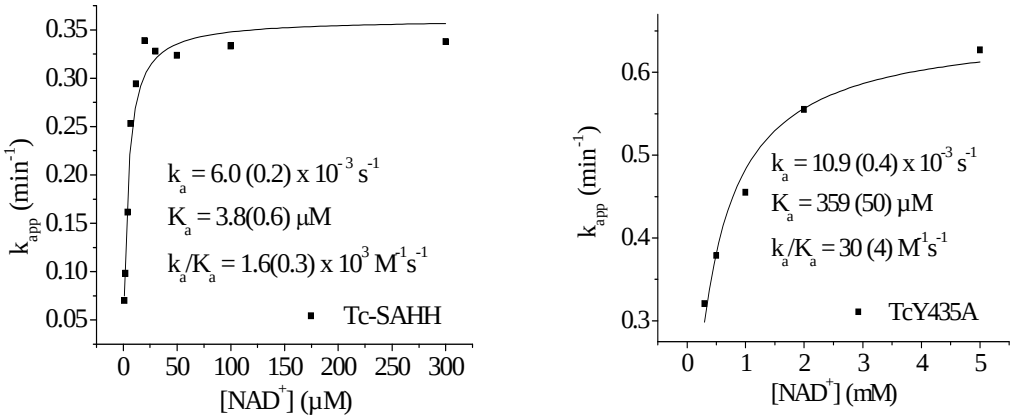

Figure 5.S2. The dependence on the concentrations of NAD^+ of the rate constants for the slow-binding phase of the association of NAD^+ with the apo-forms of mutant TcY435A and wild type Tc-SAHH (the figure of wild type Tc-SAHH is cited from our paper submitted to Biochemistry [4, 11]) at 23 °C and pH 7.4. The data in both cases have been fitted to the simple hyperbolic saturation function of equation $k_{app} = (k_a)([NAD^+]/\{K_a + [NAD^+]\})$. The parameters are shown in the figures with the standard deviations of fit in parentheses.

Table 5.SI: Full tables of residue free energy contribution and alanine scanning.

$\Delta G_{WT\text{-}Hs}$ = -75.67 (6.81) kcal/mol; $\Delta G_{WT\text{-}Tc}$ = -61.09 (4.46) kcal/mol.

Human (1a7a)	157T	158T	**191N**	217A	224V	**243E**	244I
Mutant (ΔG) (kcal/mol)	-73.80 (6.62)	-69.64 (6.37)	**-67.92 (6.24)**	-75.67 (6.81)	-73.21 (6.57)	**-64.38 (6.53)**	-72.29 (6.74)
ΔΔG (kcal/mol)	1.87	6.03	**7.75**	0	2.46	**11.29**	3.38
T. Cruzi	159T	160T	**193N**	219C	226V	**245E**	246V
Mutant (ΔG) (kcal/mol)	-56.92 (4.42)	-55.39 (3.97)	**-58.84 (4.29)**	-61.08 (4.45)	-58.05 (4.44)	**-36.23 (3.85)**	-59.52 (4.35)
ΔΔG (kcal/mol)	4.17	5.70	**2.25**	0.01	3.04	**24.86**	1.57

Human(1a7a)	276T	278C	279I	417L*	**426K***	**430Y***
Mutant (ΔG) (kcal/mol)	-73.59 (6.73)	-75.18 (6.83)	-75.60 (6.81)	-75.43 (6.80)	**-53.72 (7.12)**	**-69.29 (7.02)**
ΔΔG (kcal/mol)	2.08	0.49	0.07	0.24	**21.95**	**6.38**
T. Cruzi	278T	280N	281D	425I*	**434K***	**438Y***
Mutant (ΔG) (kcal/mol)	-58.14 (4.59)	-60.63 (4.43)	-60.25 (4.45)	-59.83 (4.52)	**-54.36 (4.58)**	**-61.55 (4.39)**
ΔΔG (kcal/mol)	2.95	0.46	0.84	1.26	**6.73**	**-0.46**

Chapter 6

Studies on Selective Anti-parasitic Inhibitors Based on Substrate Structure

6.1. Introduction

Modification of substrate structure is a common strategy in designing inhibitors. In our case, the nicotinamide cofactors are involved in a redox step of the catalytic mechanism of SAHHs [1], so that the different binding properties suggest a possible role in achieving differential inhibition of Tc-SAHH over Hs-SAHH for substrate analogs that undergo the redox reaction. However, the situation appears more complex. A screen of 122 substrate analogs kindly provided by Drs. Morris Robins and Stanley Wnuk (unpublished work) resulted in some selective inhibition of Tc-SAHH by only 12 (only one similar in activity to ribavirin, considered below) while the remainder showed no inhibition of either enzyme (89), roughly equivalent inhibition of both enzymes (10) or stronger inhibition of Hs-SAHH (11).

Ribavirin (Fig. 6.1.), an antiviral drug [2], which is an analog of adenosine, has been reported to exhibit inhibition of Hs-SAHH [3]. In this study we report the selective inactivation by ribavirin of Tc-SAHH over Hs-SAHH and some of its kinetic features.

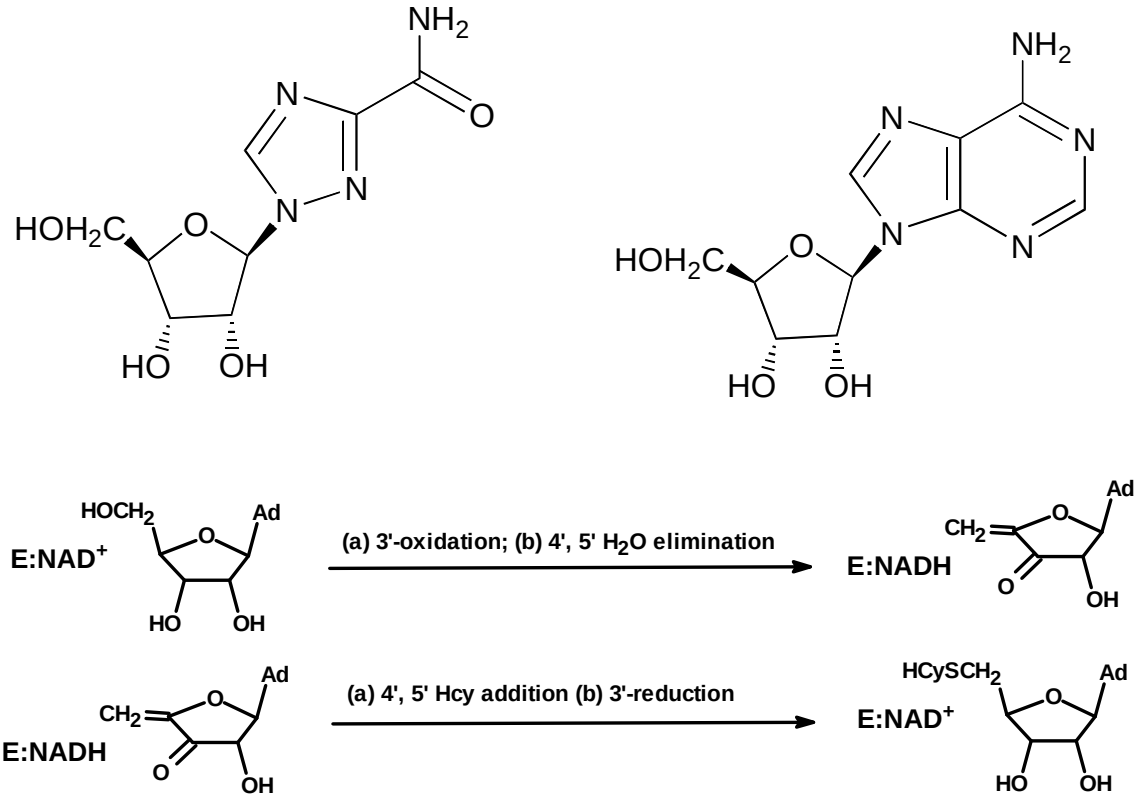

Figure 6.1. Top: Structures of ribavirin and adenosine. Bottom: Catalytic cycle of SAHHs in the synthetic direction, showing 3'-oxidation of substrate by the tightly-bound NAD^+ in the reactions leading to the intermediate, followed by 3'-reduction in the reactions leading from the intermediate to the final product.

6.2. Methods

6.2.1. Measurement of NADH content vs. fraction of inactivation of enzyme activity.

A set of ten samples of 120 μL 100 μM SAHH was incubated with 400 μM ribavirin (Sigma, R9644) in 50 mM phosphate buffer, pH 7.2, 1 mM EDTA, 100 μM NAD^+ at 37 °C for 4-9 hours. SAHH activity was measured at times roughly corresponding to 25, 50, 75 and 100 % inactivation. Once the hydrolytic activity was reduced to a chosen level, the solution was immediately frozen with dry ice/ethanol. Just before analysis, the frozen solution was thawed and 90 μL of solution was transferred into a new tube and 10 μL of 1 M Na_2CO_3/$NaHCO_3$ at pH 10.75 was added immediately. A volume of 700 μL of 95 % ethanol was added to denature the protein and release the NADH into solution. The precipitated proteins were removed by centrifugation and the supernatant was subjected to a fluorescence assay to determine the concentration of NADH released. The NADH released from SAHH that had been inactivated by NepA was measured as a control (100% NAD^+ reduced to NADH by NepA).

6.2.2. LC ESI+/MS analysis of SAHHs fully inactivated by ribavirin.

A volume of 60 μL 100 μM SAHH was incubated with 400 μM ribavirin in 50 mM phosphate buffer, pH 7.2, 1 mM EDTA, 100 μM NAD^+ at 37 °C for 4-9 hours which roughly 100 % inactivated the activity of SAHH. ESI spectra were acquired on a Q-Tof-2 (Micromass Ltd, Manchester UK) hybrid mass spectrometer operated in MS mode and acquiring data with the time-of-flight analyzer. The instrument was operated for maximum sensitivity with all lenses optimized while infusing a sample of lysozyme. The cone voltage was 60 eV and Ar was admitted to the collision cell. Spectra were acquired at 11364 Hz pusher frequency covering the mass range 800 to 3000 amu and accumulating data for 5 seconds per cycle. Time-to-mass calibration was made with CsI cluster ions acquired under the same conditions. Samples were desalted on a short column (3 cm x 1 mm ID) of reverse phase C18 resin (Zorbax, 5 μM, 300 Å). Proteins (2.5 μg) were loaded onto the reverse phase column from H_2O, washed in same and eluted with H_2O directly into the ESI source. The resulting suite of charge states in the ESI spectrum were subject to charge state deconvolution to present a "zero" charge mass spectrum using the MaxEnt1 routine in MassLynxs software. Samples were also analyzed using a different (acidic) buffer system: loading buffer and washing buffer were 1% formic acid solution and elution buffer was 90% methanol and 0.5% formic acid.

6.2.3. Kinetic model for enzyme inactivation by ribavirin.

The kinetic model used for the reaction between ribavirin and the NAD^+ form of SAHH is shown in Scheme 6.1.[a] [4].

$$E_{(NAD)} + \underset{K_I}{\rightleftharpoons} E\text{-}I_{(NAD)} \xrightarrow{k_i} E'I'_{(NADH)}$$

[a] $E_{(NAD)}$ represents the NAD^+ form of SAHH; $E\text{-}I_{(NAD)}$ represents the complex of ribavirin bound to the NAD^+ form of SAHH; $E'I'_{(NADH)}$ represents the complex of the oxidized ribavirin bound to the NADH form of SAHH; K_I represents the equilibrium dissociation constant { $K_I = [E_{(NAD)}][I]/[E\text{-}I_{(NAD)}]$}.

The velocity *v* of inactivation is given by eq 1, where $[E]_0$ represents the total concentration of enzyme in all forms.

$$v = k_i [E]_0 [I]/(K_I+[I]) \qquad (1)$$

6.2.4. Equilibrium affinity of NADH forms of SAHHs for ribavirin.

The equilibrium binding of ribavirin (R) to the enzymes reconstituted with NADH ($E_{(NADH)}$) generates a complex $E\text{-}R_{(NADH)}$ shown in Scheme 6.2.

$$E_{(NADH)} + R \underset{K_R}{\rightleftharpoons} E\text{-}R_{(NADH)}$$

The equilibrium dissociation constant K_R (= $[E_{(NADH)}][R]/[E\text{-}R_{(NADH)}]$) could serve to some degree to estimate the relative affinity of Hs-SAHH and Tc-SAHH for the unoxidized drug.

The fluorescence intensity F_0 of $E_{(NADH)}$ is greater than F, the fluorescence intensity in the presence of ribavirin. Assuming the fluorescence intensity is reduced by quenching in the complex $E\text{-}R_{(NADH)}$, F at a concentration [R] of ribavirin will be given by $F_E\ [E_{(NADH)}] + F_{ER}\ [E\text{-}R_{(NADH)}]$ where F_E and F_{ER} are the intrinsic fluorescence intensities of the two forms of the enzyme and brackets denote concentrations. The normalized decrease in fluorescence intensity $\Delta F/[E]_0$ is then given by eq 2, where $[E]_0$ is as above, the total concentration of enzyme in all forms:

$$\Delta F/[E]_0 = F_0/[E]_0 - F/[E]_0 = F_E - F_E\{K_R/([R] + K_R)\} - F_{ER}\{[R]/([R] + K_R)\} \quad (2a)$$

$$\Delta F/[E]_0 = (F_E - F_{ER})\{[R]/([R] + K_R)\} \quad (2b)$$

$$\Delta F = (F_E - F_{ER})[E]_0\{[R]/([R] + K_R)\} \quad (2c)$$

Measurement of ΔF as a function of [R] will therefore yield F_E, F_{ER} and K_R.

6.3. Results

6.3.1. Inhibition by ribavirin of Tc-SAHH and Hs-SAHH is time-dependent.

Figure 6.2. shows that ribavirin inactivates both enzymes in a first-order reaction (ribavirin in 100-fold excess over enzyme). The first-order rate constant at this concentration of ribavirin is about six-fold larger for Tc-SAHH than for Hs-SAHH (caption of Fig. 6.2.).

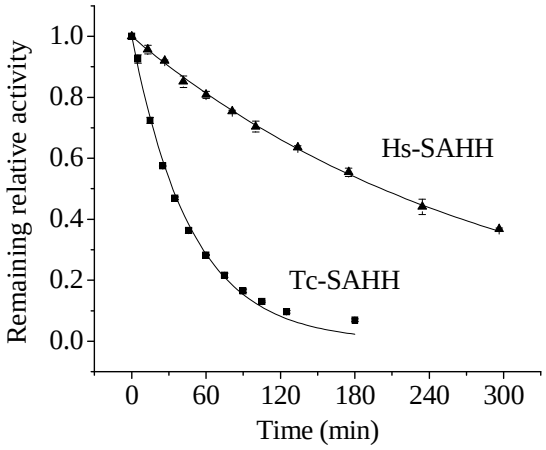

Figure 6.2. Time-dependent loss of activity of Tc-SAHH and Hs-SAHH during incubation with ribavirin. Tc-SAHH and Hs-SAHH, both 1 μM, fully reconstituted with NAD^+, were incubated with 50 μM NAD^+ and 100 μM ribavirin in phosphate buffer (pH 7.2) at 37 ºC. The activity of the enzymes was measured in the hydrolytic direction. The exponential curves shown yield first-order rate constants of (3.48 ± 0.08) x 10^{-4} s^{-1} for Tc-SAHH and (0.57 ± 0.005) x 10^{-4} s^{-1} for Hs-SAHH.

6.3.2. Inactivation by ribavirin of Hs-SAHH and Tc-SAHH is accompanied by an increase in fluorescence.

Figure 6.3. presents the time course of fluorescence emission at 450 nm (excitation 340 nm) as Hs-SAHH and Tc-SAHH are incubated with ribavirin. Fits of the data to eq 3 yield first-order rate constants of $4.05 \pm 0.002 \times 10^{-4}$ s^{-1} for Tc-SAHH and $7.54 \pm 0.006 \times 10^{-5}$ s^{-1} for Hs-SAHH, corresponding to the solid lines in Fig. 6.3.

$$F = F_{max} + (F_0 - F_{max}) \exp(-kt) \qquad (3)$$

The values of F_{max}/E_0 are $2.27 \pm 0.08 \times 10^{10}$ M^{-1} for Tc-SAHH and $1.82 \pm 0.06 \times 10^{10}$ M^{-1} for Hs-SAHH. Taking the value of the molar fluorescence of the enzymes reconstituted with NADH ($3.13 \pm 0.14 \times 10^{10}$ M^{-1} for Tc-SAHH and $2.20 \pm 0.044 \times 10^{10}$ M^{-1} for Hs-SAHH; see below in connection with Fig. 6.6.) as a standard of 100 %, the values of F_{max}/E_0 represent 72.5 ± 4.1 % (Tc-SAHH) and 82.7 ± 3.2 % (Hs-SAHH) of the fluorescence of E_{NADH}. As a control experiment, Tc-SAHH and Hs-SAHH were incubated with NepA and the final fluorescence values determined. These were, compared to E_{NADH}, 5.4 ± 0.3 % for Tc-SAHH and 2.4 ± 0.05 % for Hs-SAHH.

6.3.3 The fractional conversion of NAD^+ to NADH in Tc-SAHH and Hs-SAHH equals the fractional degree of inactivation by ribavirin.

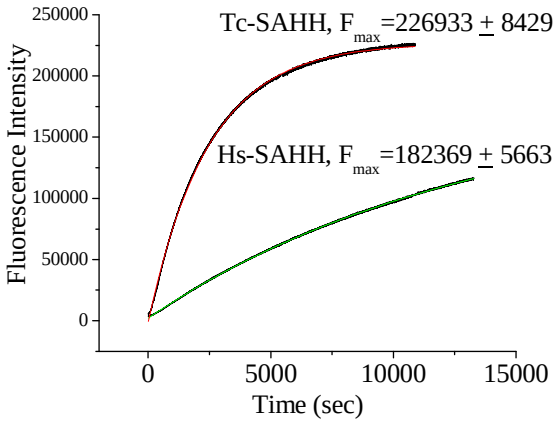

Figure 6.3. Time course of the development of fluorescence during incubation of Tc-SAHH and Hs-SAHH with ribavirin. Reconstituted NAD^+ forms of Tc-SAHH and Hs-SAHH (10 µM) were incubated with 200 µM ribavirin and 100 µM NAD^+ in 50 mM phosphate buffer (pH 7.2), 1 mM EDTA at 37 °C. The wavelengths of excitation (340 nm) and emission (450 nm) are consistent with the conversion of NAD^+ to NADH. The solid line represent fits of the data to a first-order relationship (eq 3), which yields F_0 = -549 ± 49 (Tc-SAHH), 2196 ± 11 (Hs-SAHH); k = (4.05 ± 0.002) x 10^{-4} s^{-1} (Tc-SAHH), (7.54 ± 0.006) x 10^{-5} s^{-1} (Hs-SAHH); and the values of F_{max} are shown in the figure.

In order to ascertain whether the increase in fluorescence that accompanies ribavirin inactivation arises from the conversion of NAD^+ to NADH in the course of inactivation, samples were quenched at specific levels of inactivation and the amount of NADH present was determined. Figure 6.4. shows a plot of the fractional conversion to NADH vs. the fractional level of inhibition for both Hs-SAHH and Tc-SAHH. A linear fit to the total data set yields an intercept of 0.09 ± 0.04 and slope of 0.89 ± 0.07, a linear fit to the data for Hs-SAHH yields an intercept of 0.15 ± 0.06 and slope of 0.76 ± 0.08 and a linear fit to the data for Tc-SAHH yields an intercept of 0.01 ± 0.07 and slope of 0.99 ± 0.09. Thus the fractional conversion of NAD^+ to NADH is equal to the fractional degree of inactivation for Tc-SAHH and probably for Hs-SAHH (predicted intercept 0.0 and slope 1.0).

6.3.4. Time-dependent inactivation by ribavirin of Hs-SAHH and Tc-SAHH conforms to a model of reversible binding followed by a slow inhibitory reaction.

Figure 6.5. shows plots of the first-order rate constants at various ribavirin concentrations for the time-dependent inactivation by ribavirin of Hs-SAHH and Tc-SAHH. The curves of $v/[E]_0$ vs. concentration of ribavirin [I] are described by the hyperbolic function of eq 4. This expression corresponds to a reversible-binding step (equilibrium constant K_I) followed by a slow development of inhibition with rate

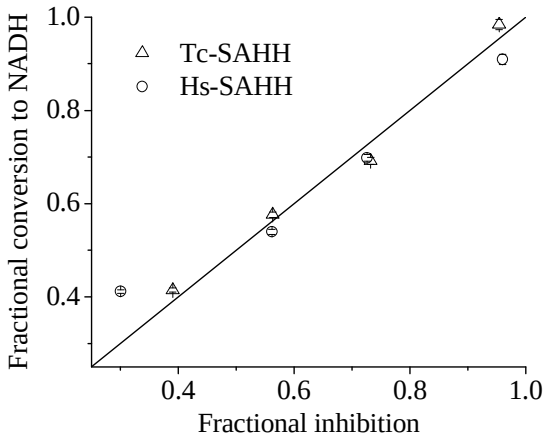

Figure 6.4. Comparison with the fractional loss of enzyme activity with the fractional conversion of enzyme-bound NAD^+ to NADH in the course of ribavirin-induced inactivation of Tc-SAHH and Hs-SAHH. Tc-SAHH and Hs-SAHH (100 μM, reconstituted with NAD^+) were incubated with 400 μM ribavirin and 100 μM NAD^+ in 50 mM phosphate buffer (pH 7.2), 1 mM EDTA at 37 °C. Samples frozen at various fractions of inhibition were later thawed and both activity in the hydrolytic direction and NADH content determined, the latter by liberation and fluorescence determination. The data for Tc-SAHH, for Hs-SAHH, and for both enzymes together are in reasonable agreement with the expectation for an equivalence of NADH formation and inhibition (see text for calculated slopes and intercepts). The straight line shown is for intercept =0 and slope = 1.

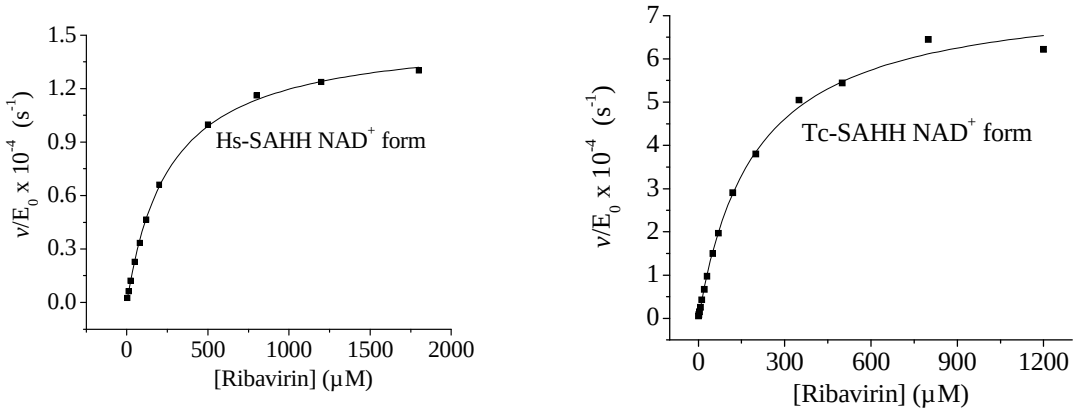

Figure 6.5. Dependence of the rate constant for slow inhibition of Tc-SAHH and Hs-SAHH on the concentration of ribavirin. Tc-SAHH and Hs-SAHH (9.07 μM, reconstituted with NAD^{+}) were incubated with various concentrations of ribavirin (0-1.8 mM) and 50 μM NAD^{+} in 50 mM phosphate buffer (pH 7.2), 1 mM EDTA at 37 °C. The initial velocity of the development of NADH was measured by use of fluorescence (excitation at 340 nm and emission at 450 nm). Data were fit to the hyperbolic saturation model (eq 4) and results are shown in Table 6.1.

constant k_i and also corresponds to various more complex models [4]. The parameters obtained from the fit of the data to eq 4 are shown in Table 6.1.

$$v/[E]_0 = k_i [I]/(K_I+[I]) \quad (4)$$

6.3.5. Ribavirin shows almost no discrimination in equilibrium binding to the NADH forms of Hs-SAHH and Tc-SAHH.

Figure 6.6. shows that incubation of Hs-SAHH and Tc-SAHH, both reconstituted with NADH, with ribavirin leads to quenching of the NADH fluorescence. No NADH was released from the enzyme, so the quenching is presumably caused by binding of ribavirin adjacent to the NADH molecule in the active site. The data were fitted to the hyperbolic-saturation model of eq 2c. The dissociation constant K_R of ribavirin from the E_{NADH}:ribavirin complex was 407 ± 6 μM for Hs-SAHH and 586 ± 12 μM for Tc-SAHH (see Supporting Information, Table S1). The initial molar fluorescence of E_{NADH} were 3.13 ± 0.14 x 10^{10} M^{-1} for Tc-SAHH and 2.20 ± 0.044 x 10^{10} M^{-1} for Hs-SAHH; the final values for the complexes with unoxidized ribavirin were 1.69 ± 0.05 x 10^9 M^{-1} (5.4 ± 0.27 % of the value for E_{NADH}) for Tc-SAHH and 1.90 ± 0.08 x 10^9 M^{-1} (8.6 ± 0.4 % of the value for E_{NADH}) for Hs-SAHH.

6.3.6. LC ESI+/MS analysis shows no evidence of covalent bond between ribavirin and SAHHs.

Table 6.1.[a]: Parameters describing the rate of slow inhibition at pH 7.2 and 37°C of Tc-SAHH and Hs-SAHH by ribavirin as a function of the concentration of ribavirin (eq 4). Experimental data and fitted curves are shown in Figure 6.5.

Parameters of eq 4	Tc-SAHH	Hs-SAHH
K_I (μM)	194 ± 12	266 ± 8
k_i (s^{-1})	7.6 ± 0.16 x 10^{-4}	1.5 ± 0.02 x 10^{-4}
k_i/K_I ($M^{-1}s^{-1}$)	3.92 ± 0.26	0.56 ± 0.017

[a]Tc-SAHH and Hs-SAHH fully reconstituted with NAD^+ (both enzymes at 9.07 μM) were incubated with ribavirin (0-1.8 mM) and 50 μM NAD^+ in 50 mM phosphate buffer (pH 7.2), 1 mM EDTA at 37°C.

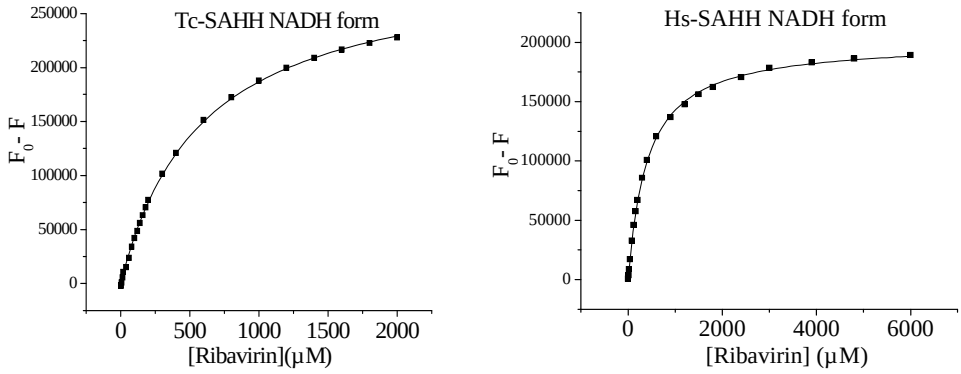

Figure 6.6. Dependence of the loss of NADH fluorescence of Tc-SAHH and Hs-SAHH, both reconstituted with NADH, on the concentration of ribavirin. The enzymes (10 μM) were incubated with various concentrations of ribavirin (0-6 mM) in 50 mM phosphate buffer (pH 7.2), 1 mM EDTA at 37 °C. Data were fit to the hyperbolic saturation model (eq 2c) and results are shown in Table S1 of the supporting information.

The deconvoluted mass spectra show that the molecular weight of SAHHs fully inactivated by ribavirin is exactly the same as that of native SAHHs (see Supporting Information, Figure S1).

6.4. Discussion

6.4.1 Ribavirin exhibits time-dependent inhibition of both Hs-SAHH and Tc-SAHH with Tc-SAHH reacting about six-fold faster.

Figure 6.2. shows that both enzymes react in a first-order fashion with ribavirin (in 100-fold excess), resulting in a completely inhibited enzyme after several hours for Tc-SAHH and considerably longer for Hs-SAHH (37 °C, pH 7.2). The ratio of first-order rate constants is around six, with Tc-SAHH reacting faster.

6.4.2. Inactivation of Hs-SAHH and Tc-SAHH by ribavirin is accompanied by reduction of NAD^+ to NADH.

Figure 6.3. shows that the fluorescence of the solution at a wavelength characteristic of NADH increases in the presence of ribavirin with rate constants that are similar to those seen for the development of inhibition (the differences are very likely related to the somewhat different reaction conditions required for the fluorescence experiment). NADH is not released into the solution, so that the reduced cofactor remains bound to the enzyme. When the inhibition experiment was

interrupted and the enzyme denatured to release NADH, the data shown in Fig. 6.4. are obtained. The figure shows that for both enzymes, the fractional degree of reduction of cofactor is essentially equal to the fractional degree of inhibition of the enzyme: thus cofactor reduction and enzyme inhibition are parallel events. This suggests that ribavirin is a Type I inhibitor according to the classification of Borchardt and Wolfe (Scheme 6.3.) [5], reacting as a substrate through the initial redox reaction. The same behavior is observed in the presence or absence of Hcy (see Supporting Information, Table III), giving some indication that, on this time scale (12 min), ribavirin undergoes 3'-oxidation but not the 4',5'-elimination reaction which would have allowed Hcy to carry it through the catalytic cycle and restore the enzyme activity. This is characteristic of other Type I inhibitors such as DHCeA and NepA, which are tightly bound in the oxidized form.

Scheme 6.3. Typical type I inactivation mechanism shown by inhibitor NepA.

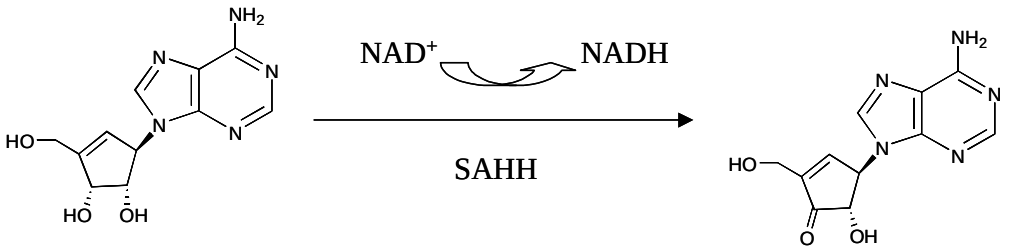

6.4.3. The kinetics of ribavirin inactivation of Hs-SAHH and Tc-SAHH correspond to the common model of time-dependent inhibition.

Figure 6.5. shows that the rate constants for time-dependent inhibition obey the general hyperbolic model for time-dependent inactivation (Scheme 6.1.) which in this case corresponds to a rapid, reversible binding step (equilibrium constant K_I) followed by the essentially irreversible oxidation step with rate constant k_i. The values of these parameters are given in Table 6.1. The initial binding is weak in both enzymes, with K_I approaching millimolar values and the affinity slightly greater for Tc-SAHH. The oxidation step is about five-fold faster for Tc-SAHH and the second-order rate constant reflecting both affinity and oxidation rates is about seven-fold greater for Tc-SAHH.

6.4.4. Fluorescence differences upon binding and oxidation distinguish ribavirin from DHCeA and NepA.

Both DHCeA and NepA in their oxidized forms quench the fluorescence of the NADH cofactor in the active site to about 2-5% of its fluorescence in E_{NADH} with no other ligand. This behavior is seen with both Hs-SAHH and Tc-SAHH. Roughly the same is true if ribavirin itself (in the reduced form) is bound to the NADH form of either enzyme. In contrast the enzyme-inhibitor complexes of ribavirin continue to exhibit around 70-80% of the fluorescence of E_{NADH}. This origin of this effect is unknown but one possibility is that the oxidized ribavirin is unstable in the active site and decomposes to generate compounds that do not quench the NADH fluorescence. The matter is under investigation.

6.4.5. LC ESI+/MS analysis excludes the possibility of irreversible covalent bond between ribavirin and SAHHs.

The LC/MS analyses were performed both in H_2O and in an acidic (1 % formic acid) environment. Water was chosen to avoid the possible acid-catalyzed degradation of the exposed ribavirin that may be covalently bound to SAHHs. Compared to native SAHHs, there is no increase of protein molecular weight in the deconvoluted mass spectrum of SAHHs fully inactivated by ribavirin. This observation shows there is no ribavirin (oxidized or reduced) or any fragment thereof covalently attached to the SAHHs. The information we have to date indicates that the conversion of NAD^+ to NADH in the SAHH active site by 3'-oxidation of ribavirin is not accompanied by or succeeded by irreversible covalent bond formation to the enzyme. Among the possible circumstances are: (a) the oxidized ribavirin, intact or as its decomposition products, either remains in the active site or departs, with the main cause of inhibition being irreversible conversion of the enzyme to the non-physiological form with NADH as the cofactor, a species which is normally restored to the NAD^+ form in the second part of the catalytic cycle (Fig. 6.1.); (b) reversible covalent binding (e.g., 3'-Schiff's base formation with lysine) is partially responsible for inhibition, the main reason still being "stalling" of the enzyme with cofactor in the wrong oxidation state.

6.5. Summary

Ribavirin shows weak inhibitory selectivity for Tc-SAHH over Hs-SAHH in its time-dependent action. It also appears to inhibit the SAHH of *P. falciparum* selectively (see Supporting Information, Table S2) and may therefore be useful as a starting point in proceeding toward more selective inhibitors.

6.6. References & Supporting Information

1. Palmer, J.L. and R.H. Abeles, *The mechanism of action of S-adenosylhomocysteinase.* J Biol Chem. , 1979. **254**(4): p. 1217-26.
2. Bougie, I. and M. Bisaillon, *The broad spectrum antiviral nucleoside ribavirin as a substrate for a viral RNA capping enzyme.* The Journal of Biological Chemistry, 2004. **279**(21): p. 22124-30.
3. Fabianowska-Majewska, K., J.A. Duley, and H.A. Simmonds, *Effects of novel anti-viral adenosine analogues on the activity of S-adenosylhomocysteine hydrolase from human liver.* Biochem Pharmacol, 1994. **48**(5): p. 897-903.
4. Cook, P.F. and W.W. Cleland, *Enzyme Kinetics and Mechanism.* Garland Sciences Publishing, New York and London, 2007: p. 196-204.
5. Wolfe, M.S. and R.T. Borchardt, *S-adenosyl-L-homocysteine hydrolase as a target for antiviral chemotherapy.* J Med Chem. , 1991. **34**(5): p. 1521-30.

Supporting information: Table 6. I[a]. Parameters describing the loss of NADH fluorescence from the NADH forms of Tc-sAHH and Hs-SAHH as a function of the concentration of ribavirin (eq 2c). Experimental data and fitted curves are shown in Figure 6.6.

Parameters of eq 2c	Tc-SAHH	Hs-SAHH
F_E (μM^{-1})-F_{ER} (μM^{-1})	29638.4 =31326.7-1688.3	20994.4 =21994.3-1899.8
F_E : F_{ER}	18.56: 1	11.6: 1
K_R (μM)	586 ± 12	407 ± 5.5

[a]Tc-SAHH and Hs-SAHH fully reconstituted with NADH (both enzymes at 10 μM) were incubated with ribavirin (0-6 mM) in 50 mM phosphate buffer (pH 7.2), 1 mM EDTA at 37 °C.

Supporting information: Table 6.II[a]: Inactivation of Hs-SAHH, Tc-SAHH and Pf-SAHH by ribavirin. Activity assay of SAHHs was performed in the synthetic direction by use of HPLC.

Inhibition (%)	Hs-SAHH	Tc-SAHH	Pf-SAHH	Time
Ribavirin	-7.7	15.6	9.9	30 min
Ribavirin	13.0	52.5	41.7	4 hours

[a]Tc-SAHH and Hs-SAHH fully reconstituted with NAD^+ (both enzymes at 0.816 μM) were incubated with 198 μM ribavirin in 50 mM phosphate buffer (pH 7.2), 1 mM EDTA at 22 °C for 30 min or 4hours.

Supporting information: Table 6. III: Data of Figure 6.4.

		Activity Inhibition (%)	NADH Content (%)
Tc-SAHH		39.04 ± 2.58 %	41.47 ± 0.45 %
Tc-SAHH		56.30 ± 5.42 %	57.62 ± 0.56 %
Tc-SAHH		73.24 ± 2.10 %	69.20 ± 0.76 %
Tc-SAHH		95.42 ± 13.3 %	98.42 ± 1.11 %
Tc-Positive (NepA)	Control	97.31 ± 10.85 %	100 ± 0.97 %

		Activity Inhibition (%)	NADH Content (%)
Hs-SAHH		30.07 ± 1.37 %	41.17 ± 0.40 %
Hs-SAHH		56.17 ± 0.96 %	53.98 ± 0.56 %
Hs-SAHH		72.63 ± 1.69 %	69.81 ± 0.70 %
Hs-SAHH		96.01 ± 4.29 %	90.94 ± 1.08 %
Hs-Positive (NepA)	Control	98.43 ± 9.94 %	100 ± 1.07 %

Supporting information: Figure 6.S1: The deconvoluted mass spectra of native Hs-SAHH (a) and inactivated Hs-SAHH by ribavirin (b).

(a)

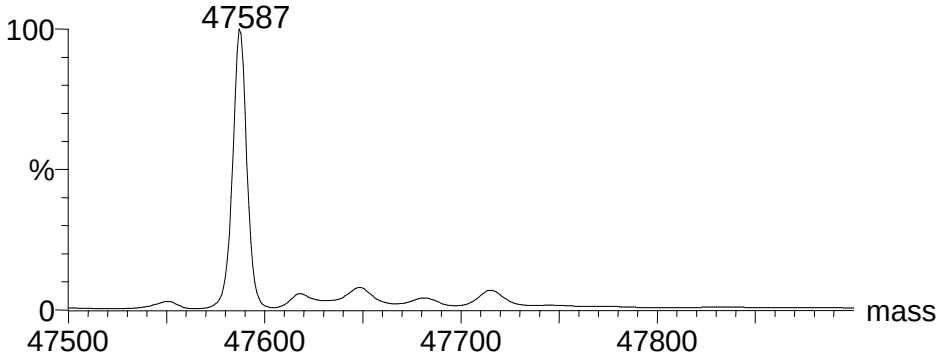

(b)

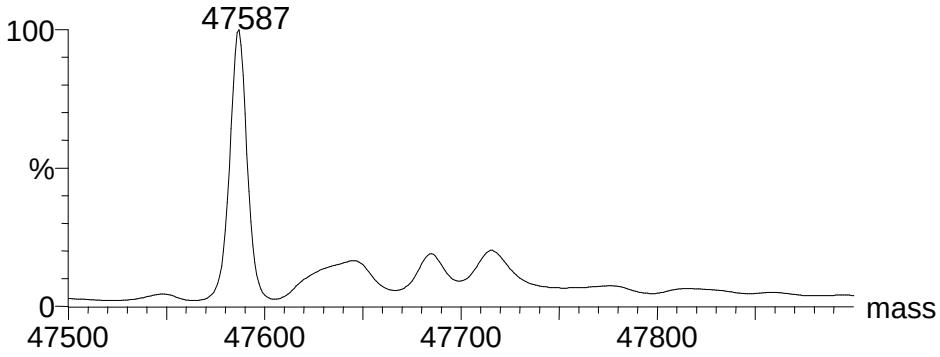

Chapter 7

Conclusion and Future Work

7.1. Summary and conclusion

In both mammals and parasites, SAHH plays a unique and important role in regulating methylation of macromolecules and small molecules. The goals of my project are to conduct comparative investigations of the properties of human and parasite SAHHs, which can be lead to design selective inhibitors against parasite SAHH over Hs-SAHH. This dissertation presents systematic studies on different kinetic and thermodynamic properties of cofactor NAD(H) association and dissociation between Hs-SAHH and Tc-SAHH using biochemical, biophysical and computational methods, as well as research on selective inhibitors against the parasitic enzyme Tc-SAHH.

Chapter 1 summarizes the structure and mechanism of Hs-SAHH and Tc-SAHH, which share more than 70 % identity in sequence. Both SAHHs are homotertramers and each subunit includes one substrate-binding domain, one cofactor-binding domain and an extended C-terminal tail. The kinetics and inhibitor binding are comparable in Hs-SAHH and Tc-SAHH. There is no significant difference in structure detected by comparing their available crystal structures.

Furthermore, it was reported that some properties of parasite enzymes are different from those of the human enzyme, such as parasite enzyme Tc-SAHH binding with cofactor more loosely than Hs-SAHH. **Chapter 2** describes the basic features of cofactor association and dissociation to Hs-SAHH and Tc-SAHH. The equilibrium and kinetic properties of the association and dissociation of the cofactor NAD^+ from Hs-SAHH and Tc-SAHH are qualitatively similar but quantitatively distinct. Both enzymes bind NAD^+ in a complex scheme. The four active sites of the homotetrameric apo-enzyme appear to divide into two numerically equal classes of active sites. One class of sites binds cofactor weakly and generates full activity very rapidly (in less than a minute). The other class binds cofactor more strongly but generates activity only slowly (over 30 min). In the case of Tc-SAHH, the final affinity for NAD^+ is roughly micromolar and this affinity persists as the equilibrium affinity. In the case of Hs-SAHH, the slow-binding phase terminates in micromolar affinity also, but over a period of hours, the dissociation rate constant decreases until the final equilibrium affinity is in the nanomolar range. The slow binding of NAD^+ by both enzymes exhibits saturation kinetics with respect to the cofactor concentration but binding to Hs-SAHH has a maximum rate constant around 0.06 s^{-1}, while the rate constant for binding to Tc-SAHH levels out at 0.006 s^{-1}. In contrast to the complex kinetics of association, both enzymes undergo dissociation of NAD^+ from all four sites in a single first-order reaction. The equilibrium affinities of both Hs-SAHH and Tc-SAHH for NADH are in the nanomolar range. The dissociation rate constants and the slow-binding association rate constants for NAD^+ show a complex temperature

dependence with both enzymes, but the cofactor always dissociates more rapidly from Tc-SAHH than from Hs-SAHH, the ratio being around 80-fold at 37 °C and the cofactor binds more rapidly to Hs-SAHH than to Tc-SAHH above about 16 °C. These features present an opening for selective inhibition of Tc-SAHH over Hs-SAHH, demonstrated with the thioamide analogs of NAD^+ and NADH. Both analogs bind to Hs-SAHH with about 40 nanomolar affinities but much more weakly to Tc-SAHH (0.6 to 15 micromolar). Nevertheless, both analogs inactivated Tc-SAHH to the extent of 60% (NAD^+ analog) or 100% (NADH analog) within 30 min, while inhibition of Hs-SAHH approached 30% only after 12 h. The rate of loss of activity is equal to the dissociation rate of the cofactor and thus 80-fold faster at 37 °C for Tc-SAHH.

To provide explanations on the differential cofactor binding properties between Hs-SAHH and Tc-SAHH, **Chapter 3** identified a local structure factor, helix 18, as a target. The binding of NAD^+ and NADH to SAHH appears structurally to be mediated by helix 18, formed by seven residues near the C-terminus of the adjacent subunit. Helix-propensity estimates indicate decreasing stability of helix 18 in the order Hs-SAHH > Tc-SAHH > Ld-SAHH > Pf-SAHH, which would be consistent with previous observations. We report the properties of Hs-18Pf-SAHH, the human enzyme with plasmodial helix 18, and Tc-18Hs-SAHH, the trypanosomal enzyme with human helix 18. Hs-18Tc-SAHH, the human enzyme with trypanosomal helix 18, was also prepared but differed insignificantly from Hs-SAHH. Association of

NAD^+ with Hs-SAHH, Hs-18Pf-SAHH, Tc-18Hs-SAHH, and Tc-SAHH exhibited biphasic kinetics for all enzymes. A thermal maximum in rate, attributed to the onset of local structural alterations in or near the binding site, occurred at 35, 33, 30, and 15 °C, respectively. This order is consistent with some reversible changes within helix 18 but does require the influence of other properties of the "host enzyme." Dissociation of NAD^+ from the same series of enzymes also exhibited biphasic kinetics with a transition to faster rates (that is the larger enthalpy of activation more than compensated by larger entropy of activation) at temperatures of 41, 38, 36, and 29 °C, respectively. This order is also consistent with changes in helix 18 but again requiring the influence of other properties of the "host enzyme." Global unfolding of all fully reconstituted holo-enzymes occurred at around 63 °C, confirming that the kinetic transition temperatures did not arise from a major disruption of protein structure.

Chapter 4 identified another structure element responsible for the difference between cofactor binding properties of Hs-SAHH and Tc-SAHH, β-sheet A in the Rossmann motif. Mutagenesis, which was used in Chapter 3, was also performed in this study. Mutations V215T and V217C in β-sheet A of the Rossmann motif of Hs-SAHH result in a "parasitized" enzyme Hs-βATc-SAHH, with β-sheet A similar to that of Tc-SAHH. Mutations T214V and C216V of Tc-SAHH result in a "humanized" enzyme Tc-βAHs-SAHH with β-sheet A similar to that of the Hs-SAHH. Both Hs-βATc-SAHH and Tc-βAHs-SAHH possess intact homotetrameric structures and

secondary structure nearly identical to those of the parent enzymes. The catalytic kinetics are also unaffected by these mutations. However, the kinetics of association and dissociation of the NAD^+ cofactor show significant effects. The first-order dissociation rate constants of the mutant enzymes fall below the large dissociation rate constant of Tc-SAHH and above the small dissociation rate constant of Hs-SAHH. Cofactor dissociation for Hs-βATc-SAHH is only slightly faster than for Hs-SAHH and dissociation for Tc-βAHs-SAHH is substantially slower than for Tc-SAHH, as expected if the structure of β-sheet A is more robust to mutational effects in Hs-SAHH than in Tc-SAHH. The temperature dependence of the rate constant for cofactor dissociation is biphasic for both mutant and wild-type enzymes, with the Eyring curves for the mutants lying between those for the wild-type enzymes; again the mutational effect is larger for Tc-SAHH than for Hs-SAHH. The association process of the cofactor with apo-Hs-βATc-SAHH follows the same fast-binding/slow-binding scheme observed with the wild-type enzymes and with very similar kinetics (in particular, initial binding at micromolar levels of cofactor). In contrast, Tc-βAHs-SAHH underwent cofactor binding only at millimolar levels, such that it was not possible to establish clearly that the overall kinetic scheme was the same as Hs-SAHH, Hs-βATc-SAHH, and Tc-SAHH. The kinetics of cofactor association with Tc-βAHs-SAHH was, however, qualitatively and quantitatively similar to that of the wild-type Pf-SAHH. These results support the view that drug-design targeted to the cofactor binding site is a promising avenue for anti-parasitic therapy.

Based on the available X-ray structures of the SAHHs, the Molecular Mechanics-Generalized Born Surface Area (MM-GBSA) method was applied with computational alanine scanning to predict residues which are important for the differential cofactor binding properties of Hs-SAHH and Tc-SAHH, within 5 Å of the cofactor NAD(H) binding site. **Chapter 5** describes the computational predictions and experimental evidence. The only non-identical residues in this range make no contribution to differential cofactor binding between Hs-SAHH and Tc-SAHH. On the other hand, four pairs of *identical* residues are shown by computational alanine scanning to differentiate cofactor binding to Hs-SAHH and Tc-SAHH. Experimental mutagenesis was performed to test these predictions for a lysine and tyrosine residue of the C-terminal extension that penetrates a partner subunit to form part of the cofactor binding site. The K431A mutant of Tc-SAHH (TcK431A) loses its cofactor binding affinity but retains the wild type tetrameric structure, while the corresponding mutant of Hs-SAHH (HsK426A) loses cofactor affinity and also tetrameric structure [Ault-Riche et al. (1994) *J Biol Chem.* 269(50):31472-8.] The tyrosine mutants HsY430A and TcY435A change the NAD^+ association and dissociation kinetics, with HsY430A increasing the cofactor equilibrium dissociation constant from around 10 nM (Hs-SAHH) to about 800 nM and TcY435A increasing the cofactor equilibrium dissociation constant from around 100 nM (Tc-SAHH) to about 1 mM. Both changes result from larger increases in off-rate combined with smaller decreases in on-rate. Overall, the lysine and tryptophan predicted by computational alanine scanning play important roles in differential cofactor binding of SAHHs.

Further attempts to design and search for selective inhibitors against Tc-SAHH were performed. Besides the cofactor-binding site identified as a plausible target site based on above obtained data (Chapter 2-5), the substrate-binding domain as a traditional design site for inhibitor was selected. Ribavirin (1, 2, 4-triazole-3-carboxamide riboside) is a well-known antiviral drug. Ribavirin has also been reported to inhibit Hs-SAHH. **Chapter 6** describes how ribavirin, which is structurally similar to adenosine, produces time-dependent inactivation of Hs-SAHH and Tc-SAHH. Ribavirin binds to the adenosine-binding site of both SAHHs and reduces the NAD^+ cofactor to NADH. The reversible binding step of ribavirin to Hs-SAHH and Tc-SAHH has similar K_I values (266 and 194 μM), but the slow inactivation step is five fold faster with Tc-SAHH. Ribavirin may provide a structural lead for design of more selective inhibitors of Tc-SAHH as potential anti-parasitic drugs.

Overall, studies on differential cofactor association and dissociation properties between Hs-SAHH and Tc-SAHH should help us to better understand these two enzymes and lead to the design of more selective inhibitors for the treatment of Chagas disease.

7.2. Potential future work

Besides the extended C-terminal tail and the first β-sheet of the Rossman motif, it is possible that additional structural elements may cause differences in the properties between the human and parasite enzymes. Improved computational methods can be very helpful in providing more accurate and useful information in this regard.

As mentioned in Chapter 2, the cofactor binding process consists of two phases: a fast-binding phase (the dead time of binding) and a slow-binding phase. Stopped-flow rapid mixing is a technique which can detect ligand-binding reactions occurring on time scales as short as a few milliseconds. So the kinetics of cofactor binding to apo-SAHHs in the fast-binding phase can be measured by this method. Analysis of this cofactor fast-binding phase should improve our cofactor association model which was created based on data primarily from the slow-binding phase. Moreover, the binding process of cofactor to the apo-form of SAHHs can be simulated using available crystal structures and these data could improve our understanding of cofactor binding.

In Chapter 5, computational alanine scanning predicted that four pairs of identical residues of Hs-SAHH and Tc-SAHH could cause differential cofactor binding properties. Due to limited time and computer resources, only two pairs of residues (LYS and TYR located on C-terminal tail) were chosen for this mutagenesis study. The other two pairs of identical residues (ASN located in the hinge region and

GLU located in cofactor-binding domain) could also be mutated to alanine for further studies. If the cofactor binding properties of these mutations matches the computational predictions, this will confirm that residue ASN_{191} of Hs-SAHH and residue GLU_{245} of Tc-SAHH could be evaluated for their roles in cofactor association and dissociation.

Finally, Tc-SAHH is one of the parasite SAHHs of significant interest. Similar studies could be performed on other parasite enzymes, such as Pf-SAHH and Ld-SAHH, to help design either broad-spectrum or more specific anti-parasitic drugs.